ATG2A interacts with RAB1A and ARFGAP1 positive membranes during autophagosome biogenesis

Devin M. Fuller[1,2], Yumei Wu[1-5#], Florian Schueder[1,6#], Burha Rasool[1], Shanta Nag[1], Justin L. Korfhage[1], Rolando Garcia-Milian[7], Katerina D. Melnyk[1], Joerg Bewersdorf[1,8,9,10,11], Pietro De Camilli[1-5], Thomas J. Melia*[1,2]

[1] Department of Cell Biology, Yale University School of Medicine, New Haven, CT
[2] Aligning Science Across Parkinson's (ASAP) Collaborative Research Network, Chevy Chase, 20 MD
[3] Department of Neuroscience, Yale University School of Medicine, New Haven CT
[4] Howard Hughes Medical Institute, Yale University School of Medicine, New Haven, CT
[5] Program in Cellular Neuroscience Neurodegeneration and Repair, Yale University School of Medicine, New Haven, CT
[6] Department of Microbial Pathogenesis, Yale School of Medicine, New Haven, CT, USA
[7] Bioinformatics Support Hub, Yale Medical Library, Yale School of Medicine, 333 Cedar St, New Haven, CT 06510
[8] Department of Biomedical Engineering, Yale University, New Haven, CT, USA
[9] Nanobiology Institute, Yale University, West Haven, CT, USA
[10] Kavli Institute for Neuroscience, Yale School of Medicine, New Haven, CT, USA
[11] Department of Physics, Yale University, New Haven, CT, USA
[#] these authors contributed equally

*Corresponding author: Thomas Melia

Email: Thomas.melia@yale.edu

Author Contributions: TJM and DMF conceptualized the project. FS and JB designed and performed the FLASH-PAINT analysis. YW and PDC designed and performed the correlative light electron microscopy experiments. DMF performed all other experiments reported in this study with contributions from BR, SN, JLK, RGM and KDM The manuscript was prepared by DMF and TJM with input from all authors.

Competing Interest Statement: FS and JB filed patent applications with the U.S. patent office covering FLASH-PAINT. JB has licensed IP to Bruker Corp. and Hamamatsu Photonics. JB is a founder of panluminate, Inc.

Abstract

Autophagosomes form from seed membranes that expand through bulk-lipid transport via the bridge-like lipid transporter ATG2. The origins of the seed membranes and their relationship to the lipid transport machinery are poorly understood. Using proximity labeling and a variety of fluorescence microscopy techniques, we show that ATG2A localizes to extra-Golgi ARFGAP1 puncta during autophagosome biogenesis. ARFGAP1 itself is dispensable during macroautophagy, but among other proteins associating to these membranes, we find that RAB1 is essential. ATG2A co-immunoprecipitates strongly, albeit indirectly, with RAB1A, and siRNA-mediated depletion of RAB1A/B blocks autophagy downstream of LC3B lipidation, similar to ATG2A depletion. Further, when either autophagosome formation or the early secretory pathway is perturbed, ARFGAP1 and RAB1A accumulate at ectopic locations with autophagic machinery. Our results indicate that ATG2A engages a RAB1A complex on select early secretory membranes in support of autophagosome biogenesis.

Significance Statement

This study expounds upon the role of early secretory membranes in autophagosome biogenesis. The authors demonstrate that RAB1/ARFGAP1 positive membranes are essential to autophagy and are recruited to the phagophore assembly site at an early step of autophagosome biogenesis. These membranes interact with the bridge-like lipid transport protein ATG2A and are positive for LC3B and WIPI2, suggesting that RAB1 membranes are a direct source for autophagosome formation.

Main Text

Introduction

Macroautophagy is a cellular degradative pathway in which a seed vesicle grows to encapsulate a target cargo, closes to form the complete autophagosome, and subsequently fuses with the lysosome. This transient organelle forms *de novo* in approximately ten minutes and requires the delivery of millions of lipids[1]. ATG2 proteins function as bridge-like bulk lipid transport proteins[2-5] and are essential during the membrane expansion step of autophagosome biogenesis. We propose that ATG2 bridges the ER and the developing phagophore, thereby allowing lipids to cross the cytosol through a long hydrophobic groove[3]. At the phagophore, lipids are equilibrated between both leaflets of the bilayer via the ATG9 scramblases[6-8]. As such, ATG9 is essential to macroautophagy and is a key component of the seed membranes that ultimately expand during ATG2-mediated lipid transport[9, 10].

In addition to ATG9 vesicles, several other membrane sources have been proposed to be involved in autophagosome biogenesis. In particular, both genetics and biochemistry implicate an essential role for the early secretory pathway. In yeast, some COP-II vesicle and ER exit site (ERES) proteins contribute to starvation-mediated autophagy at a stage that is downstream of formation of the pre-autophagosome structure (PAS)[11, 12]. Furthermore, yeast ERES naturally colocalize with the autophagic cargo Ape1[13], and that colocalization increases when autophagosome growth is stalled by depletion of essential factors[13, 14]. Autophagy proteins themselves collect at ERES; both imaging and cross-linking studies indicate a close association between the two membranes and disruption of ERES activity through depletion of Sec12 dramatically reduces Atg8 puncta formation[15]. Finally, the direct integration of yeast COPII-derived membranes into developing phagophores is suggested by the detection of the COP-II cargo Axl2-GFP, a transmembrane protein, at both phagophores and mature autophagosomes[16].

In human cell lines, genetic or pharmacological disruption of the COPII-related small GTPase SAR1A reduces the frequency of autophagic events[17]. Following biochemical fractionation of cellular membranes, the ER-to-Golgi Intermediate Compartment (ERGIC) is especially competent for supporting in vitro lipidation by LC3B, the primary marker of autophagic structures[17, 18] and clusters of COPII positive membranes can be seen accumulating adjacent to phagophores[19]. Like in yeast, these studies can be interpreted as a key role for ERES or ERGIC membranes in forming or expanding autophagosome membranes. As starvation-mediated macroautophagy drives substantial remodeling of both the ERES and ERGIC membranes[18, 20], including the formation of subdomains with unique protein-dependent organelle-organelle contact sites[21], it is possible that the ERES/ERGIC contribution to autophagy represents a distinct subcompartment of these membrane structures.

Presumably, any contribution of an early secretory membrane must ultimately coordinate with recruitment of ATG9 vesicles, in order to ensure that the lipid transport machinery is competent to expand the phagophore membrane. Several studies have postulated an early fusion intermediate in phagophore formation, such as the description of the HyPas compartment where vesicles bearing distinct autophagy proteins (ATG16L1 and FIP200) were observed to coalesce early in autophagosome biogenesis[22]. Intriguingly, when the lipid transporter ATG2 is genetically depleted from cells, all of the essential autophagy machinery including ATG9 concentrates into large compartments[9, 23-25]. Correlative light and electron microscopy of these structures indicate they are large assemblies of ATG9 vesicles surrounded by more complex membranes which harbor FIP200 and WIPI2, among other proteins[9, 26]. These complex membranes often adopt a cup-like shape, leading us to name them “proto-phagophores”[9]. The origins of the proto-phagophores have been unknown.

In this study, we demonstrate that ATG2A is enriched during autophagosome biogenesis at RAB1/ARFGAP1 positive membranes. Although both proteins can be found within the ERGIC compartment, proximity data and colocalization analyses in secretory pathway disrupted cells suggest that RAB1 and ARFGAP1 membranes involved in ATG2 recruitment are distinct from generic ERGIC membranes. Genetic depletion experiments indicate that RAB1 and ATG2 function at a similar step in autophagosome formation and further these proteins can be isolated together in a complex. Finally, both ARFGAP1 and RAB1 co-localize with proto-phagophores, implying these membranes can recruit much of the key early autophagy machinery and may be dynamically remodeled into cup-like morphologies.

Results

ATG2A is proximal to early secretory membranes

To determine the local proteome adjacent to ATG2A, we used a proximity labeling approach. We fused the biotinylation enzyme APEX2 and a green fluorescent marker to the amino-terminus of ATG2A (APEX2-EGFP-ATG2A) and expressed this construct in ATG2A/B double knockout cells (ATG2 DKO cells). In this way, the APEX2 enzyme will biotinylate cellular proteins in close proximity to the expressed ATG2A fusion protein[27]. To ensure that the APEX2-EGFP-ATG2A construct is active and correctly localized, we measured the restoration of macroautophagy in these cells by following LC3B flux and p62 clearance (Fig. S1A-C). While both LC3B-II and p62 dramatically accumulate in the ATG2 DKO cells, this accumulation is almost entirely reversed upon re-expression of APEX2-EGFP-ATG2A.

We also validated that biotinylation in these cells depends upon the presence of APEX-EGFP-ATG2A and a full reaction. In cells expressing APEX2-EGFP-ATG2A, biotin is only observed when both the biotin substrate (biotin phenol) and the reaction promoter (hydrogen peroxide) are included (Fig. S1D,E). Likewise, streptavidin-mediated immunoprecipitation revealed a strong enrichment of biotinylated material only when the full reaction conditions were employed (Fig.

S1F). Furthermore, the anti-biotin and GFP signals colocalized establishing that biotinylation is favored at sites proximal to ATG2A (Fig. S1D).

Mass spectrometry of proteins isolated by streptavidin-mediated immunoprecipitation was performed using a three state quantitative SILAC experiment[27] with light, medium, and heavy isotopes as follows: no hydrogen peroxide as a negative control, a full reaction in complete media, and a full reaction in starvation media and 100 nM bafilomycin. When comparing both the heavy and medium isotope states to the light state, mass spectrometry analysis revealed an abundance of autophagy related proteins in both full media and under starvation (Figs. 1A, S1G, respectively). The majority of these proteins were cargo adaptors such as NBR1, p62 (SQSTM1), and TAX1BP1, suggesting that the target cargo is immediately adjacent to the biogenesis machinery during autophagosome maturation. We also observed a clear enrichment of ERES or COPII proteins including SEC16A, SEC23A, SEC23IP, and SEC24B/C. Additional ERES proteins such as TFG and SEC31A were also enriched in some, but not all, of the three replicates. In addition, ARFGAP1, a COPI effector that is primarily localized to the Golgi but also found in earlier secretory membranes, was one of the two most enriched proteins in both full media and starvation. Both ARFGAP1 and the COPII proteins suggest ATG2 is localizing to the early secretory pathway.

ATG2A is recruited to ARFGAP1 membranes during autophagosome biogenesis

As an orthogonal method to assess the proximity of ATG2A to early secretory components, we performed FLASH-PAINT, a super resolution technique with high multiplexing capabilities[28]. FLASH-PAINT offers sub-organelle resolution while simultaneously allowing us to screen >10 proteins. ATG2 DKO cells stably expressing GFP-ATG2A were starved and then immunostained for autophagic proteins (GFP-ATG2A, p62, and LC3B), ERES proteins (Tango1, SEC24C, SEC31A, SEC16A, TFG), and markers of COPI-positive membranes (ARFGAP1 and COPI). All proteins were concurrently labeled with primary antibodies that were in turn identified by their association with secondary antibodies with unique DNA barcodes (Fig. S1I). A fluorophore conjugated imager DNA strand and adaptor strands were added to target the imager to the correct secondary antibody. Eraser strands were added in between rounds of imaging to outcompete the adaptor and allow for sequential labeling. In this way, the sub-cellular localization of all ten proteins could be established within the same image.

In these images, the Golgi can easily be identified as a perinuclear ribbon staining strongly for both ARFGAP1 and COP1 (magenta and purple respectively, Fig. S1J). In addition, there are bright puncta throughout the cell (pink arrow heads) stained with TFG and SEC31A, indicating that they are ERES. ARFGAP1 and COPI frequently also accumulated at ERES (made more obvious in the top-right inset, where TFG and SEC31 are removed), consistent with previous reports that COPI vesicles facilitate ER to Golgi transport in human cells[29-31]. GFP-ATG2A is mostly cytosolic, however small accumulations of ATG2 could be found at ERES and were generally observed to be proximal to ARFGAP1/COP1 (inset; brackets). Note that clusters of LC3B and p62 are also present. Occasionally, non-ERES accumulations of p62 could be observed in close proximity to LC3B and ATG2A (lower insets), and here again ATG2 is proximal to ARFGAP1.

Critically, we can directly measure the nominal proximity of each protein relative to the others under investigation by quantifying the median distance between all ten tested proteins within 200 nm of each individual protein (Fig. S1K). All early secretory pathway proteins closely associate with each other, including the COPI proteins ARFGAP1 and β-COP. As the majority of ATG2A was cytosolic, its average distances from other proteins were greater, however, within this cohort of candidate proteins, we found that ATG2A is most closely associated with p62 and ARFGAP1 (15nm and 16nm respectively; top row of Fig. S1K), exactly consistent with the APEX screen.

The APEX and FLASH-PAINT datasets provided a clear but static result that ATG2A is recruited to ARFGAP1 positive structures. To determine whether this recruitment was coincident with phagophore formation, we stably expressed GFP-ATG2A and TagBFP-LC3B in ATG2 DKO cells in order to identify phagophores. ATG2A primarily localizes to phagophores and lipid droplets, whereas LC3B primarily localizes to phagophores, autophagosomes and autolysosomes. Where these two proteins colocalize strongly suggests a growing phagophore in the process of membrane expansion (Figs. 1B). To assess co-localization with phagophores, we expressed candidate early secretory proteins labeled with red fluorophores (Fig. 1C,D; see Fig. S1H for analysis strategy**)**. ARFGAP1-TagRFP colocalized with ~90% of actively forming phagophores, whereas only ~30% of phagophores were coincident with the ERES markers mRuby-SEC23A or RFP-p125a/SEC23IP. Further, while the ARFGAP1 signal was largely concentrated in the Golgi, phagophores most frequently colocalized with extra-Golgi ARFGAP1 puncta.

Finally, we compare our results to the subcellular localization of ARFGAP1 established by global organelle profiling available at the database at https://organelles.sf.czbiohub.org[32]. ARFGAP1 is enriched on autophagic membranes positive for LC3B as well as endolysosomal and early secretory membranes (Fig. 1E). Strikingly, ARFGAP1 was most highly enriched on membranes isolated via RAB1A immunoprecipitation. The autophagic proteins ATG2A, ATG2B, WDR45, and ATG9A, all of which are involved in membrane expansion of the autophagosome, were also highly enriched on RAB1A membranes. These collective results establish that both endogenous ARFGAP1 (organelle isolation, APEX, FLASH PAINT) and overexpressed ARFGAP1 (live imaging) naturally associate with ATG2A, including during phagophore biogenesis.

Autophagic flux depends upon RAB1 but not ARFGAP1

To look for a potential functional role for ARFGAP1 in autophagy, we measured autophagic flux using the HaloTag dropout assay in which liberation of a free HaloTag (HT) is indicative of lysosome-mediated proteolysis of the full-length (FL) protein[33]. We stably expressed HaloTag7-mGFP-LC3B or HaloTag7-mGFP in WT HEK293 cells and then used siRNA to knockdown various regulators or potential regulators of macroautophagy initiation (Fig. 2A,B, S2A). Despite efficient knockdown, siRNA against ARFGAP1 had no effect on flux; the ratio of free HaloTag to full-length HaloTag7-mGFP-LC3B following ARFGAP1 knockdown was similar to both nontransfected (NT) and nontargeting siRNA controls. In contrast, knockdown of the autophagy initiation factor FIP200 dramatically suppressed dropout of the HaloTag. We also looked for an interaction between ARFGAP1 and ATG2A, but even when both proteins were overexpressed, we could not detect significant interaction via co-immunoprecipitation (Fig. 3A,B). Thus, it is likely that ARFGAP1 localizes to a key membrane involved in autophagosome biogenesis but is not itself a player in initiating autophagosome formation. To examine whether the other isoforms of ARFGAP1 could redundantly contribute to autophagosome biogenesis, we knocked ARFGAP1, ARFGAP2, and ARFGAP3 down individually and collectively. Knockdown of ARFGAP2, ARFGAP3 and ARFGAP1-3 marginally increased autophagic flux (Fig. S2B,C), suggesting either no role or a minor role as negative regulators of autophagy.

As shown in (Fig. 1E), both the ATG2/ATG9 lipid transport apparatus as well as ARFGAP1 are associated to RAB1A-positive membranes. RAB1 proteins mediate ER to Golgi trafficking in the early secretory pathway. The yeast RAB1 homologue, Ypt1, is essential to autophagy[34, 35], while in mammals, genetic depletion of either RAB1A or RAB1B modestly reduces autophagic flux[36, 37]. Thus, we tested the functional and physical interaction of RAB1 proteins with ATG2. Consistent with previous results, siRNA knockdown of either RAB1A or RAB1B in our system partially inhibited flux in the Halo dropout assay (Fig. 2A,B). Strikingly, knockdown of both isoforms simultaneously was nearly as effective as knocking down FIP200, establishing that RAB1 proteins play an essential role in supporting starvation induced autophagic flux. This result was consistent with but more pronounced than previous work examining LC3B flux following RAB1A/B double knock down[38]. As an orthogonal method to examine the role of RAB1 in LC3B flux, we used H4 neuroblastoma cells with a GFP-mCherry-LC3B heterozygous knock in reporter[39].

Following knock down and starvation, we examined the ratio between GFP and mCherry by FACS. The low pH of the lysosome quenches the fluorescence of GFP at a higher rate than mCherry, resulting in a low ratio under starvation conditions as seen in the HBSS and siCNTL conditions (Fig. 2 E-G). In contrast, knock down of FIP200 or RAB1A/B resulted in an increased ratio, confirming that these proteins are necessary for proper autophagic flux. Of note, the RAB1A/B knockdown did not block flux as efficiently as the FIP200 KD. If Rab1 is essential for autophagy, this result suggests that either very few copies of RAB1 are needed to support autophagy or that another gene could be compensating for the lack of the two RAB1 isoforms.

In addition to following tagged LC3B, we also immunoblotted for endogenous LC3B in each of our siRNA experiments. We found that knockdown of either RAB1 isoform, and especially knockdown of both together leads to a clear accumulation of the membrane conjugated form of LC3B, LC3B-II (Fig. 2A,G). As LC3B overexpression can alter endogenous LC3B patterns, we confirmed this increase in a cell line expressing only HaloTag7-mGFP (Fig. 2C,D). Knockdown of RAB1A and RAB1B drove a threefold increase of LC3B-II (Fig. 2D). We also confirmed this phenotype in WT HEK293 cells in a classical LC3B flux assay with bafilomycin (Fig. S2D), where we found elevated LC3B-II levels in all conditions.

Increasing LC3B-II levels without autophagic flux is indicative of a block to macroautophagy at a late stage, downstream of initiation, and is therefore easily distinguished from the block induced by depleting FIP200 (where LC3B-II levels go down). Intriguingly, LC3B-II levels also increase when ATG2 proteins are genetically depleted (Fig. S1A,B), suggesting ATG2A and RAB1A might function concurrently. Indeed, overexpressed GFP-RAB1A could strongly immunoprecipitate flag-tagged ATG2A in our cells, indicating these proteins are in a shared complex (Fig. 2E,F). However, ATG2A and RAB1A (bound either to GDP or GTPγS) do not interact in a fully reconstituted system (Fig. 3C,D), suggesting that the interaction is indirect. In contrast, ATG2A and GABARAPL1 cleanly interact in the *in vitro* CoIP.

We also tested several other proximity hits from the biotinylation analysis for interaction with flag-tagged ATG2A, including GFP-tagged copies of ERES resident proteins SEC23A, SEC31A, SEC16A, Sar1 and all four homologs of Sec24 (Fig. S3 A-D). We found that ATG2A co-immunoprecipitated weakly with many of them, the strongest of which was SEC24D. Note that this SEC24D interaction was barely above the background of pull-down with GFP alone (Fig. 3A,B). Thus, consistent with proximity and imaging analyses, ATG2 proteins are in the general proximity of the ERES machinery, but stable protein-protein interactions appear to be limited to RAB1.

Disruption of the early secretory pathway results in the recruitment of autophagic proteins to RAB1A-positive tubular membranes

These results suggest that ATG2 engages an early secretory membrane, distinct from the ERES, in a RAB1-dependent manner. We next tested whether disruption of the early secretory system would impact the localization of ATG2A. To this end, we overexpressed SAR1BH79G, the catalytic dead mutant of the small GTPase SAR1B that recruits the COPII coat. SAR1BH79G binds the membrane and recruits the COPII coat, but is unable to release, thereby trapping COPII onto the membrane. Overexpression of this construct has been shown to reduce autophagy in starved cells[17, 36]. Consistent with those results, overexpression of SAR1BH79G-mOrange2 diminished autophagic flux of both a bulk cargo (HaloTag7-mGFP reduced ~20%) and of LC3B (HaloTag7-mGFP-LC3B reduced by ~30%) by the HaloTag degradation assay[33] (Figs 4A,B). In a parallel assay following autophagic flux instead by the changing fluorescence of tandem tagged GFP-mCherry-LC3B, we detect a similar, but statistically insignificant trend. As both assays are likely sensitive to SAR1BH79G expression levels, which vary in our transient transfection system, we also tested how LC3 puncta accumulation correlates with SAR1BH79G expression on a per cell basis. LC3B puncta number were lowest in cells expressing high amounts of SAR1BH79G

(Figs. S4A,B), consistent with a block to autophagosome formation when the secretory pathway is disrupted rather than a later impact on autophagosome clearance.

Unexpectedly, in a small subset of transfected cells (1.5±0.8%; calculated from the images in Fig. S4A,B), overexpression of SAR1BH79G under starvation conditions shifted the localization of GFP-ATG2A from a largely punctate distribution to long, tubular objects that were SAR1BH79G negative (Fig. 4C). GFP-ATG2A decorated these tubules with varying intensities approximating a beads-on-a-string pattern (e.g. arrows in Fig. 4D,E). Fluorescently tagged forms of LC3B, ARFGAP1 and RAB1A also decorated these tubules. However, these three proteins displayed the brightest intensities where ATG2A was dimmer (e.g. arrowheads in Fig. 4D,E). These three proteins, but not ATG2A, also decorated larger structures that appeared to be contiguous with the tubule, including bulbous regions at the tubule termini.

To determine the ultrastructure of these regions, we subjected GFP-ATG2A-expressing cells to correlative light and focused ion beam scanning electron microscopy (CLEM-FIB-SEM). The GFP-ATG2A fluorescence signal corresponded to thin, tubular membranes (Fig. 4F and S4D), which is consistent with the finding that ATG2A preferentially binds highly curved membranes[40]. The tubule is surrounded by ER elements, many of which appear to be in very close contact (Fig. 4F, S4C). GFP-ATG2A signal was more intense in regions with closely adjacent ER, consistent with a possible contact site localization. The tubule continued into larger structures at either end, which were GFP-ATG2-negative, and morphologically similar with the bulbous structures harboring ARFGAP1, RAB1A and LC3B in fluorescence images.

Thus, although unusual, these rare tubules afforded an opportunity to demonstrate that ATG2, ARFGAP1 and RAB1A target the same membrane, easily resolvable even at confocal resolution. ATG2 collects where ER is closely adjacent, and LC3B accumulates with RAB1A, implying a topological organization with LC3B and RAB1A decorating the same structure, suggesting that RAB1A membranes may be a component or progenitor of the phagophore membrane.

ARFGAP1 and RAB1A accumulate around pre-autophagic structures in ATG2 DKO cells

We previously published that very small, ATG9- and LC3B-positive vesicles accumulate in large clusters with the cargo-adaptor p62 in ATG2 DKO cells[9]. This cluster is surrounded by a shell of more complicated membranes which we termed “protophagophores” because they colocalize with other autophagy proteins such as WIPI2 and because many of them appear to adopt a cup-like shape in TEM images. Beyond this protophagophore shell, the entire structure is surrounded by ER (illustrated in Fig. 5A). Our work and others have shown that essentially all proteins involved in autophagosome biogenesis accumulate with these clusters, including FIP200, ATG14, ATG9A, ATG16L, and p62[9, 23, 24], suggesting they are repositories of autophagosome biogenesis material awaiting the arrival of ATG2 proteins. If early secretory membranes contribute directly in any way to the biogenesis event, they may also concentrate at these sites.

We therefore performed IF against various markers of the early secretory pathway in ATG2 DKO cells to look for colocalization with this compartment (represented by staining for p62 (mouse antibody) or for LC3B (rabbit antibody); Figs. 5B-D). We found that ER exit site markers such as SEC16A, SEC24C, SEC31A, and TFG were not enriched around the compartment, neither was the Golgi protein GM130 (Figs. 5B-C and S5A). ßCOP was modestly enriched, but at levels that by eye, did not suggest encapsulation of the compartment the way autophagy proteins collect. In addition, overexpressed mEmerald-ERGIC53 did not localize to the ATG2 DKO compartment (Fig. S5B). In contrast, ARFGAP1 targeted all of the ATG2 DKO compartments, forming a robust spherical shell at the periphery of the p62 signal in HEK293 ATG2 DKO cells (Fig. 4B-D), or permeating the entire compartment in HeLa ATG2 DKO cells[41] (Fig. S5C).

We were unable to find a strong RAB1A signal by immunofluorescence, however, when overexpressed, tagged versions of RAB1A also formed a sphere around the HEK293 ATG2 DKO

compartment (Fig. 5D. Both ARFGAP1 and SNAP-RAB1A colocalized with WIPI2 (Fig. 5E), consistent with a model whereby these membranes arrive at the PAS prior to ATG2A recruitment and subsequent autophagosome biogenesis.

ARFGAP1 accumulates at the ATG2 DKO compartment independently of the Golgi

The vast majority of ARFGAP1 is found at the Golgi, but ATG2A specifically localizes to extra-Golgi ARFGAP1 puncta (Fig. 1C, S1J). Consistent with a non-Golgi origin for these membranes, both natural and induced perturbations of Golgi structure have no impact on the recruitment of ARFGAP1 membranes to the p62-rich compartments in ATG2 DKO cells. First, in the course of these studies we observed that ARFGAP1 persistently colocalized with p62 in cells undergoing mitosis (Fig. 6A,B,C), even as the Golgi fragments and dissipates. Second, when cells were treated with brefeldin A to inhibit the formation of the Golgi[42], ARFGAP1 again persistently colocalized with p62 (Fig. 6B,C). As brefeldin A specifically targets GBF1, the GEF for the ARF proteins[43], this result also suggests that ARFGAP1 localization to the p62 compartment is independent of GTP bound ARF proteins. Third, overexpression of GFP-SidM/DrrA, an enzyme from *Legionella Pneumophila* which acts as both a GEF[44, 45] and a GDF[46] for RAB1, fragments the Golgi[44] and sequesters RAB1 to the plasma membrane[45]. We found that following GFP-SidM expression in our cells, ARFGAP1 maintained colocalization with p62, even as the Golgi-associated ARFGAP1 as well as the Golgi-marker GM130 were completely dissipated (Fig. 6D, S6A). Thus, the ARFGAP1 localizing to the p62 compartment is not influenced by dispersal of the Golgi and does not colocalize with other Golgi markers, implying a non-Golgi origin for these structures.

Finally, we tested whether the GAP domain of ARFGAP1 or the ALPS motif are necessary for its localization to the PAS, by comparing the colocalization of various tagged constructs with GFP-ATG2A and TagBFP-LC3B (Fig. S6A). Disruption of the GAP domain via the well characterized R50K mutation had no impact on its localization to the ATG2/LC3B positive phagophores (Fig. S6B). Mutation of the ALPS domain (L207D, V279D) altered ARFGAP1 distributions in the cell such that specific localizations could no longer be quantified (the redistribution to the cytoplasm created a high background that was difficult to properly threshold). Nonetheless, even in this condition there remained clear accumulations of this construct at phagophores indicating that recruitment is not strongly dependent upon the ALPS motif. As these elements of ARFGAP1 are essential to its Golgi function, these results further suggest that the ARFGAP1/RAB1A membranes involved in autophagosome biogenesis derive from early secretory membranes prior to the Golgi.

Discussion

Here we describe an interaction of ARFGAP1/RAB1-positive membranes with the autophagic biogenesis machinery including the lipid transporter ATG2. These membranes likely derive from a privileged region of the ERGIC consistent with the literature tying these intermediate secretory membranes to autophagy[17, 21]. In particular, the presence of both ARFGAP1 and RAB1 plus the general proximity to ERES proteins across a variety of assays is consistent with an early secretory origin for these membranes. Intriguingly, ARFGAP1 and RAB1 coalesce around the periphery of the ATG2 DKO compartment exactly where we previously described complex cup-shaped membranes, so called proto-phagophores[9], accumulate. We do not detect any other ERES or ERGIC markers at these sites, implying proto-phagophores derive from only a subdomain of the ERGIC which we suspect is remodeled specifically for the purpose of supporting autophagy.

How do the ERGIC-derived RAB1 membranes contribute to autophagosome formation? Ypt1, the yeast homologue of RAB1A, was identified early on as a genetic regulator of autophagy[34], and subsequently a number of studies have connected both Ypt1 and RAB1 to autophagosome

biogenesis, but the precise mechanism of action remains contentious. In yeast, Ypt1 has been shown to interact with Atg1[35] and Atg17[47], highly suggestive of a role in regulating or recruiting the kinase machinery driving initiation of autophagosome biogenesis. Human RAB1A binds the VPS34 complex favoring conformations that likely support PI3P formation[48]. Thus, either or both of the early acting complexes in autophagosome biogenesis may engage RAB1 proteins. In this study, we find that RAB1 depletion elevates LC3B-II levels, suggesting that RAB1 acts either downstream or independently from the lipidation machinery. Further, we present two orthogonal and highly quantitative methods to follow LC3B degradation in the lysosome. Both methods unambiguously show a clear, albeit partial, genetic dependence of LC3B degradation upon RAB1 consistent with RAB1 promoting autophagy. As we detect RAB1A at the ATG2 DKO compartment, RAB1A recruitment appears to precede ATG2A recruitment to the PAS, consistent with an interaction with either the ULK1 or VPS34 complexes, but is not essential to support LC3B-II formation on early autophagy membranes.

We propose that ARFGAP1/RAB1 membranes are directly integrated into the phagophore prior to ATG2 recruitment. The fusion of vesicular sources has been proposed as a general mechanism for phagophore biogenesis[49, 50]. For example, the HyPas model postulates that FIP200 vesicles from the *cis*-Golgi fuse with endosomally derived ATG16L1 vesicles to create the nucleating structure for autophagosome formation[22]. Recent reports, including our own, have also identified ATG9 vesicles as a seed for autophagosome biogenesis, which expand through lipids delivered by ATG2[9, 10] and then scrambled into both leaflets by ATG9[6-8]. An integration of these models is necessary. Geometric estimates of the surface-to-volume ratio in yeast autophagosomes, gleaned from cryo-electron microscopy tomograms, suggest that as much as 20% of the membrane might derive from fusion rather than lipid transport in order to deliver luminal volume[51], which cannot be supplied by lipid transport. We therefore propose a model in which an early fusion step between ATG9A vesicles and ARFGAP1/RAB1 membranes, both of which accumulate in ATG2 DKO cells, primes the nucleating membrane for autophagosome biogenesis.

Materials and Methods

Plasmids and reagents

The following plasmids were used in this study: pLVX Puro GFP-ATG2A (Addgene 250863; Previously published[3]), pLVX Puro APEX2-GFP-ATG2A (Addgene 250864; This study; a PCR fragment containing flanking EcoRI cutsites around APEX2 was generated from pcDNA3 APEX2-NES (Addgene #49386) and was inserted into GFP-ATG2A by ligation), pCMV 3xFLAG-ATG2A (Addgene 250865; Previously published[3]), pLVX Neo TagBFP-LC3B (Addgene 250866; This study; pLVX puro TagBFP-LC3B[3] and pLVX-EGFP-IRES-Neo (Addgene #128660) were cut with EcoRI and BamHI, following which the TagBFP-LC3B fragment was ligated into the pLVX Neo backbone), pDESt47 Sar1-GFP (Addgene #67409), SAR1B-mOrange2 (Addgene #166899), SAR1BH79G2-mOrange2 (Addgene #166900), SAR1BH79G-3xFLAG (Addgene 250867; This Study; A BamHI-3xFLAG-NotI fragment was generated by oligo annealing, following which it was ligated into the SAR1BH79G-mOrange2 backbone that was cut by the same restriction enzymes), SAR1B-BFP (Addgene 250872; This Study; A BamHI-BFP-NotI fragment was generated by PCR, following which it was ligated into the SAR1B-mOrange2 backbone that was cut by the same restriction enzymes), SAR1BH79G-BFP (Addgene 250873; This Study; A BamHI-BFP-NotI fragment was generated by PCR, following which it was ligated into the SAR1BH79G-mOrange2 backbone that was cut by the same restriction enzymes), mRuby-SEC23A (Addgene 36158), EGFP-SEC23A (Addgene #66609), pEGFP-SEC24A (Addgene 250868; This Study; a XhoI-SEC24A-PacI fragment was generated by PCR from HA-SEC24A which was a generous gift from the Kundu lab. The fragment was ligated into the backbone of pEGFP-SEC24D, which was cut by the same restriction enzymes), pEGFP-SEC24B (Addgene 250869; This Study; a XhoI-SEC24B-PacI fragment was generated by PCR from HA-SEC24B which was a generous gift from the

Kundu lab. The fragment was ligated into the backbone of pEGFP-SEC24D, which was cut by the same restriction enzymes), EGFP-SEC24C (Addgene 250870; This Study; a AgeI-EGFP-XhoI fragment was generated by PCR and was ligated into the backbone of pEYFP-SEC24C (Addgene #66608) which was cut by the same restriction enzymes), pEGFP-SEC24D (Addgene #32678), GFP-SEC31A (Addgene #42124), GFP-SEC16A (Addgene #36155), ARFGAP1-TagRFP (This Study; ARFGAP1-TagRFP was a gift from the Rothman lab. A frame shift and a point mutation were corrected by site directed mutagenesis), ARFGAP1-GFP (Gift from the Antonny Lab), pMRX IB HaloTag7-mGFP (Addgene # 184903), pMRX No HaloTag7-mGFP-LC3B (Addgene # 184901), pLVX GFP (Addgene 250871; This Study; a fragment containing EGFP was generated from pLVX GFP-ATG2A and was ligated into pLVX puro (Clonetech, 632159) that was cut with EcoRI using Gibson Assembly), GFP-RAB1A (Gift from the Rothman Lab), SNAP-RAB1A (Gift from the Rothman Lab), pGEX2T GST-GFP-RAB1A (Addgene 250877; this study; a GFP-RAB1A fragment was generated from the GFP-RAB1A plasmid from the Rothman lab and inserted in to the pGEX2T backbone), and pGEX2T GST-GFP-GL1 (Addgene 2508740).

Antibodies for immunoblotting were used at 1:1000 and include the following: anti-ATG2A (Cell Signaling Technology, 15011S), anti-p62 (BD BioSciences, 610832), anti-GAPDH (Abcam, ab9484), anti-LC3B (Cell Signaling Technology, 3868S), anti-RB1CC1 (Thermo Fisher Scientific, 172501AP), anti-RAB1A (Cell Signaling Technology, D3X9S), anti-RAB1B (Proteintech, 17824-1-AP), anti-ARFGAP1 (Proteintech, 13571-1-AP), anti-FLAG (Sigma-Aldrich, F1804-200UG), anti-GFP (Cell Signaling Technology, 2956S), anti-mCherry (Invitrogen, PA5-34974), ECL anti-rabbit IgG horseradish peroxidase-linked (GE Healthcare, NA934V), and ECL anti-mouse IgG horseradish peroxidase-linked (GE Healthcare, NA931V).

Antibodies for immunofluorescence were used at 1:500 and include the following: anti-Biotin (Rockland, 200-301098S), anti-GFP nanobody (Massive Photonics), anti-ARFGAP1 (Proteintech, 13571-1-AP;), anti-SEC31A (BD Biosciences, 611280), anti-SEC24C (Cell Signaling Technology, 14676S), anti-MIA3 (Tango1; Sigma, HPA055922), anti-TFG (Abcam, ab156866), anti-COPI (CMIA10; made by Rothman Lab), anti-LC3B (MBL, PM036), anti-p62 (BD BioSciences, 610832), anti-SEC16A (Abcam, ab70722), anti-SEC24D (Cell Signaling Technology, 14687S), anti-GM130 (BD Biosciences, 610823), anti-ERGIC53 (Abcam, EPR6979), Alexa Fluor 405 goat anti-rabbit IgG (Thermo Fisher Scientific, A31556), Alexa Fluor 405 goat anti-mouse IgG (Thermo Fisher Scientific, A31553), Alexa Fluor 594 goat anti-rabbit IgG (Thermo Fisher Scientific, A11037), Alexa Fluor 647 goat anti-rabbit IgG (Thermo Fisher Scientific, A21245), and Alexa Fluor 647 goat anti-mouse IgG (Thermo Fisher Scientific, A21236).

The following reagents were purchased for FLASH-PAINT: Cy3B-modified DNA oligonucleotides were custom-ordered from IDT. Sodium chloride 5 M (cat: AM9759) were obtained from Ambion. Ultrapure water (cat: 10977-015) was purchased from Invitrogen. µ-Slide 8-well chambers (cat: 80807) were purchased from ibidi. Methanol (cat: 9070-05) was purchased from J.T. Baker. Glycerol (cat: G5516-500ml), protocatechuate 3,4-dioxygenase pseudomonas (PCD) (cat: P8279), 3,4-dihydroxybenzoic acid (PCA) (cat: 37580-25G-F) and (+−)-6-hydroxy-2,5,7,8- tetra-methylchromane-2-carboxylic acid (Trolox) (cat: 238813-5 G) were ordered from Sigma. 1× Phosphate Buffered Saline (PBS) pH 7.2 (cat: 10010-023) was purchased from Gibco. Paraformaldehyde (cat: 15710) were obtained from Electron Microscopy Sciences. Bovine serum albumin (cat: 001-000-162) was ordered from Jackson ImmunoResearch. Triton X-100 (cat: T8787-50ML) was purchased from Sigma-Aldrich. DNA labeled Nanobodies were obtained from Massive Photonics.

SiControl, FIP200, RAB1A, RAB1B, and ARFGAP1 were acquired from Horizon Discovery (D-001810-10-05, L-0082383-00-0005, L-008958-01-0005, L-013321-02-005; Horizon Discovery).

Cell culture

HEK293 cells (ATCC, CRL_1573), H4 (CVCL_1239), and HeLa (CVCL_0030) cells were cultured at 37°C and 5% CO2 in DMEM (Thermo Fisher Scientific, 11965092) supplemented with 10% FBS (Thermo Fisher Scientific, 10438062) and 1% penicillinstreptomycin (Thermo Fisher Scientific, 15140122). Cells were starved by incubation in Earle's Balanced Salt Solution (Thermo Fisher Scientific, 24010043) for biochemical assays or in Hank's Balanced Salt Solution (Thermo Fisher Scientific, 14025092) for live cell imaging assays and treated with 0.1 µM bafilomycin A1 (Enzo, BML-CM110-0100) for 2 h.

Lentivirus production and transduction

HEK293 cells were seeded into a 10-cm plate. At 70% confluence, cells were transfected with 4.3 µg psPAX2 (Addgene #12260), 0.43 µg pCMV-VSV-G (Addgene, #8454), and 4.3 µg target plasmid using 20 µl Lipofectamine 3000 (Thermo Fisher Scientific, L3000008). DNA was added to 500 µl Opti-MEM (Thermo Fisher Scientific, 31985070) and Lipofectamine 3000 to 500 µl Opti-MEM in separate 1.5 ml microcentrifuge tubes. The tubes were then mixed and left for 10 min before adding the mixture dropwise to cells in fresh DMEM. After overnight incubation at 37°C, the medium was replaced with fresh DMEM. Cell medium was then collected after 24-48 h and filtered with a 0.45-µm syringe filter (Pall, 4184). Generated virus was either used immediately or was aliquoted and stored at −80°C. HEK293 cells to be transduced were seeded into a 6-well plate. Undiluted virus was added to cells and incubated at 37°C for 24 h. The medium was replaced with fresh DMEM and left for another 24 h. The cells were then treated with 2 µg/ml puromycin (Clontech, 631306), 2 mg/ml Geneticin (Thermo Fisher Scientific, 10131035), or 10 µg/ml Blasticidin (Gibco, A11139-03) for at least 2 wk. For the case of pMRX No HaloTag7-mGFP-LC3B, which lacked a selection marker, the cells were transduced and subsequently sorted by flow assisted cell sorting to normalize GFP expression levels.

Proximity labeling

Proximity labeling was performed as previously described[27]. ATG2 DKO cells stably expressing APEX2-EGFP-ATG2A were cultured for two weeks in media containing heavy, medium, or light isotopes of arginine and lysine (Cambridge Isotope Laboratories, CLM-2265-H-PK, DLM-2640-PK, CNLM-291-H-PK; Sigma-Aldrich, 608033). All conditions were expanded to 3x15cm plates prior to proximity labeling. Heavy labeled cells were starved in EBSS and treated with 100 nM Bafilomycin A1 (Enzo, BML-CM110-0100) for 2 hrs prior to labeling. All conditions were incubated with 500 µM Biotin Phenol (Biotinyl Tyramide; Sigma-Aldrich, SML2135) for 30 min at 37°C. The heavy and medium isotope conditions were treated with 1 mM H2O2 (Sigma-Aldrich, H1009-100ML) for 1 min at room temperature. All conditions were then aspirated and scraped in quencher solution containing 10 mM sodium azide (Sigma-Aldrich, S2002-100G), 10 mM sodium ascorbate (Sigma-Aldrich, A4034-100G) and 5 mM Trolox (Sigma-Aldrich, 238813-5G) in DPBS. The cells were then spun down at 77xg for 5 min at 4°C and were resuspended in quencher solution. This process was repeated for a total of three washes. The cells were then lysed in RIPA buffer (50 mM Tris, 150 mM NaCl, 0.1% SDS, 0.5% sodium deoxycholate (Sigma-Aldrich, D6750-10G), 1% NP40 (Roche, 11754599001) and 1x protease inhibitor (Roche, 11836170001)) for 30 min prior to centrifugation for 10 min at 18,407xg at 4°C. The supernatants were collected and protein concentration was assessed via bradford assay. Heavy, medium and light cells were mixed at a 1:1:1 ratio for a combined mass of 3-4 mg of protein. The protein mixtures were subsequently incubated with streptavidin magnetic beads (Pierce, 88817) for 2 hrs at 4°C after which they were washed twice with RIPA lysis buffer, once with 1 M KCl, once with 0.1 M Na_2CO_3, once with 2 M urea in 10 mM Tris (pH 8.0) and twice with RIPA lysis buffer for each sample. All washes were performed at 4°C. The proteins were eluted off of the beads by boiling the samples in 2x LDS sample buffer (Invitrogen, NP0007). The eluted fraction was run on a gel (Invitrogen, NP0341) for a 10 minutes. The resulting gel plug was stained (Invitrogen, 46-5034) and excised and sent to the Yale Keck facility for mass spectrometry analysis.

Mass spectrometry

MS was performed at Yale Mass Spectrometry & Proteomics Resource of the W.M. Keck Foundation Biotechnology Resource Laboratory. Samples were analyzed in biological triplicates. The data were normalized to internal controls and total spectral counts. For differential analysis between the two groups 10E-04 to was added to all values, the data was log2-transformed, and an unpaired Student t-test was performed. Differentially abundant proteins were considered those with an absolute fold change > 1.5 and $p < 0.05$.

FLASH-PAINT Imaging

Cells were fixed with 4% PFA (Electron Microscopy Services, 15710-S) for 30 min. After three washes in 1xPBS for five minutes each, cells were blocked and permeabilized with 3% BSA and 0.25% Triton X-100 at room temperature for 1 h. Next, cells were incubated with the anti-ARFGAP1 antibody, anti- SEC31A antibody, and the GFP-Nanobody in 3% BSA and 0.1% Triton X-100 at 4 °C overnight. Additionally, all other primary antibodies were pre incubated with the corresponding nanobodies (Tables S1) at 4 °C overnight. The next day, after four washes (30 s, 60 s, 2× 5 min) cells were incubated with the nanobodies corresponding to ARFGAP1 antibody and SEC31A antibody for ~2 h at room temperature. Next, unlabeled excess secondary nanobodies (to block unlabeled epitopes) were added to pre-incubation antibody-nanobody mixes at room temperature for 5 min. Next, the cells were incubated with the pooled antibody-nanobody mix for ~2.5 h at room temperature. After four washes (30 s, 60 s, 2× 5 min), the sample was post-fixed with 3% PFA and 0.1% GA for 10 min. Finally, samples were washed three times with 1× PBS for 5 min each before adding the imaging solution.

The imaging solution consisted of 1x PBS and 500 mM NaCl and was supplemented with 1× Trolox, (100× Trolox: 100 mg Trolox, 430 µL 100 % Methanol, 345 µL 1M NaOH in 3.2 mL H_2O), 1× PCA (40× PCA: 154 mg PCA, 10 mL water and NaOH were mixed and pH was adjusted 9.0), and 1× PCD (100× PCD: 9.3 mg PCD, 13.3 mL of buffer (100 mM Tris-HCl pH 8, 50 mM KCl, 1 mM EDTA, 50 % Glycerol)). All three stock buffers were frozen and stored at -20 °C.

Fluorescence imaging was carried out on an inverted Nikon Eclipse Ti2 microscope (Nikon Instruments) with the Perfect Focus System, attached to a Andor Dragonfly unit. The Dragonfly was used in the BTIRF mode, applying an objective-type TIRF configuration with an oil-immersion objective (Nikon Instruments, Apo SR TIRF 60×, NA 1.49, Oil). As excitation laser, a 561 nm (1W nominal) was used. The beam was coupled into a multimode fiber going through the Andor Borealis unit reshaping the beam from a gaussian profile to a homogenous flat top. As dichroic mirror a CR-DFLY-DMQD-01 was used. Fluorescence light was spectrally filtered with an emission filter (TR-DFLY-F600-050) and imaged on a scientific complementary metal oxide semiconductor (sCMOS) camera (Sona 4BV6X, Andor Technologies) without further magnification, resulting in an effective pixel size of 108 nm. The power at the objective lens was ~10 % of the power set at the laser.

Imaging was carried out using the corresponding Imager and Adapter (Table S2, S3, S5) in imaging buffer. 25,000 frames were acquired at 25 ms exposure time. The readout bandwidth was set to 540 MHz. Laser power (@561 nm) was set to 80 mW (measured before the back focal plane (BFP) of the objective), corresponding to ~1.8 kW/cm^2 at the sample plane. After imaging the sample was subsequently washed three times with 200 µL each with 1× PBS (on the microscope) followed by an incubation with the corresponding eraser (Table S4; at 20 nM) for ~ 5 min. This process was repeated iteratively for ten sequential rounds (Table S5).

DNA-PAINT data was reconstructed, postprocessed (drift correction and alignment of imaging rounds) and rendered with the Picasso package[52].

Focused ion beam scanning electron microscopy and correlative light electron microscopy

For focused ion beam scanning electron microscopy (FIBSEM) CLEM, ATG2 DKO HEK293 cells overexpressing GFP-ATG2A were plated on 35-mm MatTek dish (MatTek, P35G-1.5-14-CGRD). The cells were starved for two hours prior to pre-fixation in 4% PFA + 0.25% glutaraldehyde and three washes in 1x PBS. Regions of interest by fluorescence light microscopy were selected and their coordinates on the dish were identified using phase contrast. Cells were further fixed with 2.5% glutaraldehyde in 0.1 M sodium cacodylate buffer, postfixed in 2% OsO4 and 1.5% K4Fe(CN)6 (Sigma-Aldrich) in 0.1 M sodium cacodylate buffer, en bloc stained with 2% aqueous uranyl acetate, dehydrated, embedded in Embed 812, and polymerized at 60°C for 48 hrs. Cells of interest were relocated based on the pre-recorded coordinates. Epon block was glued onto the SEM sample mounting aluminum stub and platinum en bloc coating on the sample surface was carried out with the sputter coater (Ted Pella, Inc.). The cell of interest was relocated under SEM imaging based on pre-recorded coordinates and FIB-SEM imaged in a Crossbeam 550 FIB-SEM workstation operating under SmartSEM (Carl Zeiss Microscopy GmbH) and Atlas 5 engine (Fibics, Inc.). The imaging resolution was set at 7 nm/pixel in the X, Y axis with milling being performed at 7 nm/step along the Z axis to achieve an isotropic resolution of 7 nm/voxel. Images were aligned and exported with Atlas 5 (Fibics, Inc.), further processed and segmented with DragonFly Pro software (Object Research Systems [ORS], Inc.).

Expi293 culture and transfection

3xFLAG-ATG2A was expressed and purified from Expi293 suspension cells. Cells were cultured at 37°C, 8% CO2 in vented PETG flasks (Thermo Scientific, Nalgene; 4115-0500) with 125 rpm rotation. Prior to transfection, cells were grown to 3-5 x 106 cells/mL then diluted to 2.5x106 cells/mL and allowed to grow for 18- 24 hours. Upon reaching 4.5-5.5 x 106 cells/mL, the culture was diluted to 3 x 106 cells/mL with fresh media. Cells were transfected with 100 µg plasmid per 100 mL of cultured cells. For every 100 mL of cells, 100 µg DNA was diluted in 5 mL OptiMEM. 300 µL of 1 mg/mL polyethylenimine linear 25k (Polyscience, 23966) was diluted into 5 mL OptiMEM in a separate tube. Both tubes were incubated for 5 minutes at room temperature then combined and further incubated for 30 minutes. The DNA/PEI mixture was then added dropwise into Expi293 cultures. 12-18 hours after transfection, protein expression was enhanced using 700 µL of 500 mM valproic acid. Cells were then harvested after 48-72 hours.

3xFLAG-ATG2A purification

Cell pellets were resuspended in 10 mL purification buffer A (500 mM NaCl, 20 mM HEPES, pH: 8.0, 10% glycerol, 1 mM TCEP) for every 100 mL of original culture volume. Purification buffer A was supplemented with 1x EDTA-free protease inhibitor cocktail (Roche; 11873580001). Cells were then lysed by subjecting pellet resuspensions to 6 freeze/thaw cycles in liquid nitrogen The lysates were then clarified by centrifugation at 18,500 x G, and supernatants were transferred to 150 µL of anti-Flag M2 agarose resin per 100 mL of initial culture volume (prewashed with 10 mL purification buffer A). Lysates were incubated with beads under mild agitation for 2 hours at 4 °C. Lysates and beads were then passed through a gravity filtration column and washed with 4 CVs of purification buffer. Beads were then incubated with 2.5 mM ATP and 5 mM Mg2+ in purification buffer overnight at 4 °C. Columns were then washed with 2 CVs of purification buffer, followed by elution with 50 µL of 1 mg/mL 3x-Flag (DYKDDDDK) peptide (ApexBio Technology; A6001) per 100 mL of initial culture volume. Protein concentration was determined against a BSA standard curve by Coomassie staining prior to subsequent assays. Proteins were flash frozen in liquid nitrogen for storage at -80 °C.

Recombinant protein expression and purification from *E. Coli*

For all in vitro experiments, GFP-GL1 refers to protein expressed and purified from constructs ending at the reactive glycine (G116) of GL1, as this construct was previously used for lipidation experiments in the absence of ATG4 proteins. In summary, human GFP-GL1 and GFP-RAB1A were cloned in the pGEX-2T GST vector. The proteins were expressed in BL21-Gold (DE3)

competent cells (Agilent Technologies; 230132). The cells were cultured in 4 liters of Luria Bertani broth (LB) medium with 50 mg/ml carbenicillin (C1389; Sigma-Aldrich) and induced with 0.5 mM isopropyl β-D-thiogalactopyranoside (IPTG). Bacterial pellets were treated with EDTA-free protease inhibitor tablets in thrombin buffer (20 mM Tris pH 7.5, 100 mM NaCl, 5 mM $MgCl_2$, 2 mM $CaCl_2$, 1 mM DTT). The cells were broken in a cell disrupter, and the lysate was incubated with pre-washed glutathione agarose beads (G4501; Sigma-Aldrich) for 3 h at 4°C. The beads were washed three times and then incubated with thrombin (10 µl of thrombin [T6884; Sigma-Aldrich], 500 µl of thrombin buffer, 0.5 µl of DTT, 500 µl of beads) to cut the proteins from GST tags overnight at 4°C. Purified proteins were stored in 20% glycerol at −80°C.

Lysis, gel electrophoresis, and immunoblotting

Cells were collected by scraping in PBS. The cells were centrifuged at 500 g for 3 min at 4°C, and lysed in lysis buffer (10 mM Tris pH 7.5, 150 mM NaCl, 0.5 mM EDTA, 0.5% NP-40) with EDTA-free protease inhibitor cocktail (Sigma-Aldrich, 11873580001) on ice for five minutes. Lysates were collected after centrifugation at 16,000 g for 10 min at 4°C. Total protein concentration was determined by a bradford assay (BioRad, 5000006). 50-100 µM DTT (American Bio, AB00490-00010) and 1xLDS (Invitrogen, NP0007) loading buffer were added to each sample, which were then electrophoresed on precast Bis-Tris gels (Thermo Fisher Scientific, NP0341BOX or NP0322BOX). Gels were subsequently transferred to Immobilon-FL PVDF membranes (Sigma-Aldrich, IPFL00010) at 30-35 V for 90 min.

The membranes were blocked with 5% BSA (Sigma-Aldrich, A9647) in PBS-T (PBS containing 0.1% Tween 20; Thermo Scientific, CAS 9005-64-5) for 1 h at room temperature and incubated with primary antibody (diluted 1:1,000 in PBS-T containing 5% BSA [Sigma-Aldrich, A9647] and 0.03% sodium azide (Sigma-Aldrich, S2002)) overnight at 4°C. Membranes were washed three times in PBS-T before incubation with the secondary antibody which was diluted 1:5,000 in PBS-T containing 0.5% Omniblock (American Bio, AB10109-00100) for 1 h. Membranes were then washed three times in PBST and treated with SuperSignal West Femto substrate (Thermo Fisher Scientific, 34096) for 5 min before imaging with the Bio-Rad VersaDoc imaging system.

Immunoprecipitation

For immunoprecipitation experiments, 15 cm plates were seeded and transfected upon reaching 80-90% confluency. The next day, the cells were collected by scraping, washed 1x in PBS, and lysed as previously described. Following quantification of protein levels by a Bradford assay, equal amounts of protein were added to pre-washed GFP-Trap beads (Proteintech, gtma-20). The volume was increased to 500 uL and the bead/lysate slurry was incubated at 4°C for two hours while rotating. The beads were pelleted using a magnetic rack and washed five times in lysis buffer (10 mM Tris pH 7.5, 150 mM NaCl, 0.5 mM EDTA, 0.5% NP-40) with EDTA-free protease inhibitor. The target proteins were eluted by boiling the beads for 10 min in 2x LDS loading buffer.

Densitometry and quantification

Densitometry quantifications of immunoblots and in-gel fluorescence images were performed using ImageJ software. For LC3B and p62 clearance analysis (Fig. S1 A-C), the band intensity of LC3B or p62 for each condition was normalized against the GAPDH intensity of that lane. To normalize each replicate, each value was divided by the mean value of the entire replicate. This normalization technique was also employed in the co-immunoprecipitation experiments. Statistical significance was determined by two-way ANOVA followed by a Tukey multiple comparison test to compare cell types. To quantify the co-immunoprecipitation reactions, the intensity of the 3xFLAG-ATG2A IP band was ratioed against the intensity of its corresponding input band. Following normalization, statistical significance was determined by a one (Fig. S3 A-D) or two-way (Fig. 2E-F) ANOVA followed by a Dunnett multiple comparison test to comparing

each sample to the control lane. For the HaloTag flux assay (Fig. 2A, 2B, 3A, 3B), the Halotag flux rate was calculated as the ratio of the free Halotag band divided by the unprocessed Halotag band. Statistical significance was determined by a one (Fig. 2 A and B) or two-way (Fig 3 A and B) ANOVA followed by a Dunnett multiple comparison test to comparing each sample to the control lane. For one way ANOVA tests, data distributions were assumed to be normal. For two way ANOVA tests, the Geisser-Greenhouse correction was used as equal variability was not assumed. All data are $n = 3$ or greater and represent biological replicates. All data were plotted with mean ± SD, and all significance values were considering adjusted P value based on grouped analyses in Prism 10 (GraphPad). Asterisks indicate significance: *, $P < 0.05$; **, $P < 0.01$; ***, $P < 0.001$; ****, $P < 0.0001$. All blots were adjusted in contrast for better visualization of the bands in the figures.

LC3B flux analysis

WT, ATG2 DKO and ATG2 DKO + APEX2-GFP-ATG2A HEK293 cells were cultured in 6-well plates to 70-90% confluence. At the beginning of the assay, the media was replaced with fresh DMEM, DMEM containing 100 nM bafilomycin A1, or EBSS containing 100 nM bafilomycin A1. After a 2 hour incubation, cells were harvested by scraping, washed with 1x PBS, and lysed. 20 µg of protein from each sample were analyzed by SDS-PAGE and immunoblotting for ATG2A, p62, GAPDH, and LC3B.

HaloTag flux assay

HEK293 WT stably expressing either HaloTag7-mGFP or HaloTag7-mGFP-LC3B were cultured in 6-well plates to 60-70% confluence prior to transfection with either SAR1B/SAR1BH79G-mOrange2 for one day (Fig. 3A) or siRNA for two days (Fig. 2A). SAR1B transfection was performed using Lipofectamine 3000 (Thermofisher Scientific, L3000015) according to the manufacturer's protocol. SiRNA transfection was performed using Dharmafect (Horizon Discovery, T-2001-01) according to the manufacturer's protocol. The cells were incubated with 100 nm TMR-conjugated HaloTag ligand (Promega, G8251) for 30 min. Following two washes with 1xPBS, the cells were starved in EBSS for four hours. The cells were then collected and lysed. Following SDS-PAGE separation, in gel fluorescence was immediately measured with a ChemiDoc MP Imaging System (BioRad). Images were taken at 30 s and 100 s exposures. The gel was then transferred and immunoblotted against mCherry and GAPDH (Fig 3A) or FIP200, RAB1A, RAB1B, ARFGAP1, GAPDH, and LC3B (Fig 2A).

GFP-mCherry-LC3B Flux analysis by FACS

H4 cells and H4 cells with a GFP-mCherry-LC3B heterozygous knock-in tag were seeded in a six well plate. Following a three day siRNA knock down, the cells were subject to a four hour starvation period in HBSS. They were subsequently trypsinized, pelleted, resuspended in HBSS, and passed through a filter prior to FACS data acquisition. The cell population was gated to ensure a single, live cell population. The ratio between the GFP and mCherry intensity was plotted as a histogram using FlowJo 10 and the ratio between the average values of each replicate was plotted using Prism 10. Three biological replicates were combined and statistically assessed using a one-way ANOVA followed by a Dunnett multiple comparison test. All data were plotted with mean ± SD, and all significance values were considering adjusted P value based on grouped analyses in Prism 10 (GraphPad). Asterisks indicate significance: *, $P < 0.05$; **, $P < 0.01$; ***, $P < 0.001$; ****, $P < 0.0001$.

Immunofluorescence

Cells seeded on coverslips were fixed in 4% PFA (Electron Microscopy Sciences, 15710), washed three times with PBS, and permeabilized in PBS containing 0.1% Saponin (Sigma-Aldrich, 47036) and 3% BSA. Incubation with primary antibodies was done at 4C for 18-24 hrs

and secondary antibodies at room temperature for 1 hr at indicated concentrations (see Reagents). After each antibody incubation, cells were washed three times in PBS containing 0.1% Saponin and 3% BSA. The coverslips were mounted on precleaned microscope slides with Fluoromont-G mounting reagent (Southern Biotech, 0100-01). Images were acquired on an inverted Zeiss LSM 880 laser scanning confocal microscope with AiryScan, using Zen acquisition software (Fig S1D) or a Nikon CSU-W1 SoRa 60x oil objective, using the Nikon Elements software (Fig. 1C, 3C-F, S3A, S3C, 4A, 4C, 4E, 4F). All images were processed using ImageJ software. Images are displayed either as maximum intensity projections or single confocal slices as stated in the figure legends.

To assess the enrichment factor of early secretory proteins around the ATG2 DKO compartment (Fig. 4D), the phagophore channel which was denoted by either LC3B or p62 was masked and duplicated. Following outlier removal, one masked image was dilated and the other eroded. Following an XOR function, the resulting signal formed a ring around the ATG2 DKO compartment and the early secretory protein channel(s) were measured using this ROI. Separately, the early secretory protein channel was masked using a manual threshold and measured. The enrichment factor was calculated as $(Mean_{compartment}-Min_{cell})/(Mean_{cell}-Min_{cell})$. Three biological replicates were combined and statistically assessed using a one-way ANOVA followed by a Dunnett multiple comparison test. All data were plotted with mean ± SD, and all significance values were considering adjusted P value based on grouped analyses in Prism 10 (GraphPad). Asterisks indicate significance: *, $P < 0.05$; **, $P < 0.01$; ***, $P < 0.001$; ****, $P < 0.0001$.

Live cell imaging

Cells were plated on poly-d-lysine coated MatTek dishes (MatTek, P35GC-1.5-14-C). The following day the cells were transfected using Lipofectamine 3000 (Thermo Fisher Scientific, L3000015) according to the manufacturer's protocol for 18-24 hrs. The cells were starved in HBSS (Thermo Fisher Scientific, 14025092) for 2-4 h and imaged in the same solution at 37°C. All images were analyzed using ImageJ and are displayed as maximum intensity projections.

For phagophore quantification (Fig. 1 C and D), each channel was masked using a manual threshold and outliers were removed. The ATG2A and LC3B channels were merged using the AND function and quantified as the total number of phagophores. The phagophore channel was then merged using the AND function with the transfected gene and quantified as the number of positive phagophores. Three biological replicates were combined and the ratio of positive over total was plotted and statistically assessed using a one-way ANOVA followed by a Dunnett multiple comparison test. All data were plotted with mean ± SD, and all significance values were considering adjusted P value based on grouped analyses in Prism 10 (GraphPad). Asterisks indicate significance: *, $P < 0.05$; **, $P < 0.01$; ***, $P < 0.001$; ****, $P < 0.0001$.

Data Availability

The data, code, protocols, and key lab materials used and generated in this study are listed in a Key Resource Table alongside their persistent identifiers at Table S7.

Acknowledgments

This work was supported by grants from the National Institutes of Health (R01 GM100930 and R35 GM153482 to TJM; R01 GM151829 to JB; DA018343 to PDC), F31 AG079606 to DMF and F31 DK136246 to JLK. This research was also funded in part through Aligning Science Across Parkinson's (ASAP-025173 to TJM and PDC) through the Michael J. Fox Foundation for Parkinson's Research (MJFF) and the Howard Hughes Medical Institute (HHMI; PDC). FS acknowledges support from the Human Frontier Science Program (LT000056/2020-C). JB acknowledges support by the Wellcome Leap Foundation. We would like to thank Bruna Mafra de

Faria, Michael Hanna, and Jeff Coleman for their support and reagent sharing. We would further like to thank Juan Bonifacino for the gift of the HeLa ATG2 DKO cells as well as the H4 GFP-mCherry-LC3B KI cells. Imaging was supported by the Yale Center for Cellular and Molecular Imaging (both the fluorescence and electron microscopy facilities). We also thank the MS & Proteomics Resource at Yale University for providing the necessary mass spectrometers and the accompany biotechnology tools funded in part by the Yale School of Medicine and by the Office of The Director, National Institutes of Health (S10OD02365101A1, S10OD019967, and S10OD018034). The funders had no role in study design, data collection and analysis, decision to publish, or preparation of the manuscript.

References

1. Melia, T.J., Lystad, A.H. & Simonsen, A. Autophagosome biogenesis: From membrane growth to closure. *J Cell Biol* **219** (2020).
2. Osawa, T. *et al.* Atg2 mediates direct lipid transfer between membranes for autophagosome formation. *Nat Struct Mol Biol* **26**, 281-288 (2019).
3. Valverde, D.P. *et al.* ATG2 transports lipids to promote autophagosome biogenesis. *J Cell Biol* **218**, 1787-1798 (2019).
4. Maeda, S., Otomo, C. & Otomo, T. The autophagic membrane tether ATG2A transfers lipids between membranes. *Elife* **8** (2019).
5. Osawa, T., Ishii, Y. & Noda, N.N. Human ATG2B possesses a lipid transfer activity which is accelerated by negatively charged lipids and WIPI4. *Genes Cells* **25**, 65-70 (2020).
6. Matoba, K. *et al.* Atg9 is a lipid scramblase that mediates autophagosomal membrane expansion. *Nat Struct Mol Biol* **27**, 1185-1193 (2020).
7. Maeda, S. *et al.* Structure, lipid scrambling activity and role in autophagosome formation of ATG9A. *Nat Struct Mol Biol* **27**, 1194-1201 (2020).
8. Ghanbarpour, A., Valverde, D.P., Melia, T.J. & Reinisch, K.M. A model for a partnership of lipid transfer proteins and scramblases in membrane expansion and organelle biogenesis. *Proceedings of the National Academy of Sciences* **118**, e2101562118 (2021).
9. Olivas, T.J. *et al.* ATG9 vesicles comprise the seed membrane of mammalian autophagosomes. *J Cell Biol* **222** (2023).
10. Sawa-Makarska, J. *et al.* Reconstitution of autophagosome nucleation defines Atg9 vesicles as seeds for membrane formation. *Science* **369** (2020).
11. Ishihara, N. *et al.* Autophagosome Requires Specific Early Sec Proteins for Its Formation and NSF/SNARE for Vacuolar Fusion. *Molecular Biology of the Cell* **12**, 3690-3702 (2001).
12. Hamasaki, M., Noda, T. & Ohsumi, Y. The Early Secretory Pathway Contributes to Autophagy in Yeast. *Cell Structure and Function* **28**, 49-54 (2003).
13. Suzuki, K., Akioka, M., Kondo-Kakuta, C., Yamamoto, H. & Ohsumi, Y. Fine mapping of autophagy-related proteins during autophagosome formation in Saccharomyces cerevisiae. *J Cell Sci* **126**, 2534-2544 (2013).

14. Tan, D. *et al.* The EM structure of the TRAPPIII complex leads to the identification of a requirement for COPII vesicles on the macroautophagy pathway. *Proceedings of the National Academy of Sciences* **110**, 19432-19437 (2013).
15. Graef, M., Friedman, J.R., Graham, C., Babu, M. & Nunnari, J. ER exit sites are physical and functional core autophagosome biogenesis components. *Mol Biol Cell* **24**, 2918-2931 (2013).
16. Shima, T., Kirisako, H. & Nakatogawa, H. COPII vesicles contribute to autophagosomal membranes. *J Cell Biol* **218**, 1503-1510 (2019).
17. Ge, L., Melville, D., Zhang, M. & Schekman, R. The ER–Golgi intermediate compartment is a key membrane source for the LC3 lipidation step of autophagosome biogenesis. *Elife* **2** (2013).
18. Ge, L., Zhang, M. & Schekman, R. Phosphatidylinositol 3-kinase and COPII generate LC3 lipidation vesicles from the ER-Golgi intermediate compartment. *Elife* **3** (2014).
19. Hayashi-Nishino, M. *et al.* A subdomain of the endoplasmic reticulum forms a cradle for autophagosome formation. *Nat Cell Biol* **11**, 1433-1437 (2009).
20. Ge, L. *et al.* Remodeling of ER-exit sites initiates a membrane supply pathway for autophagosome biogenesis. *EMBO Rep* **18**, 1586-1603 (2017).
21. Li, S. *et al.* A new type of ERGIC-ERES membrane contact mediated by TMED9 and SEC12 is required for autophagosome biogenesis. *Cell Res* **32**, 119-138 (2022).
22. Kumar, S. *et al.* Mammalian hybrid pre-autophagosomal structure HyPAS generates autophagosomes. *Cell* **184**, 5950-+ (2021).
23. Bozic, M. *et al.* A conserved ATG2-GABARAP family interaction is critical for phagophore formation. *EMBO Rep* **21**, e48412 (2020).
24. Feng, X. *et al.* Local membrane source gathering by p62 body drives autophagosome formation. *Nat Commun* **14**, 7338 (2023).
25. Velikkakath, A.K., Nishimura, T., Oita, E., Ishihara, N. & Mizushima, N. Mammalian Atg2 proteins are essential for autophagosome formation and important for regulation of size and distribution of lipid droplets. *Mol Biol Cell* **23**, 896-909 (2012).
26. Gudmundsson, S.R. *et al.* Morphology of Phagophore Precursors by Correlative Light-Electron Microscopy. *Cells* **11** (2022).
27. Hung, V. *et al.* Spatially resolved proteomic mapping in living cells with the engineered peroxidase APEX2. *Nat Protoc* **11**, 456-475 (2016).
28. Schueder, F. *et al.* Unraveling cellular complexity with transient adapters in highly multiplexed super-resolution imaging. *Cell* **187**, 1769-1784 e1718 (2024).
29. Weigel, A.V. *et al.* ER-to-Golgi protein delivery through an interwoven, tubular network extending from ER. *Cell* **184**, 2412-2429.e2416 (2021).
30. Wong-Dilworth, L. *et al.* Nanoscale imaging reveals the mechanisms of ER-to-Golgi transport via a dynamic tubular-vesicular network. *bioRxiv*, 2023.2010.2027.563951 (2023).

31. Westrate, L.M., Hoyer, M.J., Nash, M.J. & Voeltz, G.K. Vesicular and uncoated Rab1-dependent cargo carriers facilitate ER to Golgi transport. *J Cell Sci* **133** (2020).
32. Hein, M.Y. *et al.* Global organelle profiling reveals subcellular localization and remodeling at proteome scale. *Cell* (2024).
33. Yim, W.W., Yamamoto, H. & Mizushima, N. A pulse-chasable reporter processing assay for mammalian autophagic flux with HaloTag. *Elife* **11** (2022).
34. Lynch-Day, M.A. *et al.* Trs85 directs a Ypt1 GEF, TRAPPIII, to the phagophore to promote autophagy. *Proc Natl Acad Sci U S A* **107**, 7811-7816 (2010).
35. Wang, J. *et al.* Ypt1 recruits the Atg1 kinase to the preautophagosomal structure. *Proc Natl Acad Sci U S A* **110**, 9800-9805 (2013).
36. Carlos Martín Zoppino, F., Damián Militello, R., Slavin, I., Álvarez, C. & Colombo, M.I. Autophagosome Formation Depends on the Small GTPase Rab1 and Functional ER Exit Sites. *Traffic* **11**, 1246-1261 (2010).
37. Gyurkovska, V. *et al.* Dual function of Rab1A in secretion and autophagy: hypervariable domain dependence. *Life Sci Alliance* **6** (2023).
38. Lamb, C.A. *et al.* TBC1D14 regulates autophagy via the TRAPP complex and ATG9 traffic. *EMBO J* **35**, 281-301 (2016).
39. Jia, R. & Bonifacino, J.S. Negative regulation of autophagy by UBA6-BIRC6-mediated ubiquitination of LC3. *Elife* **8** (2019).
40. Kotani, T., Kirisako, H., Koizumi, M., Ohsumi, Y. & Nakatogawa, H. The Atg2-Atg18 complex tethers pre-autophagosomal membranes to the endoplasmic reticulum for autophagosome formation. *Proceedings of the National Academy of Sciences of the United States of America* **115**, 10363-10368 (2018).
41. Mailler, E. *et al.* The autophagy protein ATG9A enables lipid mobilization from lipid droplets. *Nat Commun* **12**, 6750 (2021).
42. Lippincott-Schwartz, J., Yuan, L.C., Bonifacino, J.S. & Klausner, R.D. Rapid redistribution of Golgi proteins into the ER in cells treated with brefeldin A: evidence for membrane cycling from Golgi to ER. *Cell* **56**, 801-813 (1989).
43. Helms, J.B. & Rothman, J.E. Inhibition by brefeldin A of a Golgi membrane enzyme that catalyses exchange of guanine nucleotide bound to ARF. *Nature* **360**, 352-354 (1992).
44. Machner, M.P. & Isberg, R.R. Targeting of host Rab GTPase function by the intravacuolar pathogen Legionella pneumophila. *Dev Cell* **11**, 47-56 (2006).
45. Murata, T. *et al.* The Legionella pneumophila effector protein DrrA is a Rab1 guanine nucleotide-exchange factor. *Nat Cell Biol* **8**, 971-977 (2006).
46. Machner, M.P. & Isberg, R.R. A bifunctional bacterial protein links GDI displacement to Rab1 activation. *Science* **318**, 974-977 (2007).
47. Yao, W. *et al.* TOR-mediated Ypt1 phosphorylation regulates autophagy initiation complex assembly. *EMBO J* **42**, e112814 (2023).
48. Cook, A.S.I. *et al.* Structural pathway for PI3-kinase regulation by VPS15 in autophagy. *Science*, eadl3787 (2025).

49. Ravikumar, B., Moreau, K., Jahreiss, L., Puri, C. & Rubinsztein, D.C. Plasma membrane contributes to the formation of pre-autophagosomal structures. *Nat Cell Biol* **12**, 747-757 (2010).
50. Knaevelsrud, H., Carlsson, S.R. & Simonsen, A. SNX18 tubulates recycling endosomes for autophagosome biogenesis. *Autophagy* **9**, 1639-1641 (2013).
51. Bieber, A. *et al.* (Cold Spring Harbor Laboratory, 2022).
52. Schnitzbauer, J., Strauss, M.T., Schlichthaerle, T., Schueder, F. & Jungmann, R. Super-resolution microscopy with DNA-PAINT. *Nat Protoc* **12**, 1198-1228 (2017).

Figures and Tables

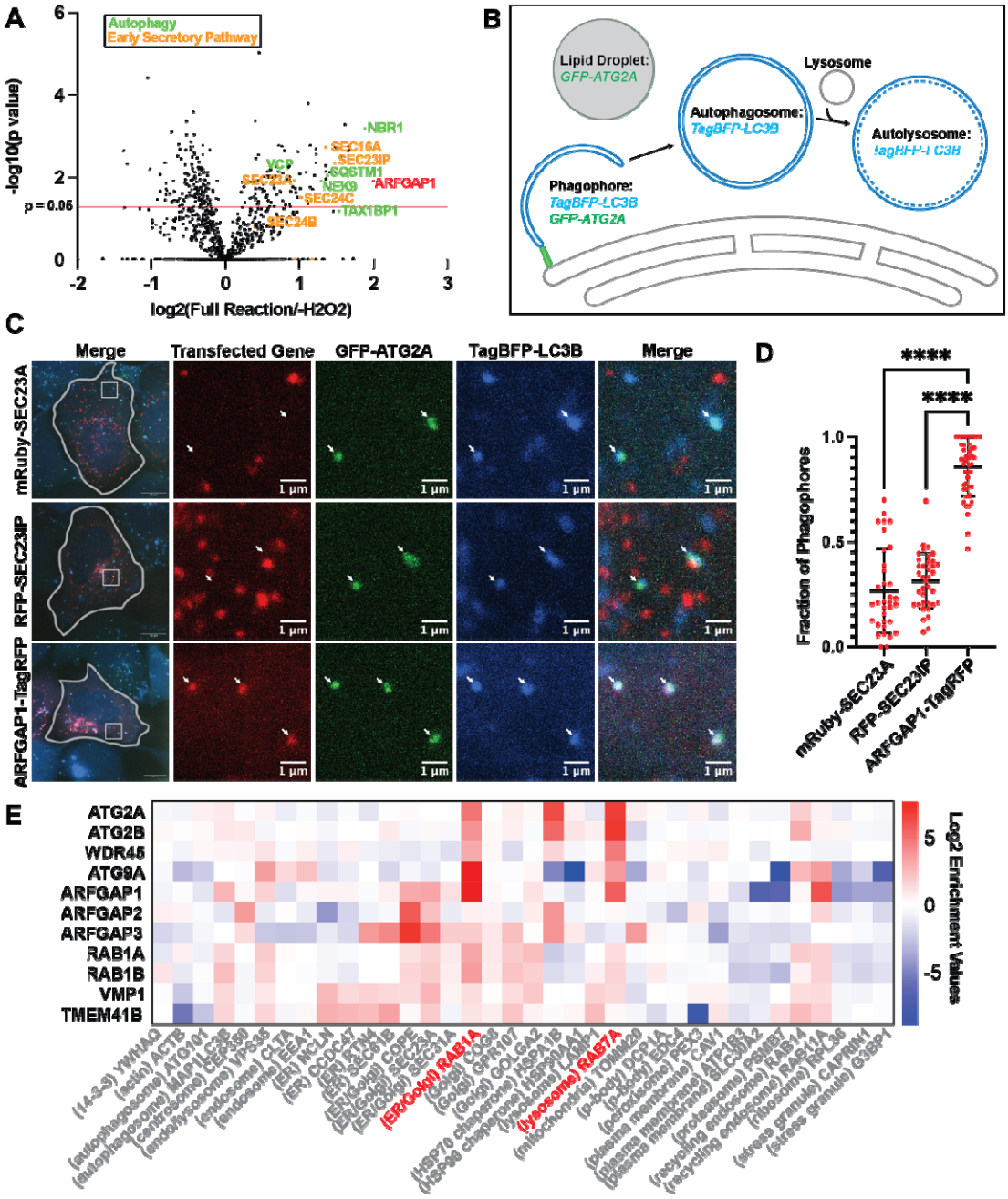

Figure 1. ATG2A is proximal to ARFGAP1 positive membranes. (A) Proximity labeling of HEK293 ATG2 DKO cells stably expressing APEX2-GFP-ATG2A was performed as previously described[27]. Three biological replicates were averaged and plotted as the log2 ratio between the full labeling reaction in complete media over cells that were not treated with hydrogen peroxide on the x axis, and -log10 of the p-value on the y axis. The red line demonstrates the p-value cutoff of 0.05. The proteomics revealed an enrichment of autophagy (labeled in green) and early secretory

proteins (COPII/ER Exit Site proteins are labeled in orange, ARFGAP1 is labeled in red). **(B)** Strategy to identify phagophores by live cell imaging. Phagophores are defined as sites where both GFP-ATG2A and TagBFP-LC3B co-localize. **(C-D)** Live cell imaging of ATG2 DKO cells stably expressing GFP-ATG2A and TagBFP-LC3B and transfected with mRuby-SEC23A or RFP-SEC23IP/p125a or ARFGAP1-TagRFP. The cells were starved for 2-4 hours prior to imaging. The fraction of phagophores (white arrows) that colocalized with the third fluorescent protein (transfected gene) was quantified and plotted in (D). The gray lines show the cell periphery and the insets focus on representative phagophores. Statistical significance was assessed by one way ANOVA. *, adjusted P value <0.05. **, adjusted P value <0.01. ***, adjusted P value <0.001. ****, adjusted P value <0.0001. Data from three biological replicates were pooled for each condition. Maximum intensity projections of confocal images. **(E)** Global organelle profiling data from https://organelles.sf.czbiohub.org[32]. Whole organelle profiles were established by pulling down endogenously tagged proteins and performing quantitative proteomics. The enrichment value for each protein were calculated by taking the difference in median log2 LFQ values between the replicates and the null distribution.

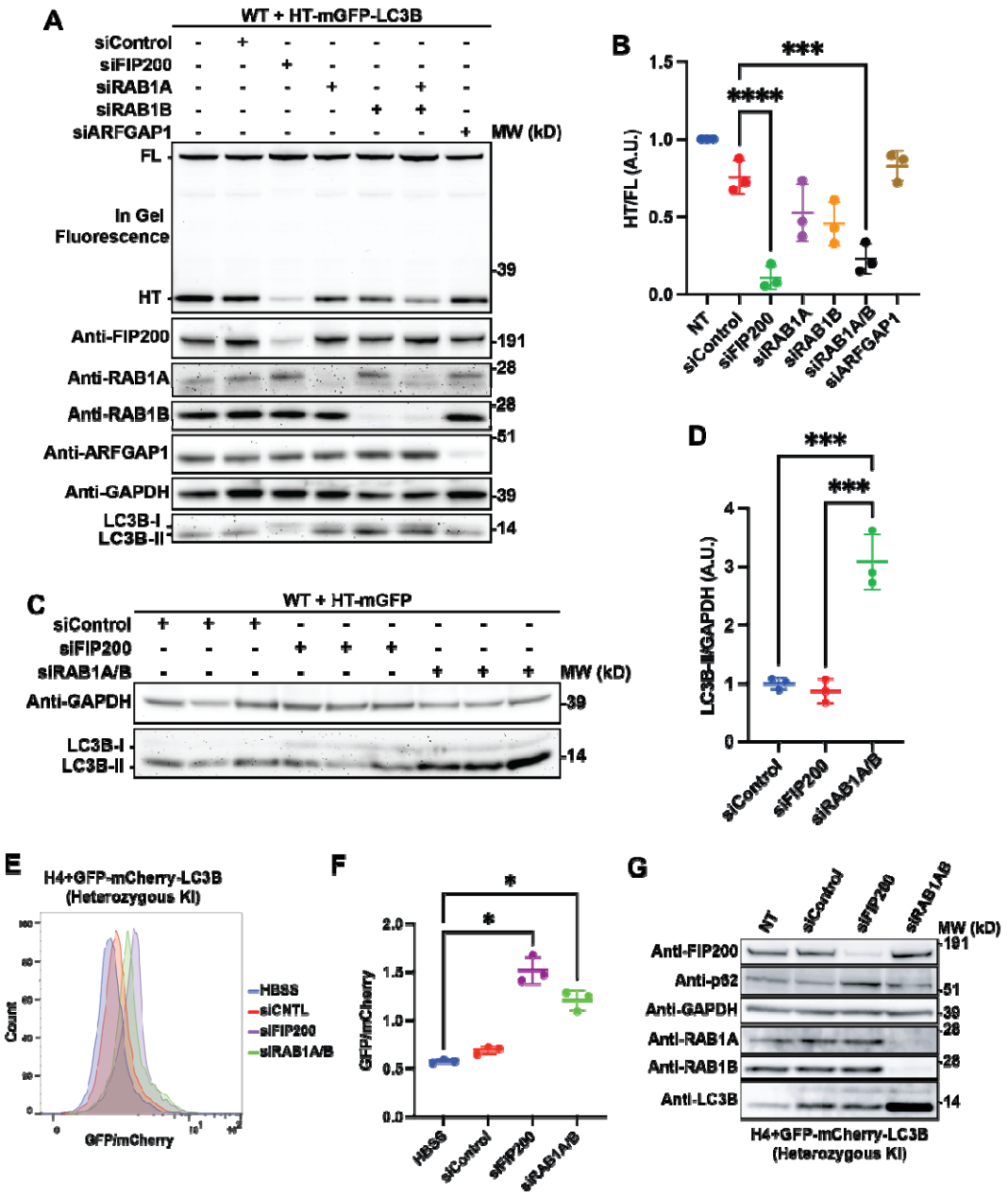

Figure 2. Autophagic flux depends upon RAB1 but not ARFGAP1. (A-B) In gel fluorescence image (top panel) and immunoblots demonstrating that siRNA KD of RAB1 inhibits autophagic flux in cells starved in EBSS for four hours. In gel fluorescence reveals HaloTag7s moiety bound to the TMR ligand. Indicated bands are full length (FL) HT-mGFP-LC3B protein and HaloTag7 after cleavage (HT) in the lysosome. The ratio between FL and HT demonstrates autophagic flux, quantified in (B). Statistical significance was assessed by one way ANOVA. *, adjusted P value <0.05. **, adjusted P value <0.01. ***, adjusted P value <0.001. ****, adjusted P value <0.0001. Data from three biological replicates were collected for each condition**. (C-D)** Immunoblot of lysates from three biological replicates demonstrating that siRNA KD of RAB1 results in an accumulation of LC3B-II in cells starved in EBSS for four hours. The band intensity of LC3B-II was normalized against the intensity of GAPDH for each lane. To normalize each replicate, each

individual value was divided by value of the non-transfected sample. Statistical significance was assessed by one way ANOVA. *, adjusted P value <0.05. **, adjusted P value <0.01. ***, adjusted P value <0.001. ****, adjusted P value <0.0001. **(E-G)** FACS data demonstrating that RAB1A/B KD results in a block in autophagic flux. H4 cells with a heterozygous GFP-mCherry-LC3B endogenous tag were transfected with siRNA for three days, following which they were starved in HBSS for four hours and analyzed by FACS. The ratio between GFP and mCherry is an indicator of autophagic flux, as the GFP signal is quenched in the lysosome. This ratio is displayed in histograms in (E) for one replicate and as averages in (F). The KDs of each protein can be seen in (G).

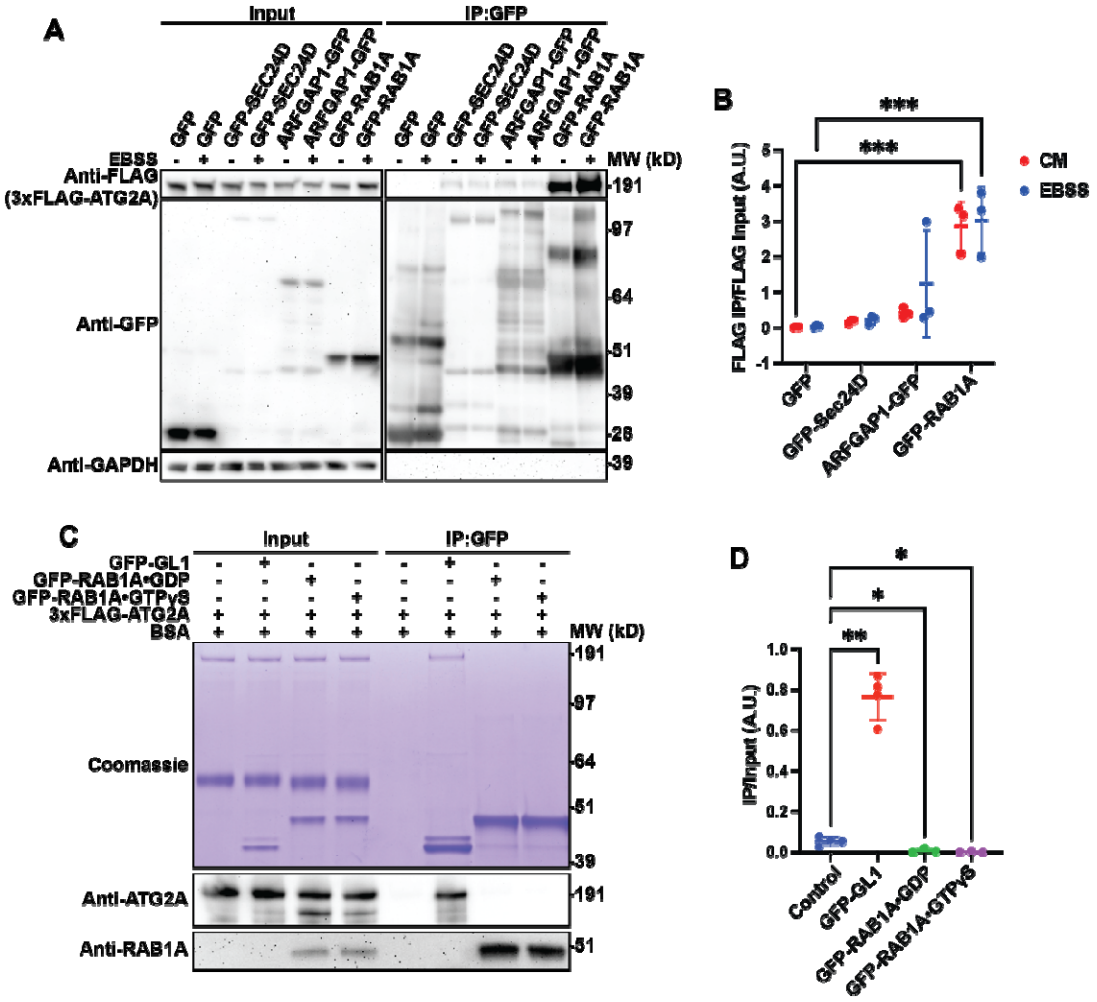

Figure 3. ATG2A interacts indirectly with RAB1A. (A-B) Immunoblot showing CoIP between GFP-RAB1A and 3xFLAG-ATG2A compared to the same reaction with other GFP-tagged early secretory proteins. The cells were incubated with either complete media or EBSS for four hours prior to harvesting. For the CoIP, ~3 mg of cell lysate was used per condition (slight deviations in total amount between replicates, but not between lanes). To quantify the results, the intensity of the 3xFLAG-ATG2A IP signal was ratioed against the input signal. To normalize each replicate, each individual value was divided by the average of the replicate. Statistical significance was assessed by two way ANOVA. *, adjusted P value <0.05. **, adjusted P value <0.01. ***, adjusted P value <0.001. ****, adjusted P value <0.0001. The media was not a significant source of variation (p = 0.3535). **(C-D)** A fully reconstituted CoIP reaction between GFP tagged bait proteins and 3xFLAG-ATG2A reveals no direct interaction between RAB1A and ATG2A. GST tagged GFP-GABARAPL1 (GL1) and GFP-RAB1A were purified from *E. Coli*, during which process the GST tag was proteolytically removed. The purified proteins were then used in a CoIP reaction using GFP trap beads as in (A), but with no cell lysate present in the reaction. BSA was used to block the beads and as a negative control. To quantify the results, the intensity of the 3xFLAG-ATG2A IP signal was ratioed against the input signal. To normalize each replicate, each individual value was divided by the average of the replicate. Statistical significance was assessed by one way ANOVA. *, adjusted P value <0.05. **, adjusted P value <0.01. ***, adjusted P value <0.001. ****, adjusted P value <0.0001.

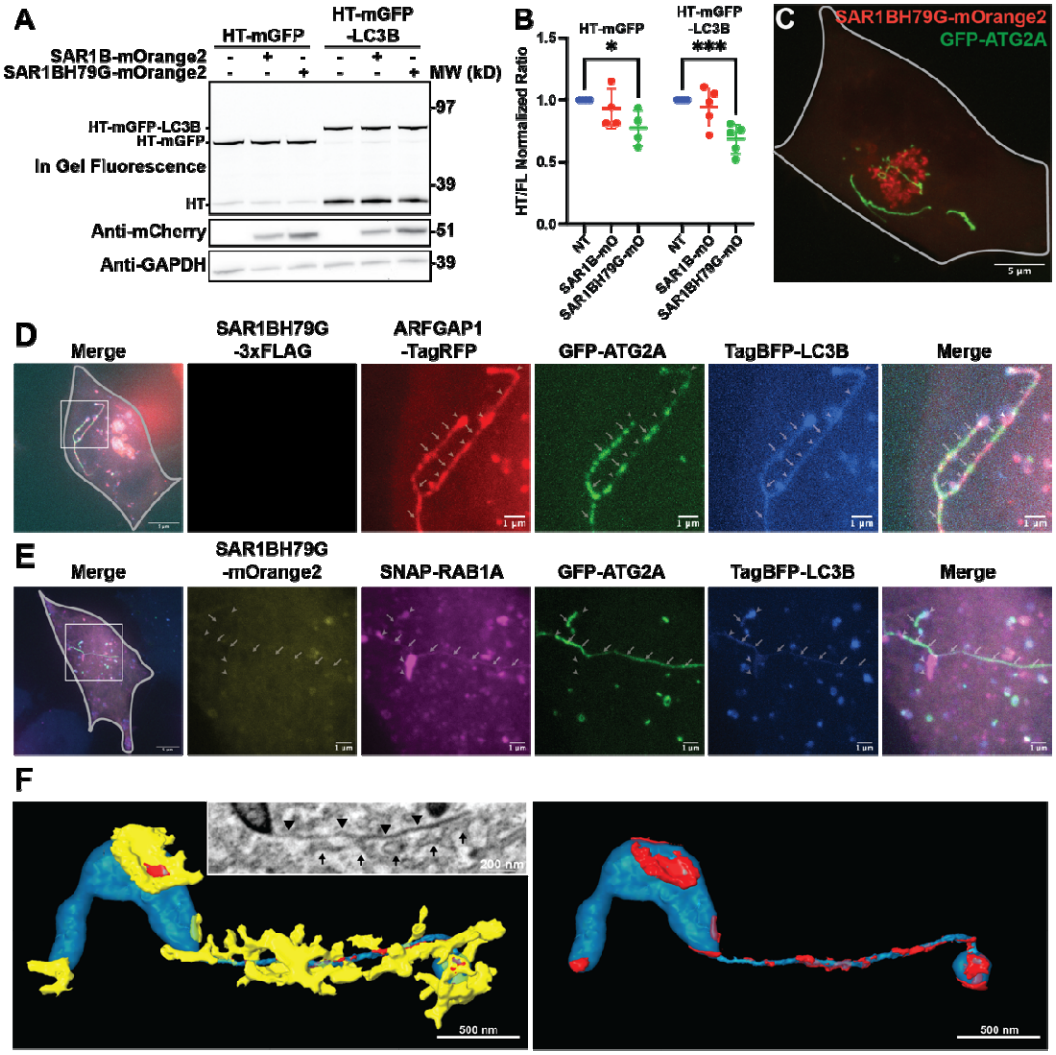

Figure 4. ATG2A, LC3B, ARFGAP1, and RAB1A localize to tubules following disruption of the early secretory pathway. (A-B) In gel fluorescence image (top panel) and immunoblots demonstrating that SAR1BH79G-mOrange2 (mO) overexpression negatively affects autophagic flux in cells starved in EBSS for four hours. The ratio between the FL and the free HT represents the autophagic flux in each condition (as in Fig. 2 A/B) and is plotted in (B). Statistical significance was assessed by two way ANOVA. *, adjusted P value <0.05. **, adjusted P value <0.01. ***, adjusted P value <0.001. ****, adjusted P value <0.0001. Data from four biological replicates were collected for each of the HT-mGFP conditions and five replicates were collected for each of the HT-mGFP-LC3B conditions. **(C)** Live cell imaging of ATG2 DKO cells stably expressing GFP-ATG2 that were transfected with SAR1BH79G-mOrange2 and starved for two hours. Note that GFP-ATG2A forms long tubules that do not colocalize with the SAR1BH79G-mOrange2 signal. Maximum intensity projection of a confocal image. Gray line was added to show cell outline. **(D-E)** Live cell imaging demonstrates the localization of ARFGAP1-TagRFP (D) and SNAP-RAB1A (E) on GFP-ATG2A/TagBFP-LC3B positive tubules following SAR1BH79G overexpression. Arrows denote thin GFP-ATG2A positive tubules whereas arrow heads denote thicker tubules that lack most GFP-ATG2A but contain high levels of LC3B, ARFGAP1, and RAB1A. Maximum intensity projections of confocal images. **(F)** CLEM-FIBSEM of cells prepared as in (C). GFP-ATG2A fluorescence corresponds to a thin tubular membrane that is connected to a thicker tubule. The

small inset in the left image shows a single SEM slice. The arrowheads are pointing to the tubule which is segmented and displayed in turquoise in the larger image, whereas the arrows are pointing at adjacent ER tubules which are segmented and displayed in the larger image in yellow. At many points, these ER structures come into very close apposition with the tubule which is denoted in red. The ER structures are removed in the right image for better visualization of the ATG2A positive tubule.

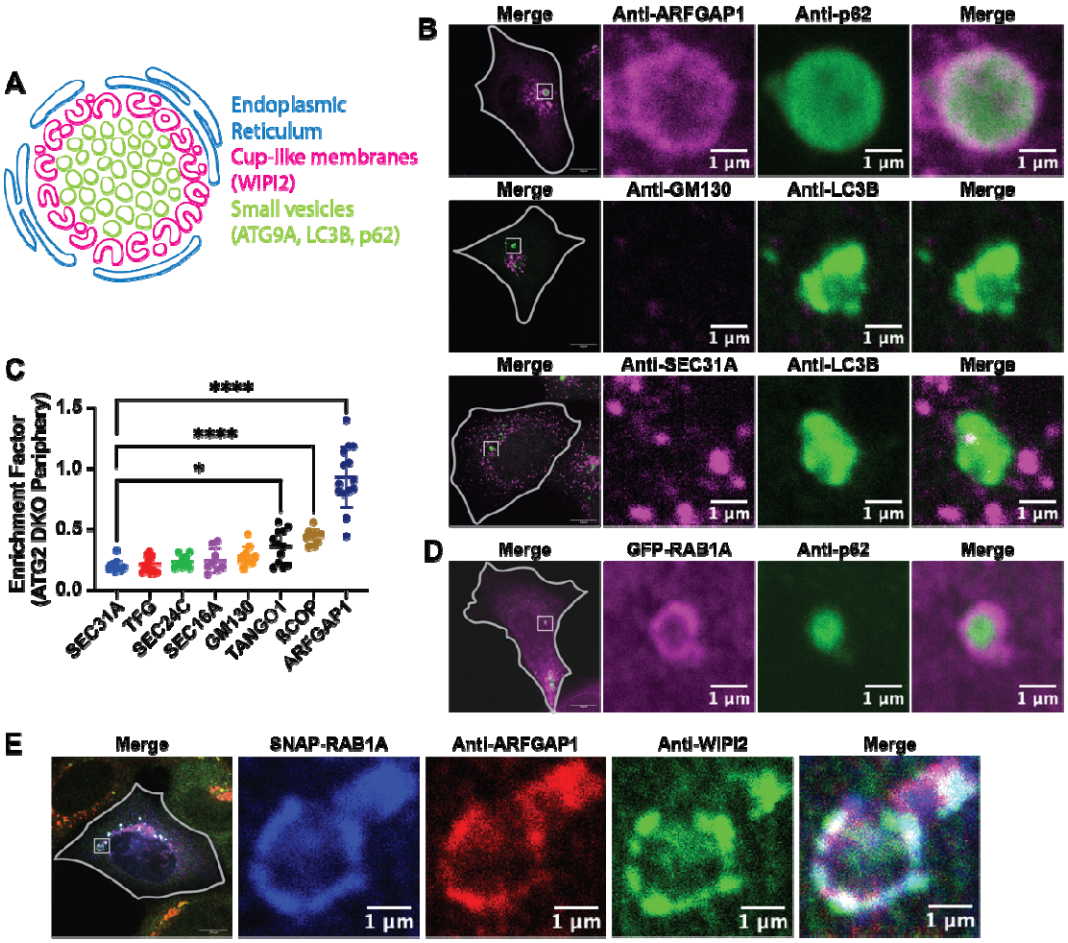

Figure 5. ATG2 deletion results in the accumulation of ARFGAP1 and RAB1A on autophagic membranes. (A) Schematic of the membranes that accumulate at the ATG2 DKO compartment based off the TEM images in Olivas et al[9]. The core of the compartment contains small vesicles that stain for ATG9A, LC3B, and p62. The periphery of the compartment is comprised of more complicated cup shaped membranes that stain for WIPI2. The entire compartment is enwrapped by ER tubules. **(B)** Immunofluorescence images demonstrating the distribution of early secretory membranes around the ATG2 DKO compartment which is marked by either p62 (mouse antibody) or LC3B (rabbit antibody). The images presented are single confocal slices of the center of the ATG2 DKO compartment. The gray lines show the cell periphery and the insets focus on the largest accumulation of p62 or LC3B in the cell. **(C)** Quantification of the images in (C) and in Sup Fig 4A. The enrichment factor is equal to the mean of the given protein at the periphery of the ATG2 DKO compartment compared to its mean throughout the cell. Statistical significance was assessed by one way ANOVA. *, adjusted P value <0.05. **, adjusted P value <0.01. ***, adjusted P value <0.001. ****, adjusted P value <0.0001. Data from three biological replicates were pooled together for each of the conditions. **(D-E)** Immunofluorescence images demonstrating the enrichment of overexpressed GFP-RAB1A (D) or SNAP-RAB1A (E) at the periphery of the ATG2 DKO compartment as determined by the presence of p62 (D) or WIPI2 (E). Presented as a single confocal slice. The gray lines show the periphery of the cell and the insets focus on ATG2 DKO compartments that are distal from the Golgi.

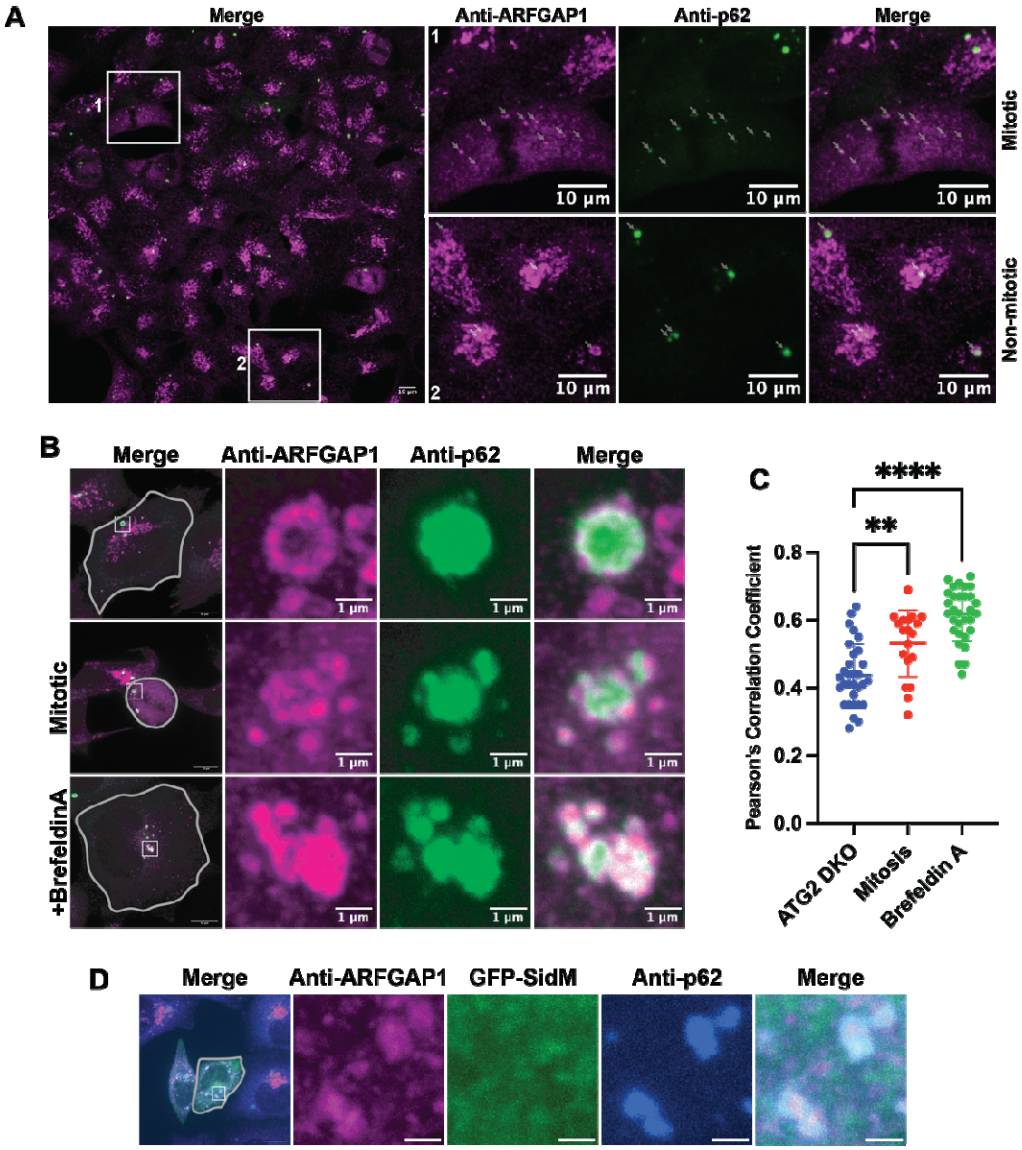

Figure 6. ARFGAP1 accumulation at the ATG2 DKO compartment is independent of the Golgi. (A) Immunofluorescence microscopy demonstrates that ARFGAP1 colocalizes with p62 in ATG2 DKO cells. Inset 1 highlights a cell undergoing mitosis, in which the colocalization of these two markers persists as denoted by the arrows. Inset 2 shows several cells, a ring-like accumulation of ARFGAP1 around p62 is clearly visible, separate from the Golgi. Maximum intensity projection of a confocal image. **(B-C)** Immunofluorescence images showing that perturbations which disrupt Golgi formation don't affect the recruitment of ARFGAP1 to the ATG2 DKO compartment. HEK293 ATG2 DKO cells were treated or not treated with 5 µg/ml Brefeldin A for one hour, following which they were immunostained against ARFGAP1 and p62. The gray lines show the periphery of the cell and the insets focus on ATG2 DKO compartments as seen by the p62 accumulations. Colocalization between ARFGAP1 and p62 was assessed in (C) using the Pearson's Correlation Coefficient. In the untreated sample, cells were separated into two groups: mitotic and non-mitotic, based on the ARFGAP1 fluorescence pattern. Statistical significance was assessed by one way ANOVA. *, adjusted P value <0.05. **, adjusted P value

<0.01. ***, adjusted P value <0.001. ****, adjusted P value <0.0001. **(D)** Immunofluorescence image demonstrating that Golgi disruption by SidM/DrrA overexpression did not perturb the colocalization between ARFGAP1 and p62. HeLa ATG2 DKO cells were transfected with GFP-SidM and then immunostained against ARFGAP1 and p62. The gray line shows the periphery of the cell and the inset focuses on the largest accumulation of p62.

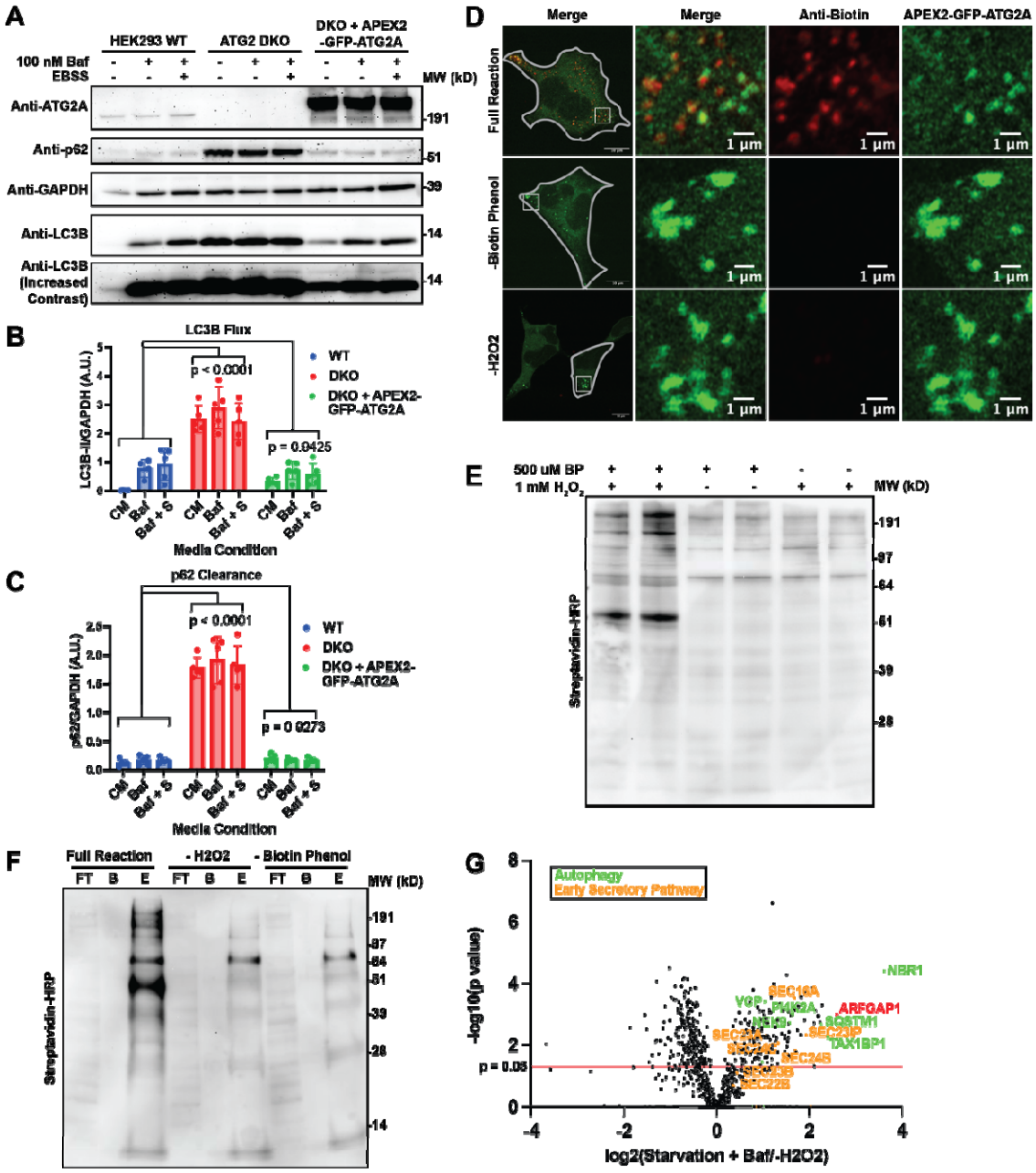
A
HEK293 WT
ATG2 DKO
DKO + APEX2 -GFP-ATG2A
100 nM Baf
EBSS
MW (kD)
Anti-ATG2A
Anti-p62
Anti-GAPDH
Anti-LC3B
Anti-LC3B (Increased Contrast)
191
51
39
14
14
B
LC3B Flux
LC3B-II/GAPDH (A.U.)
p < 0.0001
p = 0.0425
WT
DKO
DKO + APEX2-GFP-ATG2A
CM
Baf
Baf + S
Media Condition
C
p62 Clearance
p62/GAPDH (A.U.)
p < 0.0001
p = 0.9273
WT
DKO
DKO + APEX2-GFP-ATG2A
CM
Baf
Baf + S
Media Condition
D
Merge
Merge
Anti-Biotin
APEX2-GFP-ATG2A
Full Reaction
-Biotin Phenol
-H2O2
1 µm
E
500 uM BP
1 mM H2O2
MW (kD)
Streptavidin-HRP
191
97
64
51
39
28
F
Full Reaction
- H2O2
- Biotin Phenol
FT
B
E
MW (kD)
Streptavidin-HRP
191
97
64
51
39
28
14
G
Autophagy
Early Secretory Pathway
-log10(p value)
p = 0.05
NBR1
SEC16A
YOP1
PI4K2A
ARFGAP1
SQSTM1
SEC22B
TAX1BP1
SEC24B
log2(Starvation + Baf/-H2O2)

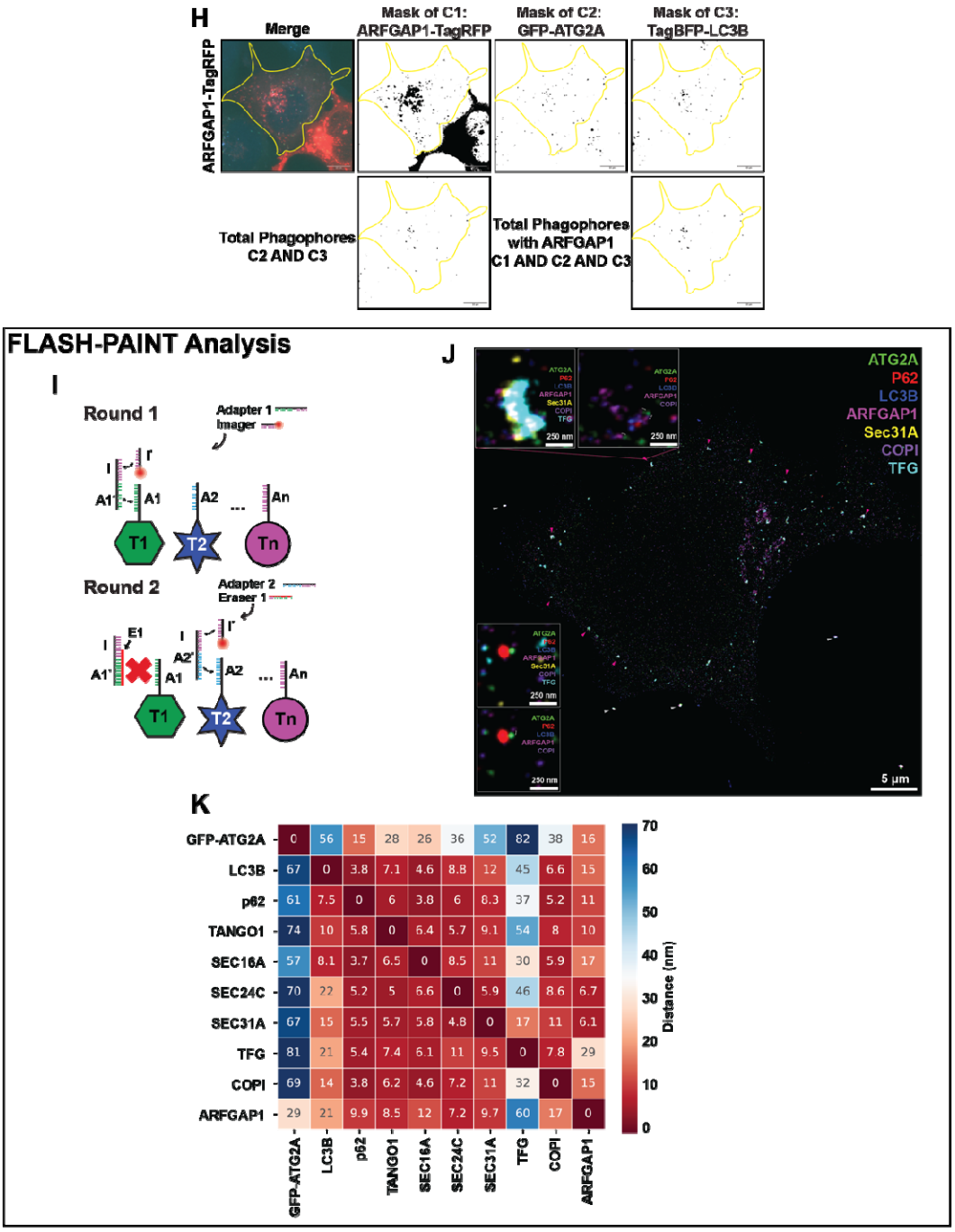

Supplemental Figure 1. ATG2A and ARFGAP1 colocalize during starvation. (A-C) Immunoblot showing the restoration of LC3B flux (B) and p62 clearance (C) in ATG2 DKO cells stably expressing APEX2-GFP-ATG2A. The restoration of a wild type phenotype indicates that the fusion protein is both localizing and functioning properly. The band intensity of LC3B (B) and p62 (C) were normalized against the intensity of GAPDH for each lane. To normalize each replicate, each individual value was divided by the average of the replicate. Statistical significance was assessed by two way ANOVA. Data from five biological replicates were collected for each condition, save for the WT + Baf and WT + Baf + EBSS, which each had four replicates. **(D-F)**

Single slice confocal immunofluorescence images (D) and immunoblots (E-F) demonstrating that the addition of biotin phenol and hydrogen peroxide to ATG2 DKO cells stably expressing APEX2-GFP-ATG2A results in the biotinylation of proteins proximal to ATG2A. The omittance of either biotin phenol or hydrogen peroxide resulted in the loss of the anti-biotin signal, save for endogenously biotinylated proteins. The immunoblot in (F) demonstrates that the biotinylated proteins can be enriched on streptavidin beads. **(G)** Proximity labeling of HEK293 ATG2 DKO cells stably expressing APEX2-GFP-ATG2A was performed as described in Fig. 1A. **(H)** An example of the workflow to calculate phagophore fraction as seen in (Fig. 1D). **(I-K)** FLASH-PAINT analysis confirming the proximity of ATG2A to ARFGAP1. ATG2 DKO cells stably expressing GFP-ATG2A were labeled with all of the antibodies listed in (J), which in turn were preincubated with secondary antibodies with unique DNA sequences as depicted in (H). Each target (T1, T2… Tn) was visualized sequentially by adding an adaptor DNA strand that matched the target sequence (A1, A2… An) and an additional sequence to recruit the imager DNA strand (H). To remove the imager strand from each sequential target, a unique eraser strand was added that recognized the entirety of the adaptor sequence (e.g. A1) and part of the imager sequence, resulting in the total sequestration of the adaptor DNA strand. The subsequent adaptor sequence was then added to visualize the next target protein. Seven of the ten visualized proteins are depicted in (I), which highlights the proximity of ATG2A and ARFGAP1 at autophagic and early secretory membranes. The heatmap presented in (J) shows the median distance within 200 nm between all visualized proteins. (I); pink arrow heads = ERES. white arrow heads = exogenous beads used as a fiduciary marks in imaging. (I; insets), brackets indicate immediate proximity of ATG2 (green) and ARFGAP (maroon) as frequently observed in ERES.

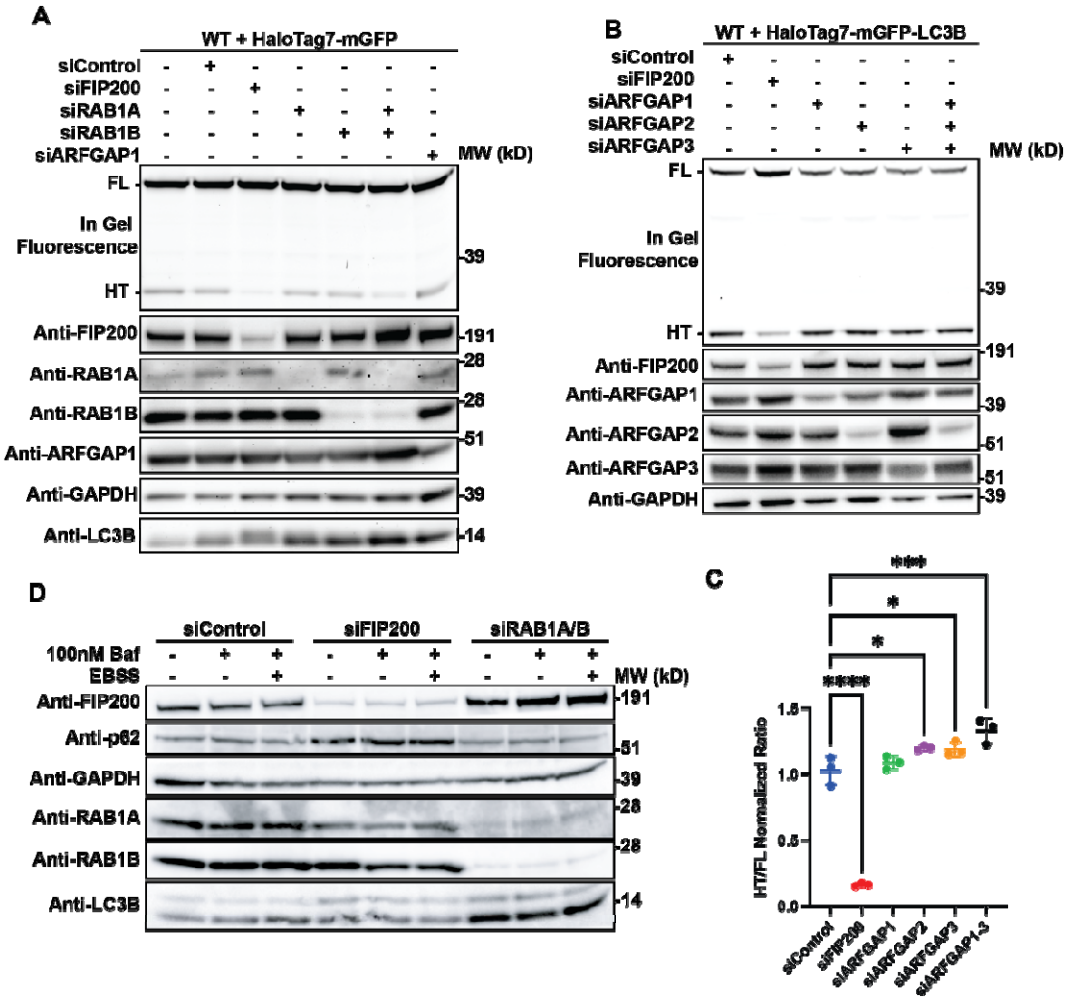

Supplemental Figure 2. Autophagic flux depends upon RAB1 but not ARFGAP1. (A) In gel fluorescence image (top panel) and immunoblots demonstrating that siRNA KD of RAB1 inhibits autophagic turnover of a cytosolic reporter of bulk autophagy. In gel fluorescence reveals HaloTag7s moiety bound to the TMR ligand. Indicated bands are full length (FL) HT-mGFP protein and HaloTag7 after cleavage (HT) in the lysosome. **(B-C)** In gel fluorescence image (top panel) and immunoblots demonstrating that siRNA KD of ARFGAP1-3 slightly promotes autophagic turnover of a HaloTag7-mGFP-LC3B reporter. In gel fluorescence reveals HaloTag7s moiety bound to the TMR ligand. Indicated bands are full length (FL) HT-mGFP protein and HaloTag7 after cleavage (HT) in the lysosome. The ratio between FL and HT demonstrates autophagic flux, quantified in (C). Statistical significance was assessed by one way ANOVA. *, adjusted P value <0.05. **, adjusted P value <0.01. ***, adjusted P value <0.001. ****, adjusted P value <0.0001. Data from three biological replicates were collected for each condition**. (D)** Immunoblot showing the impact of siRAB1 knockdown on LC3B-II levels. HEK293 WT cells were not treated or treated with 100 nM bafilomycin A1 or EBSS and 100 nM bafilomycin A1.

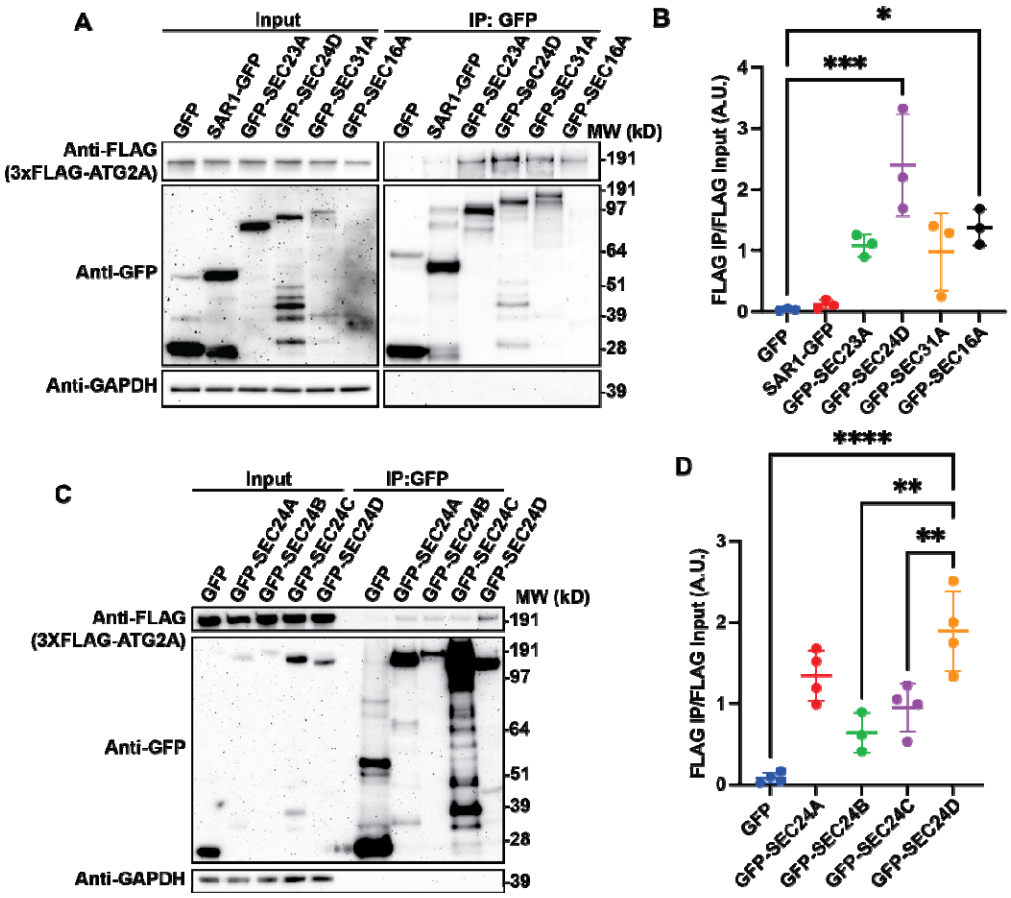

Supplemental Figure 3. ATG2A CoIPs weakly with ER Exit Site proteins. (A-D) Immunoblot showing the weak CoIP between 3xFLAG-ATG2A and various ER Exit Site proteins. For the CoIP, ~3 mg of cell lysate was used per condition (slight deviations in total amount between replicates, but not between lanes). Immunoblots quantified as in Fig. 2B. Statistical significance was assessed by one way ANOVA. *, adjusted P value <0.05. **, adjusted P value <0.01. ***, adjusted P value <0.001. ****, adjusted P value <0.0001.

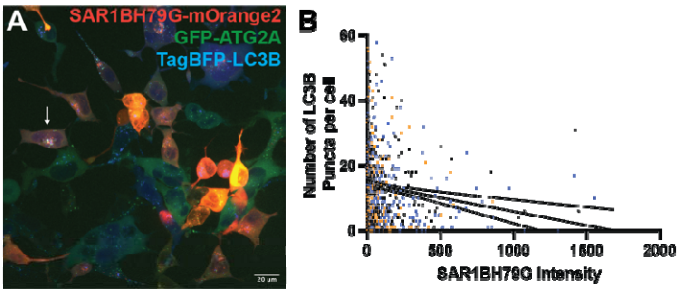

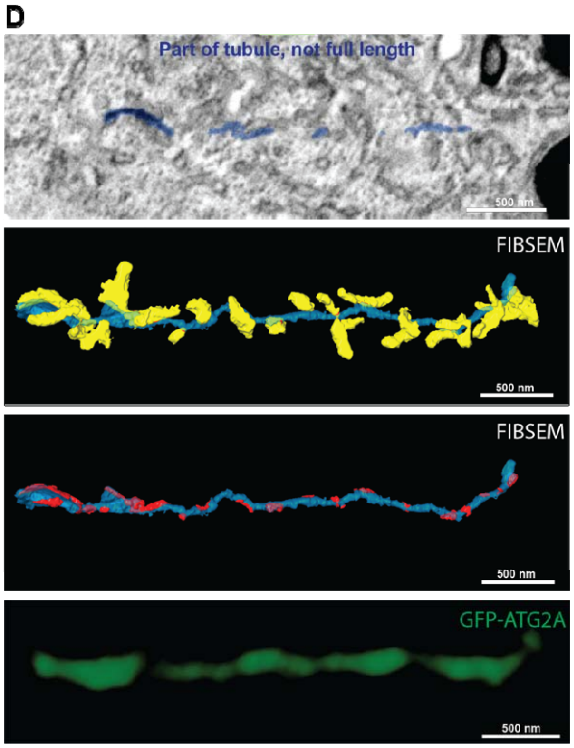

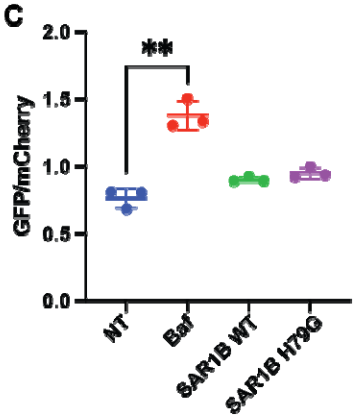

Supplemental Figure 4. SAR1BH79G overexpression hinders autophagy and leads to the formation of ATG2A positive membrane tubules. (A-B) Live cell imaging shows that SAR1BH79G overexpression negatively correlates with LC3B puncta number. ATG2 DKO cells stably expressing GFP-ATG2A and BFP-LC3B were transfected with SAR1BH79G-mOrange2 and starved for 2 hours. The number of transfected cells with GFP-ATG2A tubules (white arrow in A) was counted against the total number of transfected cells, resulting in a formation rate of 1.5±0.8%. ROIs were drawn over each transfected cell, and the resulting SAR1BH79G intensity was plotted against the number LC3B puncta in (B). A linear trendline was added in black with a 95% confidence interval. **(C)** FACS data demonstrating that SAR1BH79G overexpression only results in a partial block in autophagic flux. H4 cells with a heterozygous GFP-mCherry-LC3B endogenous tag were transfected with SAR1B-mOrange2 or SAR1BH79G-mOrange2 overnight, following which they were starved in HBSS for four hours and analyzed by FACS. The ratio between GFP and mCherry is an indicator of autophagic flux, as the GFP signal is quenched in the lysosome. This ratio is displayed as averages. Statistical significance was assessed by one way ANOVA. *, adjusted P value <0.05. **, adjusted P value <0.01. ***, adjusted P value <0.001. ****, adjusted P value <0.0001. **(D)** CLEM-FIBSEM of cells prepared as in (Fig. 4C). GFP-ATG2A fluorescence corresponds to a thin tubular membrane. A single slice SEM slice is depicted in (i). Note that the segmented tubule comes in and out of the plane of this slice, so the tubule that is highlighted in turquoise is not complete. The yellow arrows are pointing at adjacent ER structures

which are segmented and displayed in (ii) in yellow. At many points, these ER structures come into very close apposition with the tubule which is denoted in red. The ER structures are removed in (iii) for better visualization of the tubule. The GFP-ATG2A fluorescence signal is depicted in (iv).

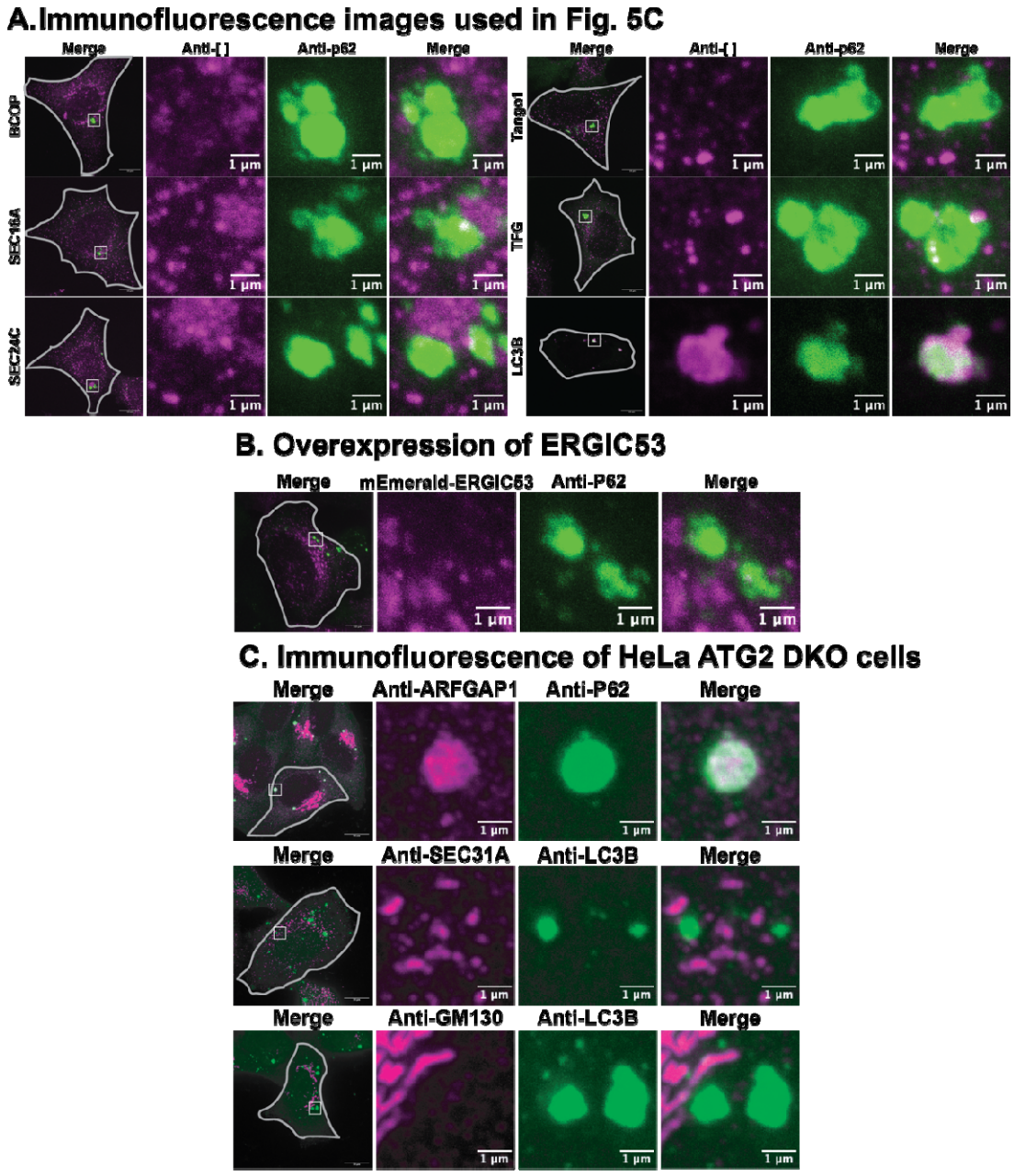

Supplemental Figure 5. Most early secretory markers are not enriched at the periphery of the ATG2 DKO compartment. (A-B) Immunofluorescence images demonstrating the distribution of endogenous (A) or overexpressed (B) early secretory membranes around the ATG2 DKO compartment which is marked by p62. The images presented are single confocal slices of the center of the ATG2 DKO compartment. The gray lines show the cell periphery, and the insets focus on the largest accumulation of p62 in the cell. The images in (A) were used in the analysis of Fig. 5C. **(C)** Immunofluorescence images in HeLa ATG2 DKO cells demonstrating a distribution of early secretory proteins as in HEK293 ATG2 DKO cells. Of note, whereas ARFGAP1 localized to the ATG2 DKO compartment in both HEK293 and HeLa cells, the distribution of ARFGAP1 was markedly different.

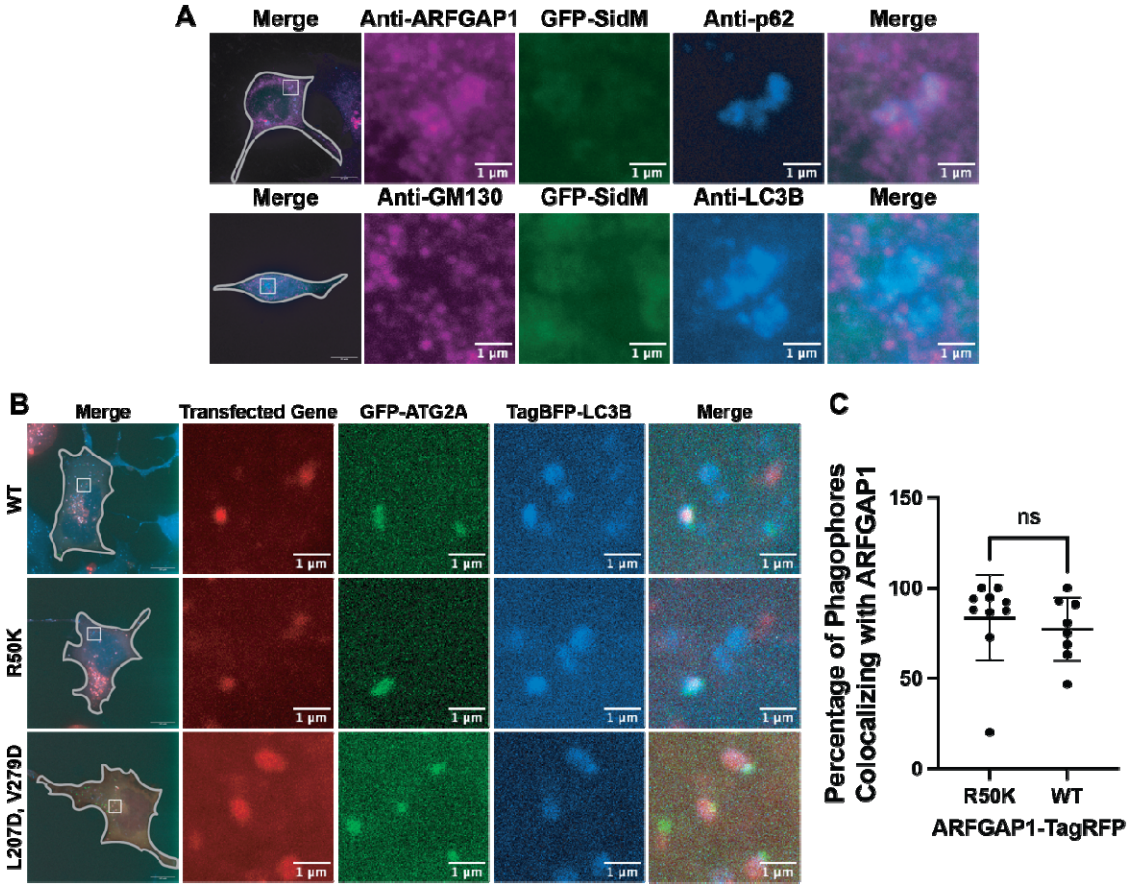

Supplemental Figure 6. ARFGAP1 localizes to PAS independently of the Golgi, GAP activity, and ALPS motif. (A) Immunofluorescence images demonstrating that whereas GFP-SidM overexpression results in the complete dissipation of GM130 signal, ARFGAP1 still colocalized with the p62 signal. **(B-C)** Live cell imaging demonstrating the colocalization between ARFGAP1 mutants and phagophores, as denoted by the overlap between GFP-ATG2A and TagBFP-LC3B. Quantification for the WT and R50K construct was performed as in (Fig. 1C). Stastical significance was assessed using a two-tailed t-test.

Table S1. Antibody Targets and Sequences for FLASH PAINT

Target	**Nanobody**	**Sequence (3' → 5')**
ATG2A-GFP	Anti-GFP-Nanobody-A3	NB - TT TCTTCATTAGCG
TFG	Anti-Rabbit-Nanobody-A15	NB - TT ATAGTGATTGGA
TANGO1	Anti-Rabbit-Nanobody- A39	NB - TT TTATGTTCTGCT
SEC24C	Anti-Rabbit-Nanobody-A8	NB - TT ATGTTAATGGGT
SEC16A	Anti-Rabbit-Nanobody-A38	NB - TT ATTTAGTGTAGC
LC3B	Anti-Rabbit-Nanobody-A20	NB - TT ATATGATCTCCG
SEC31A	Anti-Mouse-Nanobody-A27	NB - TT AAAAAGTTCGAG
ARFGAP1	Anti-Rabbit-Nanobody-A10	NB – TT ATAATGGATGGG
COPI	Anti-Mouse-Nanobody-A25	NB – TT ATAATCATGCTC
p62	Anti-Mouse-Nanobody-A36	NB – TT ATAACAGAATCG

Table S2. Imager Sequence

Imager name	**Sequence**	**3'-mod**
R2-6nt	TGGTGG	Cy3B

Table S3. Adaptor Sequences

Adapter Name	**Sequence (3' → 5')**
A3-5xR2	ACCACCACCACCACCACCA AA CGCTAATGAA
A15-5xR2	ACCACCACCACCACCACCA AA TCCAATCACT
A39-5xR2	ACCACCACCACCACCACCA AA AGCAGAACAT
A8-5xR2	ACCACCACCACCACCACCA AA ACCCATTAAC
A38-5xR2	ACCACCACCACCACCACCA AA GCTACACTAA
A20-5xR2	ACCACCACCACCACCACCA AA CGGAGATCAT
A27-5xR2	ACCACCACCACCACCACCA AA CTCGAACTTT
A10-5xR2	ACCACCACCACCACCACCA AA CCCATCCATT
A25-5xR2	ACCACCACCACCACCACCA AA GAGCATGATT
A36-5xR2	ACCACCACCACCACCACCA AA CGATTCTGTT

Table S4. Eraser sequences

Eraser Name	**Sequence (3' → 5')**
E3-5xR2	TTCATTAGCG TT TGG
E15-5xR2	AGTGATTGGA TT TGG
E39-5xR2	ATGTTCTGCT TT TGG
E8-5xR2	GTTAATGGGT TT TGG
E38-5xR2	TTAGTGTAGC TT TGG
E20-5xR2	ATGATCTCCG TT TGG
E27-5xR2	AAAGTTCGAG TT TGG
E10-5xR2	AATGGATGGG TT TGG
E25-5xR2	AATCATGCTC TT TGG
E36-5xR2	AACAGAATCG TT TGG

Table S5. Order of sequential antibody labeling for FLASH-PAINT

# Round	Protein	Adapter – Concentration	Imager – Concentration
Round 1	ATG2A-GFP	A3-5xR2 – 20 nM	R2 – 500pM
Round 2	ARFGAP1	A10-5xR2 – 20 nM	R2 – 250 pM
Round 3	SEC31A	A27-5xR2 – 20 nM	R2 – 500 pM
Round 4	SEC24C	A8-5xR2 – 20 nM	R2 – 500 pM
Round 5	Tango1	A39-5xR2 – 20 nM	R2 – 500 pM
Round 6	TFG	A15-5xR2 – 20 nM	R2 – 500 pM
Round 7	COPI	A25-5xR2 – 20 nM	R2 – 500 pM
Round 8	LC3B	A20-5xR2 – 20 nM	R2 – 500 pM
Round 9	p62	A36-5xR2 – 20 nM	R2 – 500 pM
Round 10	SEC16A	A38-5xR2 – 20 nM	R2 – 500 pM

Table S6. Mass Spectrometry Data

Protein Name	log2(Complete/ Ref)	-log10(p value)		Protein Name	log2(Starvation/ Ref)	-log10(p value)
ARFGAP1	1.990001	1.910316		NBR1	3.616668	4.402305
NBR1	1.876667	3.191361		ARFGAP1	2.596666	2.98884
APC	1.723334	0.030681		TAX1BP1	2.396666	2.251865
KLC1	1.66	2.754587		KTN1	2.276667	3.302519
PABPC4	1.653334	2.658605		SQSTM1	2.249999	2.684983
PAIP1	1.61	3.281064		ANXA11	2.233334	2.745159
GPHN	1.583333	0.02872		UBAP2L	2.183333	2.955829
KTN1	1.563333	2.520177		KLC1	2.130001	3.103247
TAX1BP1	1.526666	1.180538		NUP210	2.113333	1.322503
KIDINS220	1.49	2.119021		RAI14	2.1	2.71908
RRBP1	1.483334	2.732909		FLNA	2.053334	3.847886
SEC23IP	1.473333	2.341899		TFG	2.036666	0.034123
XRN1	1.453333	1.184407		SEC23IP	1.93	2.338303
ANXA7	1.403333	2.121564		PAIP1	1.903333	3.67719
RAI14	1.393333	1.734573		KIDINS220	1.896667	2.819156
SQSTM1	1.373333	2.040963		ACTN4	1.819999	3.564691
ANXA11	1.356667	1.969817		SPTBN1	1.806666	2.34055
EPB41L2	1.356667	2.148951		CLTC	1.760001	3.259923
UBAP2L	1.353334	2.287386		PDLIM1	1.743333	2.493008
SEC16A	1.353334	2.725806		EIF4B	1.733334	0.030319
EIF4B	1.326666	0.023212		CRKL	1.716667	1.774432
GOLGA2	1.303333	0.02279		SEC24B	1.699999	1.830301
NEK9	1.286666	1.911789		ANXA7	1.696667	1.827068
CAMK2D	1.220001	2.562478		CAMK2D	1.686668	3.128622
MAP4	1.216667	2.692122		SEC16A	1.68	3.542678
OSBPL9	1.216667	0.022193		PI4K2A	1.626666	3.001863
GEMIN4	1.216666	2.345639		FLNB	1.6	2.977772
CLTC	1.193334	2.045881		CCDC6	1.59	0.028915
GFPT1	1.17	1.71647		NEK9	1.576667	2.722235
TFG	1.166666	0.019559		XRN1	1.573333	1.637869
TTC28	1.143334	2.78476		HERC2	1.56	2.439834
PI4K2A	1.143333	1.767996		RAB3GAP2	1.55	1.677751
PARP9	1.113333	3.790284		PABPC4	1.546668	2.706853

DDX20	1.110001	1.368403		GFPT1	1.543334	2.242861
CCDC6	1.109999	0.020192		USP9X	1.543334	3.088877
WIPI2	1.103334	0.019913		TTC28	1.540002	3.817083
CRKL	1.103333	1.410823		SPAG9	1.529999	2.132198
USP9X	1.093333	2.129857		CAPRIN1	1.52	1.956944
AKAP8	1.046667	0.018195		IMPDH2	1.513334	4.28233
GSPT1	1.033334	0.018008		LASP1	1.483334	0.025228
SEC24C	1.023334	1.515652		CTTN	1.48	2.237308
SPAG9	1.01	1.73575		USP47	1.473335	1.801441
FLNA	1.003333	2.082767		DDX20	1.473333	2.332358
BICD2	0.98	0.017706		GPHN	1.42	0.025761
CYFIP2	0.976666	2.628189		GEMIN4	1.416666	3.112823
CTTN	0.966667	1.522253		RRBP1	1.406667	2.38415
TP53	0.963334	1.161234		EMC1	1.376667	0.025002
MON2	0.943335	1.634557		KIF5B	1.37	3.349187
FASN	0.936666	1.7441		ASNS	1.330001	0.022212
SEC13	0.933333	0.016427		SEC24C	1.326666	2.086397
WNK1	0.923335	1.103603		AIMP1	1.32	1.787589
CPNE3	0.923334	1.09517		HGS	1.32	0.02361
SEC23A	0.923332	1.927333		DBN1	1.316668	0.02333
AIMP1	0.913335	1.127301		MYCBP2	1.316668	0.024818
PDLIM1	0.913333	1.168642		ITPR2	1.316666	1.393081
SPTBN1	0.906667	1.77298		MAVS	1.313333	0.023553
SEC24B	0.9	1.117323		KIF11	1.31	2.804458
COIL	0.883333	1.651347		SYNCRIP	1.31	2.82914
USP47	0.880001	1.293738		SMN1	1.306666	0.023018
FLNB	0.873334	1.894586		GNPDA1	1.29	2.246103
CAST	0.873333	0.015417		MACF1	1.29	2.737995
KIF5B	0.866666	2.01843		GOLGB1	1.276667	2.164892
CNOT1	0.863333	1.948862		FASN	1.253334	2.588918
GOLGB1	0.863333	1.348179		ATP6V0A1	1.233333	0.022366
HERC2	0.860001	1.041792		PRKAR1A	1.226668	3.966267
ESYT1	0.86	2.266855		LARP1	1.226666	2.309467
DBN1	0.859999	0.01524		CNOT1	1.216667	2.015865
RARS1	0.840001	1.956198		CPNE3	1.210002	2.026714
KIF11	0.833334	2.243385		CACYBP	1.2	6.617983
DYNC2H1	0.82	0.923149		HSD17B11	1.19	1.88206

GPD2	0.81	0.014152		PCM1	1.19	1.340342
HSD17B11	0.806667	1.333526		ASCC3	1.186667	1.554012
CAPZA1	0.796667	2.652704		ESYT1	1.18	3.556717
GAPDH	0.783335	1.235337		PABPC1	1.173332	3.068128
ATP6V0A1	0.783333	0.014205		PRDX2	1.153332	2.190462
PSMB6	0.779999	0.012988		SYNGR2	1.149999	0.020275
IARS1	0.773333	2.108558		MON2	1.146666	1.782477
SEC24A	0.77	0.014227		UPF1	1.146666	1.258344
TMEM159	0.77	0.013295		TRIM32	1.143333	0.020521
EPB41L3	0.77	1.424795		WIPI2	1.143333	0.020618
MAP1B	0.766667	1.046008		DYNC2H1	1.14	1.194385
ASCC3	0.763334	0.963272		CYFIP2	1.136667	3.071749
CARM1	0.763333	2.757326		IQGAP1	1.133334	3.154983
MAVS	0.76	0.01363		RASA1	1.13	0.021025
RAB3GAP2	0.76	0.799928		AHNAK	1.116668	2.265218
EML4	0.756667	0.013555		RTN3	1.110001	2.697115
PPP4R1	0.753333	0.014023		AGL	1.109999	0.019413
GSR	0.743333	0.012896		APPL1	1.106667	0.020369
PRKAA1	0.743333	1.635135		TP53	1.096666	1.15255
MACF1	0.733334	1.659033		MAP4	1.093333	2.316438
RPTOR	0.733334	0.013566		CTNND1	1.09	1.632224
AKAP9	0.726667	0.013127		WNK1	1.09	1.45984
IDH3G	0.726667	0.677006		EMD	1.09	2.706117
VCP	0.723333	2.133516		ITGB1	1.09	0.019389
NCOA4	0.719999	0.012672		CHUK	1.086667	0.019758
SMN1	0.716667	0.012626		SEC23A	1.076666	2.323015
IQGAP1	0.716667	2.77667		PYCR2	1.073332	1.618861
ITPR2	0.713333	0.607374		AKAP9	1.066667	0.019268
WDR45	0.713333	0.012568		NCOA4	1.063333	0.018716
RASA1	0.71	0.013212		TRIO	1.059999	1.815803
SYNCRIP	0.706668	2.13789		VCL	1.056666	2.857458
ANK3	0.696667	1.050332		STIP1	1.043333	1.608922
NME1	0.689999	1.110755		TTC37	1.04	2.260872
ATXN2L	0.689999	0.012001		TAGLN2	1.036667	2.747229
AIMP2	0.686666	1.587641		VCP	1.036666	3.408178
PPP5C	0.683333	2.26293		RB1CC1	1.033334	0.018547

MYCBP2	0.680001	0.012822		RELA	1.030001	1.233324
RANBP2	0.68	2.0243		BAG2	1.026667	0.017229
PSMC6	0.663333	0.011442		CAST	1.026666	0.018068
IPO7	0.660001	1.748893		IARS1	1.016667	2.966758
LARP1	0.660001	1.304893		CAD	1.013335	2.287169
BAG2	0.656667	0.011019		SUCLG2	1.013334	0.017761
CKAP5	0.656667	1.74772		SMAD9	1.01	0.018134
EPRS1	0.653334	1.844093		CKAP5	1.006667	3.096269
UPF1	0.650001	0.696598		BICD2	1.006666	0.018183
RNF213	0.649999	0.775962		MAP1B	0.996666	1.21159
RTN3	0.640001	2.004812		OSBPL9	0.993333	0.018121
PCM1	0.636667	0.514772		DBNL	0.990001	0.01822
COG1	0.636666	0.011627		ATL1	0.986666	0.017364
CAPRIN1	0.63	0.950725		BIRC6	0.986666	0.018304
SMAD9	0.626668	0.011251		RICTOR	0.986665	1.460667
CHUK	0.626666	0.011393		PPP5C	0.976667	2.549852
KARS1	0.623333	0.011059		RARS1	0.976667	2.476349
NF1	0.62	0.011125		SEC13	0.973333	0.017132
ACLY	0.616668	1.848168		EIF3B	0.973332	2.260377
OSBPL11	0.616667	0.010927		EML4	0.963334	0.01726
NUP160	0.616666	0.611465		ANXA2	0.956665	2.797131
CCAR2	0.613332	0.695832		PDCD6IP	0.956665	1.726799
RELA	0.610001	0.831489		CORO1C	0.953334	1.110328
IMPDH2	0.61	2.201498		EPRS1	0.943335	2.858201
ACTN4	0.606665	1.396208		RHOT1	0.943333	1.357716
CYP20A1	0.603334	0.010754		EPB41L3	0.940001	1.89599
SVIL	0.603334	0.011095		ATXN2L	0.936666	0.016292
OLA1	0.603333	0.010623		ACLY	0.930002	3.102015
XPR1	0.6	0.010506		CLINT1	0.926667	2.650526
EXOC6	0.6	0.010582		CARM1	0.923333	2.61762
SCRIB	0.6	0.010678		OSBPL11	0.923333	0.016362
YTHDC2	0.596666	2.188594		SPTAN1	0.919999	1.569132
EEF1D	0.593334	0.81142		EPB41L2	0.916667	2.056007
NAP1L1	0.593334	1.297321		AKAP11	0.913333	0.016264
HGS	0.59	0.010557		TJP2	0.91	0.016718
VCL	0.583334	2.005098		WDR45	0.9	0.015799
PABPC1	0.583332	2.029144		HECTD4	0.9	0.016268
DBNL	0.580001	0.010766		CNNM4	0.893333	0.016213

ABCF2	0.58	0.010217		PRKAA1	0.893333	2.500744
GTF3C1	0.58	0.010578		EPPK1	0.889998	1.713283
BIRC6	0.576666	0.010697		MTCH2	0.88	3.237046
FAM120A	0.573333	1.431885		SEC24A	0.873334	0.016136
NBAS	0.570001	0.010375		RANBP2	0.873333	2.223492
PDCD6IP	0.569999	1.240795		FLNC	0.87	1.596474
YWHAQ	0.566666	2.142986		NF1	0.863333	0.015492
STIP1	0.563333	1.188946		AIMP2	0.85	2.44481
PPP2R2A	0.563332	0.009567		SCAMP3	0.846666	1.193247
CAD	0.560001	1.571918		PGAM5	0.836666	1.596276
PKN2	0.560001	0.808662		EIF3L	0.820001	1.852516
CSDE1	0.56	2.029759		LANCL1	0.816667	1.218794
TJP2	0.556667	0.010302		TNPO3	0.816667	1.562821
ADD1	0.553336	1.185958		NBAS	0.813334	0.014806
EZR	0.55	1.52492		TBC1D15	0.806668	2.106276
HSD17B7	0.546666	0.009479		DIAPH1	0.806667	2.696219
FLNC	0.543333	1.178046		EEF1D	0.806666	0.865209
METTL7A	0.540001	1.526896		MTOR	0.8	0.014688
SLK	0.530001	2.026822		RUFY1	0.796666	0.014182
AHSA1	0.53	0.008802		COIL	0.793333	2.189282
NAA15	0.526667	1.665783		SLK	0.790002	2.57158
UNC45A	0.526666	0.00958		EIF3CL	0.789999	2.581124
FTH1	0.523333	0.009175		HUWE1	0.789999	3.802044
ROCK2	0.516666	0.009226		IPO7	0.786666	2.452208
RPL36AL	0.513333	0.008449		EIF4G1	0.776667	1.824042
TBC1D9B	0.510001	0.009217		CANX	0.77	1.460512
USP5	0.51	1.826906		ARFGEF1	0.766666	0.014283
CTNND1	0.51	0.713914		PPP4R1	0.766666	0.014268
FYN	0.506667	0.00869		MMUT	0.76	0.01384
CORO1C	0.506666	0.869997		FTH1	0.76	0.013322
EIF3B	0.503333	1.044144		RNF213	0.749999	1.250892
AIP	0.5	0.008903		SVIL	0.749999	0.013751
EMD	0.5	1.647736		LRBA	0.743333	0.013223
ISYNA1	0.5	0.008383		PPP2CB	0.74	1.087447
TUBAL3	0.5	0.008961		ANXA6	0.733334	1.711263
SRRT	0.496667	0.008747		FKBP4	0.723335	3.375203
NUP210	0.493334	0.43725		NUP214	0.72	3.352958
ATAD3B	0.493333	0.008534		PRDX1	0.719999	2.168034

DIAPH1	0.49	1.727705		NUBPL	0.716667	0.012043
GEMIN5	0.49	0.008658		POLR2B	0.716666	0.012927
PPP2CB	0.486666	0.78479		DYNC1H1	0.713333	2.769012
LANCL1	0.48	0.66879		TJP1	0.713333	0.012842
MRI1	0.476667	0.592221		CALCOCO1	0.71	0.01258
RTCB	0.476667	0.754787		YTHDC2	0.71	3.069445
EIF3L	0.476667	1.234045		CAMK2G	0.706666	0.012371
PRDX2	0.476666	1.099195		PARD3	0.703334	0.012415
HECTD4	0.473333	0.008554		WBP2	0.703334	0.011928
TARS1	0.47	0.819399		VAV2	0.703333	1.218438
DOCK7	0.463333	0.00821		PARP9	0.689999	2.68417
RB1CC1	0.46	0.008255		GATD3B	0.686666	0.012102
CTBP1	0.46	0.007898		TPM3	0.683334	0.01214
RHOT1	0.46	0.491174		IQGAP2	0.683333	0.012177
VAV2	0.459999	0.54668		RAB7A	0.680001	1.042758
CTNNB1	0.456666	0.008057		ROCK2	0.676666	0.012084
TAGLN2	0.456666	1.748429		GSR	0.673333	0.011682
LASP1	0.453334	0.007711		COG1	0.673332	0.012296
USP10	0.453333	0.912064		PTPN1	0.67	2.711739
DNAJC7	0.450001	0.007838		ANXA1	0.663334	2.421839
CACYBP	0.45	5.023192		MOV10	0.663333	0.011784
POLD1	0.446666	0.448973		STAU1	0.66	0.011594
ANXA1	0.443333	2.55011		RRAGC	0.656666	0.011824
SEPTIN7	0.443333	0.45394		TRIM25	0.656666	1.89382
EIF3CL	0.443332	1.414989		KRT19	0.656665	1.058541
MAGED2	0.439999	1.368284		USP10	0.65	1.249028
NCAPD2	0.436668	0.762459		ACSL3	0.639999	2.487796
TUBA1A	0.436667	1.927462		MARCKS	0.636666	0.011207
ANXA2	0.436666	1.239304		NCAPD2	0.633334	1.735295
DPYSL2	0.436666	0.007664		LPCAT1	0.633334	1.745
PLS3	0.43	1.352432		AARS1	0.63	1.278388
AHNAK	0.423334	0.588593		GOLGA2	0.63	0.011167
DTX3L	0.423334	0.007193		PLEC	0.63	0.790626
HDLBP	0.423334	0.810856		TLN1	0.623334	1.466547
MTOR	0.419999	0.00771		CEP55	0.620001	0.010744
SMARCA4	0.416667	0.660496		ABI1	0.62	0.011034
AS3MT	0.416667	0.007538		TMEM159	0.62	0.010736

RNPEP	0.416666	0.007335		PSMC4	0.616667	0.786661
ULK1	0.413335	0.878106		DGLUCY	0.616667	0.011298
COPB2	0.413334	2.461216		TUBA1A	0.616666	2.828419
FKBP8	0.413333	0.007216		XPR1	0.616666	0.010795
ACTB	0.413333	1.486585		DOCK7	0.613333	0.010869
OGT	0.413333	0.007463		GTF3C1	0.613333	0.011186
POLR2B	0.413333	0.007454		HIP1R	0.613333	0.010732
TTC37	0.410001	0.801303		PLS3	0.613333	1.871595
ABCE1	0.41	1.163999		TARS1	0.610001	1.108472
DYNC1H1	0.406666	1.731928		NUP155	0.6	2.057821
TRIO	0.403334	0.801988		IPO5	0.596667	2.374289
PLCG1	0.403333	0.00713		TUBGCP3	0.596667	1.862355
EIF3D	0.400001	1.595448		OSBPL8	0.589999	1.542563
TLN1	0.4	0.839522		LRRFIP1	0.586667	0.010505
KIF2A	0.4	3.369478		FAM120A	0.586665	1.860909
SPTAN1	0.399999	1.02415		OLA1	0.576668	0.010154
SYNGR2	0.396666	0.006992		CSDE1	0.576667	2.246528
NUMA1	0.393333	1.443254		NAA15	0.576667	1.440271
APPL1	0.39	0.007178		TRAPPC11	0.57	0.010393
FKBP4	0.383335	1.876983		NUP160	0.57	0.435467
ECPAS	0.383334	0.993956		SEC31A	0.566668	0.009762
GNPDA1	0.383334	0.672854		PRKAG1	0.566666	1.808671
SEC23B	0.383334	0.806593		GPD2	0.56	0.009783
RFC1	0.383333	0.006953		METTL7A	0.56	1.478544
TRIM25	0.383332	1.527959		HELZ	0.559999	0.010515
KRT36	0.38	0.006554		GAPDH	0.556667	0.98021
MARCKS	0.376667	0.00663		ANK3	0.556667	0.839715
TUBGCP2	0.376666	0.006726		RANGAP1	0.556667	0.009655
PAK4	0.376666	0.00681		SUGT1	0.556667	0.009999
VAPA	0.373334	0.006431		ELP1	0.553333	1.347087
SENP3	0.370001	0.006303		FASTKD5	0.55	0.009339
YTHDF1	0.37	0.006374		FKBP8	0.549999	0.009603
HNRNPL	0.369999	0.006397		RABGAP1	0.549999	0.009876
EPS8L2	0.366667	0.006553		RABL6	0.543334	1.181496
GLO1	0.366667	0.006511		NAP1L1	0.543333	1.553457
EXOC2	0.363333	0.006427		PYCR1	0.54	0.009241
RABGAP1	0.363333	0.006548		UNC45A	0.54	0.009822

ZSWIM8	0.363333	0.006838		PLCG1	0.539999	0.009548
GART	0.360001	0.913506		SPTLC1	0.536667	1.215875
SUGT1	0.36	0.006491		AP1B1	0.536666	0.956569
TNPO1	0.359999	0.357108		BAG6	0.536666	0.009594
LRRFIP1	0.356667	0.006415		SEPTIN7	0.536666	0.676955
YWHAH	0.356666	0.00628		GCN1	0.536666	2.721607
KRT19	0.353334	0.551111		EZR	0.526667	1.838105
LRBA	0.353333	0.006284		VWA8	0.526667	0.009264
ARHGEF2	0.353333	0.488837		GTPBP6	0.523333	0.009599
RICTOR	0.353333	0.360805		ADD1	0.516668	1.207181
DDX21	0.353332	0.635194		SCRIB	0.513334	0.009136
NUDC	0.35	0.499037		DCTN2	0.51	0.009412
PSMC4	0.35	0.36694		GIGYF2	0.506667	0.008908
RABL6	0.35	0.617185		KPNB1	0.506667	2.73434
NUP214	0.346666	1.505354		TUFM	0.506667	0.43141
PSMC3	0.346666	0.305378		CCAR2	0.493333	0.568692
MOV10	0.343334	0.006098		AS3MT	0.49	0.008852
OXSR1	0.343334	1.201277		KRT18	0.49	1.007707
PTDSS1	0.343334	0.005999		CAVIN2	0.486668	0.008957
TSC1	0.343333	0.006173		DVL3	0.486666	0.008782
BAG3	0.34	0.005921		CTNNB1	0.483334	0.008524
HIP1R	0.34	0.00598		RPTOR	0.483334	0.00894
MTCH2	0.333333	1.234657		UBA6	0.483333	0.008992
ANXA6	0.330001	1.168894		TRIP13	0.480001	3.060808
LMNA	0.330001	0.005883		AARS2	0.480001	0.008168
CAPN2	0.33	0.005672		IMMT	0.48	1.761369
TES	0.329999	0.005802		GFM2	0.48	0.008171
NSDHL	0.326667	1.076282		TPR	0.476667	0.320636
RPS6KA3	0.326667	1.491267		LTA4H	0.476666	0.00845
RHOC	0.323333	0.005723		LYPLAL1	0.473333	0.008457
SSR4	0.323332	0.743314		OGT	0.466667	0.008417
HUWE1	0.319999	1.886934		WDR11	0.466666	0.00817
CEP131	0.313333	0.005745		PSMC2	0.463333	1.897314
DHCR7	0.310001	0.583886		PFKL	0.463333	0.463982
AKAP12	0.31	0.005461		DNAJC7	0.456667	0.007954
GAPVD1	0.31	0.461836		KNTC1	0.456666	0.008042
TBC1D15	0.31	0.863878		ABCF1	0.453335	0.613726
MKI67	0.306667	0.005449		BAG3	0.449999	0.007821

LAP3	0.306666	0.005481		OAS3	0.446667	0.008057
PPP1CA	0.306666	0.005474		ARMCX3	0.443333	0.007838
APRT	0.303334	0.005118		GAPVD1	0.440001	0.458555
TXNDC5	0.303334	0.005409		SEC23B	0.439999	1.099267
LNPEP	0.303333	0.005241		EXOC6	0.436667	0.007725
TRIM32	0.303333	0.005538		SMS	0.436667	1.189554
TUBA1B	0.300002	0.506899		AIP	0.436666	0.007785
RAB7A	0.300001	0.443971		IPO8	0.436666	0.007582
AP1B1	0.3	0.635842		AFDN	0.43	0.330972
PTK2	0.3	0.395728		TSC1	0.426667	0.00766
SPTLC1	0.296667	0.587331		ARHGEF2	0.426666	0.523093
HELZ	0.296666	0.0056		PAICS	0.423334	0.844877
SRP72	0.296666	0.005421		RFC1	0.423334	0.007678
PARD3	0.293334	0.005176		IQGAP3	0.42	0.00732
TPM3	0.293333	0.005251		WASHC4	0.42	0.007475
PSMC1	0.293332	0.838593		DST	0.416667	0.007485
MYG1	0.29	0.004902		ISYNA1	0.413333	0.006941
KRT18	0.286667	0.486795		ACTBL2	0.413333	2.81619
NCAPH	0.286667	0.005087		PRKD2	0.41	0.007013
FUBP1	0.283334	0.004887		KPNA2	0.406668	1.183913
DHX36	0.283333	0.004931		CDK5RAP3	0.406666	0.007342
PUM1	0.283333	0.004943		PTDSS1	0.406666	0.007097
TNPO3	0.28	0.60463		RUVBL1	0.403334	2.067239
SEC31A	0.276667	0.004766		MAGED2	0.403334	1.186103
TRIOBP	0.276667	0.004902		PTK2	0.403334	0.351757
TNIP1	0.276667	0.004877		RAB14	0.403334	1.531114
CLINT1	0.273334	0.643802		TNPO1	0.403332	0.460935
USO1	0.273334	0.004858		DHX29	0.4	0.475931
PPA1	0.273333	0.723918		PI4KA	0.4	0.436125
ATL1	0.266666	0.004692		MRI1	0.399999	0.469633
LARS1	0.263333	0.733332		DYNC1LI1	0.393334	0.006818
ACADM	0.260001	0.00453		DHX36	0.39	0.006774
HSPA1A	0.260001	1.394788		FYN	0.39	0.006703
IPO5	0.26	0.869624		PTPMT1	0.389999	0.006753
ABCF1	0.256667	0.304132		CALD1	0.386667	0.445825
DST	0.256667	0.004625		CKAP4	0.386667	1.076875
NT5DC2	0.256666	0.004519		IRAK1	0.386667	0.006664

RHEB	0.256666	0.004338		IPO11	0.386666	0.006983
OSBPL8	0.256666	0.849148		KRT8	0.386666	0.918686
IPO4	0.253334	0.004313		DTX3L	0.383333	0.006518
PSMD6	0.253334	0.637646		ECPAS	0.383333	1.241791
IQGAP2	0.253333	0.004552		CAPZA1	0.380002	1.123026
ARF5	0.25	0.004215		TFRC	0.38	1.222269
NOP58	0.25	0.004376		MAGED1	0.38	0.006587
LPCAT1	0.246667	0.735695		TRIOBP	0.376667	0.006661
ABI1	0.246667	0.004422		YBX3	0.376666	0.006658
DNMT1	0.246667	0.004428		ACTB	0.376666	1.296374
ACTBL2	0.243334	1.777488		PFN1	0.373333	1.752227
CPNE1	0.243333	0.004259		DPYSL2	0.37	0.006502
LAMP2	0.24	0.004074		TBL2	0.366667	0.006369
STAG2	0.239999	0.004237		DDX1	0.366666	0.87848
STRN	0.236668	0.004219		VPS29	0.363335	0.006151
DARS1	0.236666	0.911973		SEC22B	0.363334	0.690717
PRDX5	0.236666	0.235447		USP24	0.363334	0.006313
EIF3I	0.233334	0.004065		FUBP3	0.359999	0.913979
PRKAG1	0.233334	0.509427		NCAPG	0.356668	0.618153
TOP2B	0.233334	0.00418		ALDOA	0.356667	0.913316
MRPS9	0.233333	0.004163		HPRT1	0.356667	0.624003
AARS1	0.233332	0.362943		PSMC6	0.353333	0.006095
PCBP1	0.233332	0.860049		FAF2	0.353333	2.628884
USP24	0.230001	0.003996		LAP3	0.353333	0.006314
ERBIN	0.23	0.004051		ALDOC	0.35	0.006074
FLII	0.23	0.379965		HBS1L	0.35	0.006163
GIGYF2	0.226667	0.004006		UNK	0.35	0.006215
ARHGAP 35	0.223334	0.004141		FHL1	0.346667	0.534568
GCN1	0.223334	1.882373		LARS1	0.34	0.977754
HSPA8	0.223334	1.275585		PXN	0.34	0.005829
VPS26A	0.223334	0.003962		STRN	0.34	0.006049
CANX	0.220001	0.484371		GART	0.336669	0.750532
PELP1	0.220001	0.45859		DNAJA1	0.336667	0.005877
GPR107	0.216667	0.00394		TNIP1	0.333334	0.00587
YBX3	0.216667	0.003841		FXR1	0.333333	1.315141
GALK1	0.216666	0.003659		YWHAQ	0.333332	1.088969
FAF2	0.210001	1.638911		ARL8A	0.33	0.005796

DCTN2	0.21	0.003899		SENP3	0.326668	0.005565
DTNA	0.21	0.003696		ABCD3	0.326667	0.887484
SLC25A22	0.21	0.003673		DNAJC11	0.326667	1.109253
CHORDC1	0.21	0.003668		LMNA	0.326667	0.005824
NDUFA9	0.206668	0.333237		PDCD11	0.323334	0.005808
NUP107	0.206668	0.00359		TUBAL3	0.323334	0.005815
PRPF6	0.206668	0.310069		EIF3E	0.323333	1.351332
DDX39A	0.203334	0.597873		USO1	0.323333	0.005741
TKT	0.203334	0.21389		VPS51	0.323333	0.005644
NUP155	0.203334	0.482042		SERBP1	0.320001	0.50583
VPS29	0.203334	0.003442		AKAP12	0.32	0.005636
BAG6	0.203332	0.003658		KPNA1	0.319999	0.944259
RPL37A	0.203332	0.003214		TOR1AIP1	0.316666	0.916322
FUS	0.200001	0.003415		ARHGAP35	0.313333	0.005799
PTBP3	0.200001	0.003387		MFN1	0.306667	0.00561
TIMM44	0.2	0.37408		EPS8L2	0.303333	0.005421
FBXO22	0.2	0.003413		OSBPL3	0.300001	0.005172
FUBP3	0.2	0.799779		LNPEP	0.3	0.005184
NUP188	0.2	0.25152		ABCF2	0.296666	0.005225
PTPN1	0.2	0.65829		NUDT19	0.296666	0.005197
CLPB	0.196667	0.003387		CKB	0.293334	0.005054
KRT8	0.196666	0.339147		CTBP1	0.293333	0.005052
PXN	0.193333	0.003323		FDPS	0.293332	0.005115
RANGAP1	0.193332	0.003352		MCMBP	0.29	0.005139
CCT8	0.190001	0.762778		TARS2	0.29	0.005048
DYRK1A	0.19	0.003349		STAT1	0.289998	1.071298
SERBP1	0.186668	0.349763		PPP3CA	0.286667	0.005116
AKAP11	0.186666	0.003372		AP2B1	0.283333	0.875046
MFN1	0.186666	0.003414		FLII	0.283333	0.64426
PDCD11	0.186666	0.003352		PPP2R2A	0.283333	0.004812
SYNE2	0.186666	0.171502		ATAD1	0.280001	0.005108
ATP6V1B2	0.186665	0.003223		GEMIN5	0.28	0.004967
LIPA	0.183334	0.003157		MAPRE2	0.28	0.005076
HLA-B	0.183334	0.003147		PDXDC1	0.28	0.004871
NARS1	0.183334	0.003236		ABCE1	0.279999	1.235244

EIF3E	0.183332	0.998899		RRM1	0.279999	0.004889
TTLL12	0.180001	0.380441		TES	0.279999	0.004923
TNKS1BP1	0.18	0.00317		UTRN	0.279999	0.005031
PRKD2	0.179999	0.003092		HDLBP	0.276666	0.474897
MPRIP	0.176667	0.002984		IPO9	0.273332	0.383286
EEF1AKNMT	0.173333	0.003122		UFL1	0.27	0.272126
HNRNPH3	0.173333	0.380872		ATP2B4	0.27	0.004715
PFN1	0.173333	0.626362		SAMM50	0.27	0.004635
TRMT1L	0.173333	0.003083		DLST	0.266667	0.004643
WDR1	0.173333	0.003039		PSMC1	0.266666	0.799549
VPS35	0.170002	0.296229		TOMM70	0.266666	0.004699
DVL3	0.17	0.003067		TXNDC5	0.266666	0.004755
FXR1	0.17	0.963873		SRSF4	0.266665	0.004537
PRDX1	0.169999	0.350557		ALDH2	0.263334	0.169966
ACSL3	0.169999	0.667687		ACSF3	0.263334	0.004483
MCMBP	0.166667	0.002953		EEA1	0.263334	0.004615
SEPTIN2	0.166667	0.002884		SNTB2	0.263333	0.004693
CNNM4	0.166667	0.003024		PLIN3	0.260001	0.004607
KPNB1	0.163335	1.119087		GTPBP4	0.26	0.004527
DLST	0.163334	0.002844		VDAC2	0.26	1.224148
IPO11	0.163334	0.002962		PRDX5	0.259999	0.408099
OAS3	0.163334	0.002962		ST13	0.256667	0.004319
ZADH2	0.163334	0.002859		CLASP1	0.256667	0.00457
AFG3L2	0.163333	0.157345		PLXNB2	0.256667	0.004642
UBA1	0.159999	0.883195		GCC2	0.256666	0.004785
DDX50	0.156667	0.427246		USP5	0.253334	0.857038
ETF1	0.156667	0.659356		NSDHL	0.253333	1.010344
DCTN1	0.156666	0.971196		SEPTIN2	0.253333	0.004384
SLC12A4	0.153334	0.002714		APC	0.25	0.004589
PHF6	0.153334	0.002648		NME1	0.25	0.585836
HM13	0.150002	0.00259		RHOT2	0.246667	0.00433
PPP3CA	0.15	0.002684		PHGDH	0.243334	0.680071
UBA6	0.15	0.002809		EXOC2	0.243334	0.004314
ACO2	0.146667	0.002493		DNAJC13	0.243333	0.258564
SEC22B	0.146667	0.216339		ERBIN	0.243333	0.004286
COASY	0.146666	0.45947		VIM	0.243333	0.169349

KRT14	0.146666	0.002488		NUP93	0.243333	1.398693
SCAMP3	0.146666	0.141673		NUMA1	0.236667	1.376255
UTRN	0.146666	0.002635		VPS35	0.236667	0.525649
ARMCX3	0.143333	0.002548		ULK1	0.236666	0.32086
HSD17B10	0.143333	0.002501		NOP58	0.236666	0.004142
PHGDH	0.143333	0.526544		KRT36	0.233334	0.004035
KANK1	0.139999	0.002425		ATP6V1B2	0.233333	0.004029
OTUB1	0.139999	0.489224		YTHDF1	0.233333	0.00403
SSRP1	0.139999	0.002384		PSMC3	0.233332	0.304821
TRIP6	0.139999	0.002346		ETFB	0.23	0.795022
KYAT3	0.136667	0.002371		DNM1L	0.23	0.510034
MRE11	0.136667	0.388871		DYNLL1	0.23	0.003996
PSMA5	0.136667	0.002377		SMC4	0.23	1.242458
PSME1	0.136667	0.002436		EIF2B3	0.226667	0.004005
NME2	0.136666	0.002239		DDX21	0.226666	0.532535
DNAJA2	0.133334	0.002299		PIK3R4	0.220001	0.003926
FECH	0.133334	0.002308		SRPRB	0.220001	0.003819
NEFL	0.133334	0.002334		UGP2	0.216668	0.003787
RAD50	0.133333	0.452311		DNAJA2	0.216667	0.00373
STAT1	0.133333	0.502718		ARAF	0.216666	0.003976
SURF4	0.130001	0.389641		MYO1C	0.213333	0.003893
EI24	0.13	0.002254		CCDC88A	0.21	0.003747
PPP6C	0.13	0.002259		CLPX	0.21	0.003619
MTREX	0.126667	0.002228		SMARCC2	0.21	0.003751
TBCE	0.126667	0.00221		PRMT5	0.21	0.003736
PLXNB2	0.126666	0.002297		RTN4	0.206668	0.003444
RUVBL2	0.126666	0.226494		PKN2	0.203334	0.300602
KPNA2	0.123334	0.472944		PSME1	0.203334	0.00362
MAPRE2	0.123334	0.002236		CKMT1A	0.203333	0.854728
PLIN3	0.123334	0.002185		COPB2	0.199999	0.981474
NAT10	0.123333	0.154989		MRPL24	0.196667	0.003441
RAD21	0.123333	0.002125		DPYSL3	0.193334	0.003392
DDX5	0.120001	0.488164		HYOU1	0.193333	0.174679
TBCD	0.120001	0.002082		DARS1	0.193331	0.998018
EMC1	0.12	0.00218		PPP2R5D	0.186668	0.003337
ST13	0.116667	0.001963		KIF2A	0.186666	1.542743

ALDOC	0.116667	0.002033		CPNE1	0.183334	0.003208
GTPBP4	0.116666	0.002037		EXOC4	0.183333	0.003234
TJP1	0.116666	0.0021		GBF1	0.183333	0.151137
MAP4K4	0.113334	0.001984		ACTN1	0.18	0.003159
MRPL24	0.113333	0.001983		DCTN1	0.18	0.73285
PSMD13	0.113333	0.00195		ZSWIM8	0.18	0.0034
FAM98A	0.113333	0.001915		HSPA8	0.18	0.747581
STT3B	0.110001	0.00192		NSF	0.176668	0.463812
RCC2	0.11	0.001917		ATP2C1	0.176668	0.00302
TIGAR	0.11	0.20548		RAC2	0.176668	0.002958
FDPS	0.109999	0.001918		EIF3A	0.176667	0.246193
PRMT3	0.109999	0.001925		MAPK1	0.176667	0.003018
ALG10	0.106667	0.001812		AP3M1	0.176666	0.480155
NCLN	0.106667	0.001865		UQCR10	0.176666	0.003105
RBFOX2	0.106667	0.001859		DSP	0.173334	0.199884
RBM17	0.106667	0.001791		TBC1D9B	0.173333	0.003153
DGLUCY	0.106667	0.001974		TBCD	0.173333	0.003004
CNDP2	0.103334	0.00182		LAMP2	0.173333	0.002942
FHL1	0.103334	0.176237		COASY	0.17	0.729585
CDK5RAP3	0.103333	0.001876		G6PD	0.17	0.364132
ELP1	0.103333	0.243284		SSX2IP	0.17	0.003038
RRM1	0.103333	0.001804		PTCD3	0.169999	0.002978
IDH3A	0.1	0.143174		AASS	0.166667	0.002943
UCHL1	0.1	0.001661		DSTN	0.166667	0.25852
PSMC2	0.099999	0.646096		SEC61B	0.166667	0.002879
ATP6V1A	0.096667	0.919533		MYO6	0.166666	0.987967
COPB1	0.096667	0.425184		GNAI3	0.166665	0.002887
GDI2	0.096667	0.001715		TOMM40	0.163334	0.959233
MSH2	0.096667	0.316287		CNP	0.163333	0.218057
PGAM5	0.096667	0.233264		NT5DC2	0.163333	0.002881
RAB9A	0.096667	0.001649		ATAD3B	0.16	0.002767
EIF4G1	0.093334	0.232215		CORO7	0.16	0.224962
SND1	0.093334	0.001625		PTPN11	0.16	0.002704
NMT1	0.09	0.265328		TNKS1BP1	0.16	0.002819
RUVBL1	0.09	0.563923		HSPA1A	0.159999	0.521797
UQCR10	0.09	0.001584		CAPN2	0.156666	0.002692
SLFN11	0.09	0.001569		HADHB	0.156666	0.414458

SNRPA1	0.09	0.001518		MRPS5	0.156666	0.002671
AFDN	0.086667	0.070465		NUDC	0.156666	0.214018
AKR7A2	0.086667	0.001555		DHCR7	0.153334	0.220383
CEP55	0.086667	0.001501		PSMD2	0.153334	0.315593
RRM2B	0.086666	0.001468		SEC63	0.153334	0.002673
DPYSL3	0.083334	0.001462		TUBB3	0.153334	0.002844
HNRNPR	0.083333	0.001444		CEP131	0.153333	0.00282
KPNA1	0.083333	0.247295		PPP6R3	0.153333	0.002756
PTCD3	0.083333	0.00146		LMAN1	0.153332	0.25277
TRAPPC11	0.080001	0.001473		ALDH18A1	0.15	0.282933
SRPRB	0.08	0.001388		DHX57	0.15	0.00277
LTA4H	0.079999	0.001429		RAB21	0.15	0.230981
NFKB2	0.076667	0.001333		TRMT1L	0.15	0.002668
UNK	0.076667	0.001368		MYO1D	0.15	0.683651
H1-10	0.076667	0.001348		PUM1	0.15	0.002623
PUS1	0.076666	0.11191		VDAC3	0.146667	0.402313
PYGB	0.076665	0.15229		NAT10	0.146666	0.222063
DNAJC11	0.073334	0.135689		SLC12A2	0.146666	0.002606
EIF3G	0.073334	0.00127		UBR4	0.143334	0.213612
POLA1	0.073334	0.149821		VPS4B	0.143333	0.352042
PDXDC1	0.073333	0.00128		DTNA	0.140001	0.002467
SEC63	0.073332	0.00128		TBCE	0.140001	0.002442
HYOU1	0.066667	0.061713		YBX1	0.140001	0.002414
PRMT5	0.066667	0.001189		CHORDC1	0.136667	0.002387
CTBP2	0.066666	0.001159		TFCP2	0.136667	0.002423
DHX29	0.066666	0.065512		VAPA	0.136665	0.002354
G3BP2	0.066666	0.001173		FBL	0.133334	0.264731
EDC4	0.063334	0.001072		CHCHD3	0.13	0.384614
SLC27A4	0.063334	0.001117		CPS1	0.13	0.002305
WASHC4	0.063334	0.001135		PAK4	0.129999	0.00235
RPL15	0.063332	0.244729		PHF6	0.129999	0.002245
ARFGEF1	0.06	0.001118		AHCY	0.126667	0.809166
PSMD10	0.056667	0.000968		ATP2A2	0.126667	0.805437
DDX17	0.056666	0.168132		PPP1R12A	0.126666	0.127007
HBS1L	0.056666	0.000998		SND1	0.126666	0.002205
CDC37	0.053334	0.000893		STT3B	0.126666	0.002211

MCM2	0.053334	0.087542		NUP107	0.120001	0.002085
CLASP1	0.053333	0.000953		ATXN10	0.12	0.002101
HAX1	0.053333	0.000946		SLC38A2	0.12	0.224161
TUBGCP3	0.053333	0.095521		MYO1B	0.116668	0.269857
DNAJC13	0.053333	0.058123		GLS	0.116667	0.002007
ACTR2	0.05	0.054292		HARS2	0.116667	0.002037
CKAP4	0.05	0.162681		MAIP1	0.116667	0.002015
PGM3	0.05	0.000886		MARS1	0.116667	0.610228
TUBB6	0.05	0.000852		PCID2	0.116667	0.002139
RNH1	0.046668	0.000806		PTPN9	0.116666	0.002105
DCAKD	0.046667	0.000835		TUBB6	0.113334	0.001932
PRKAR1A	0.046667	0.188716		MYH14	0.113333	0.001998
SF1	0.046667	0.000815		TRMT2B	0.11	0.001996
ATAD1	0.046666	0.000851		PPP1CA	0.109999	0.001971
NUP133	0.046666	0.000803		ATAD3A	0.106667	0.344579
STOM	0.046666	0.086678		EARS2	0.106667	0.001884
CAPN1	0.043334	0.047683		GDI2	0.106667	0.001893
CAVIN2	0.043334	0.000797		SLC25A22	0.106667	0.001869
ALDH18A1	0.043334	0.101866		DHX30	0.100001	0.249742
GLS	0.043334	0.000746		ADO	0.1	0.001632
MAGT1	0.043334	0.000708		GALK1	0.1	0.001692
CAPZB	0.043333	0.00074		POLRMT	0.1	0.001799
GATD3B	0.043333	0.000773		TRAF2	0.099999	0.001706
DDX1	0.043332	0.109473		RBM17	0.096668	0.001624
COPA	0.040001	0.176901		GPR89A	0.096667	0.001747
CBR1	0.04	0.000696		SSR4	0.096666	0.14292
PRKDC	0.04	0.231643		KYAT3	0.093334	0.001619
PSMC5	0.036668	0.103777		RAD50	0.093334	0.302389
UBE2M	0.036667	0.04087		VPS26A	0.093334	0.001655
EEA1	0.036666	0.000643		HSD17B7	0.093333	0.001632
GNA11	0.036666	0.000638		CCT8	0.090001	0.239431
RCC1	0.036666	0.000654		EEF1AKNMT	0.09	0.001624
GPSM1	0.036666	0.000631		MAP4K4	0.09	0.001575
FDXR	0.036665	0.049863		ARL1	0.09	0.29917
STRAP	0.033333	0.000584		OXSR1	0.086667	0.383326
TRIP13	0.033333	0.232959		STOM	0.086667	0.189897

WBP2	0.033333	0.000565		TOP2B	0.086667	0.001557
ABCB10	0.033333	0.086609		NUP133	0.086666	0.001491
NDUFA4	0.033333	0.00055		NUP88	0.086666	0.001491
CCT2	0.033332	0.134502		CYFIP1	0.083333	0.001476
0	0.030001	0.000516		PPFIA1	0.083333	0.001515
CYFIP1	0.030001	0.000531		RARS2	0.083333	0.001456
PGD	0.03	0.00051		PGD	0.083333	0.001415
CAP1	0.029999	0.000517		CNN3	0.080001	0.034148
DDX3X	0.029999	0.184256		ABCB10	0.08	0.191472
FXR2	0.029999	0.016304		IARS2	0.08	0.060042
ZNF622	0.029999	0.000508		HNRNPL	0.079999	0.001383
MAP2K2	0.026667	0.000451		RUVBL2	0.079999	0.136098
COPE	0.026667	0.000468		NEFL	0.076667	0.001344
VPS51	0.026667	0.000468		SKIV2L	0.076667	0.001344
FARSB	0.026666	0.087471		TSG101	0.076667	0.001315
RPS5	0.026666	0.046297		NKRF	0.076666	0.001346
DYNC1LI 1	0.023334	0.000404		CNDP2	0.073334	0.001293
MIF	0.023334	0.098656		DNM2	0.073333	0.24347
RAB14	0.023334	0.072151		HMOX2	0.073333	0.00123
TOR1AIP 1	0.023333	0.044145		TUBGCP2	0.073333	0.001309
SUCLG2	0.023333	0.000409		RNPEP	0.073332	0.001291
PPM1F	0.023332	0.000401		RAD21	0.07	0.001206
PELO	0.02	0.000341		RRM2B	0.07	0.001186
PTPN9	0.02	0.000361		PRDX4	0.066668	0.227494
VDAC3	0.02	0.068542		CYB5R3	0.066667	0.119712
THOC2	0.02	0.000351		NUP188	0.066666	0.08768
DDX6	0.019999	0.121896		PSMD10	0.063333	0.001082
FARSA	0.016668	0.000274		SLC12A4	0.063333	0.001123
ABCD3	0.016667	0.025017		COQ8A	0.060001	0.036996
GFM1	0.016667	0.028668		CYP20A1	0.06	0.001069
PDCD6	0.016667	0.00028		GPSM1	0.06	0.001032
RRAGC	0.016667	0.000304		KCTD12	0.06	0.047505
NUBPL	0.016666	0.000284		CEP170	0.059999	0.001029
PRPF19	0.016666	0.000283		MRE11	0.056668	0.144843
VDAC2	0.016666	0.070861		H3C15	0.056667	0.000883
AGL	0.013334	0.000238		EDC4	0.056667	0.000959
ATXN10	0.013333	0.000233		PSMA3	0.053333	0.00092

RECQL	0.013333	0.052721		SCFD1	0.053333	0.000922
HNRNPH1	0.01	0.080518		DDX3X	0.053332	0.384234
UFL1	0.006667	0.008373		DDX39A	0.050001	0.097153
CMAS	0.006666	0.000116		COPE	0.050001	0.000877
PES1	0.006666	0.00012		MYH9	0.049999	0.060072
HPRT1	0.003333	0.004281		GNAS	0.046667	0.071893
CDK4	0.003333	5.68E-05		TUBB4A	0.046667	0.000822
VIM	0.003333	0.002265		CDC37	0.046666	0.000782
DNM2	6.36E-07	1.74E-06		EI24	0.046666	0.00081
EIF2S3	6.36E-07	3.52E-06		YWHAB	0.043334	0.130739
PPME1	6.36E-07	1.03E-06		ALG5	0.043334	0.040485
ARPC4	0	0		LRCH2	0.043334	0.000772
BCCIP	0	0		GNA11	0.043333	0.000754
CLIC1	0	0		PITRM1	0.04	0.000697
GNAI3	0	0		RNH1	0.04	0.000691
PAICS	0	0		AAAS	0.04	0.000687
DHX9	-6.36E-07	5.62E-06		AKAP8	0.04	0.000709
GFM2	-0.003333	5.67E-05		MRPL47	0.04	0.000727
AP3M1	-0.003333	0.009686		COPA	0.036668	0.149573
CAMK2G	-0.003333	5.83E-05		HNRNPR	0.036667	0.000636
LUC7L	-0.003333	5.99E-05		MYL6	0.036667	0.061914
PSMD1	-0.003333	5.91E-05		ZNF622	0.036667	0.000621
STAU1	-0.003333	5.93E-05		MRPS9	0.036666	0.000657
ALDOA	-0.006666	0.011442		NUP98	0.036666	0.000654
ADRM1	-0.006666	0.000115		RPL23	0.033334	0.042635
MTHFD1L	-0.006666	0.000114		PELP1	0.03	0.077301
XPO7	-0.006666	0.000114		RHEB	0.03	0.000507
IRAK1	-0.006667	0.000116		PPP6C	0.029999	0.000521
GOLGA5	-0.01	0.000165		PRPF6	0.026667	0.039765
PITRM1	-0.01	0.000174		RRAS2	0.026667	0.000449
ALDH1B1	-0.01	0.000177		CDK5RAP1	0.026667	0.000475
DNM1L	-0.01	0.012878		VPS35L	0.026667	0.000474
FASTKD5	-0.01	0.000172		OTUB1	0.023334	0.056858
FN1	-0.01	0.000169		COPB1	0.023333	0.078353
SEPTIN9	-0.01	0.000173		SPTLC2	0.023333	0.000422
SPTLC2	-0.01	0.000181		PCBP1	0.023333	0.052439
PRDX3	-0.013332	0.012952		AP3B1	0.02	0.116089

GNB1	-0.013333	0.051886		PDIA4	0.02	0.000343
HK1	-0.013333	0.096503		NCAPH	0.02	0.000355
CUL1	-0.013334	0.000234		ATP1A1	0.016668	0.185352
NUP98	-0.013334	0.000238		FUS	0.016667	0.000286
EEF1G	-0.013334	0.048485		AP3D1	0.016666	0.00029
PCBP2	-0.013335	0.078967		MTHFD1L	0.016666	0.000286
CDK5	-0.016665	0.000285		FUBP1	0.013335	0.000231
DLD	-0.016666	0.000288		TMPO	0.011667	0.000205
KDELR1	-0.016666	0.000276		PRKDC	0.010001	0.058605
SLC12A2	-0.016666	0.000297		RAB18	0.010001	0.000172
ERAP1	-0.016667	0.000291		PPP2R1A	0.009999	0.022075
SAMM50	-0.016667	0.000286		CUL2	0.006667	0.000117
EPPK1	-0.016668	0.022515		HSD17B10	0.006667	0.000116
NXF1	-0.019999	0.000344		ATP2B1	0.006666	0.000117
YBX1	-0.019999	0.000346		EIF3I	0.006666	0.000116
YWHAE	-0.019999	0.063415		SMC3	0.006666	0.02263
LAS1L	-0.020001	0.03318		FECH	0.003333	5.78E-05
SCFD1	-0.020001	0.000346		YWHAE	0.003333	0.008681
TUBB2A	-0.023331	0.060445		DYRK1A	0.003333	5.9E-05
MAD2L1	-0.023333	0.000392		ESYT2	0.003333	5.79E-05
HNRNPA2B1	-0.023333	0.088529		KARS1	0	0
CAND1	-0.026665	0.093107		MRPL10	0	0
NSF	-0.026665	0.040673		NUBP2	0	0
DNAJA1	-0.026666	0.000466		HK1	-1.91E-06	1.53E-05
HSP90AA1	-0.026666	0.333163		NCKAP1	-0.003333	0.00847
INPPL1	-0.026666	0.000459		NPEPPS	-0.003333	0.008515
ARL1	-0.026667	0.080884		MMS19	-0.006666	0.011753
CNP	-0.026667	0.037771		GLRX3	-0.006667	0.006064
PRMT1	-0.026667	0.000462		OGDH	-0.006667	0.000121
PRPSAP2	-0.026667	0.000454		POGZ	-0.006667	0.000116
PSMA3	-0.026667	0.000461		RAB11A	-0.006667	0.015251
ZC3H18	-0.026667	0.000471		ACADM	-0.006668	0.000116
HSPA4	-0.03	0.044741		CAPZB	-0.006668	0.000114
HSPH1	-0.03	0.000528		PFKP	-0.009998	0.031115
ILF3	-0.03	0.000515		CDK5	-0.009999	0.000171
NPEPPS	-0.03	0.070509		LBR	-0.009999	0.066407

PSMB2	-0.03	0.000525		SMC2	-0.01	0.02198
DPM1	-0.033334	0.118606		CUL1	-0.010001	0.000176
SUPT16H	-0.033334	0.00055		KDELR1	-0.013333	0.000221
IQGAP3	-0.033334	0.000587		MEPCE	-0.013333	0.000239
SLC38A2	-0.033334	0.03598		STK4	-0.013334	0.000228
NUP93	-0.033335	0.108513		IKBKG	-0.016666	0.000289
PURA	-0.036666	0.293767		MAT2A	-0.016666	0.000282
RAB6A	-0.036666	0.000614		MKI67	-0.016667	0.000296
PFKL	-0.036666	0.032182		ELAVL1	-0.019999	0.049589
VPS35L	-0.036666	0.000654		KRT14	-0.02	0.000341
CLPX	-0.036667	0.000636		DDX50	-0.020001	0.036876
IDH3B	-0.036667	0.07092		G3BP1	-0.023332	0.000397
PPP2R1A	-0.036667	0.055097		PTBP3	-0.023333	0.000397
TSG101	-0.036667	0.000631		PURA	-0.023334	0.204328
WDR11	-0.036667	0.000649		RAP2C	-0.026666	0.000445
MEPCE	-0.04	0.000719		MACROD 1	-0.026667	0.000477
RTN4	-0.04	0.000671		SAR1A	-0.026667	0.000441
ATP2B1	-0.040001	0.000704		EIF5B	-0.026667	0.000468
PI4KA	-0.040001	0.035106		RAB1B	-0.026667	0.000458
ERGIC1	-0.043333	0.000751		ORC5	-0.03	0.000536
U2SURP	-0.043333	0.000782		DDX5	-0.033332	0.106675
CALU	-0.043334	0.000771		VARS1	-0.036666	0.00064
ME2	-0.043334	0.00075		EIF3G	-0.036667	0.000636
PPP6R3	-0.043334	0.000783		MYG1	-0.036667	0.000624
UGGT1	-0.043334	0.000756		TBRG4	-0.036667	0.00063
CSE1L	-0.046666	0.273669		RPS6KA3	-0.04	0.150776
FLOT2	-0.046667	0.035093		TUBB2A	-0.043333	0.14334
MATR3	-0.046667	0.136683		PSMB6	-0.043334	0.000734
NFS1	-0.046667	0.000804		CTPS1	-0.046666	0.05239
TUBB3	-0.046667	0.00087		OGA	-0.046667	0.000806
DHX15	-0.046667	0.178972		PEX11B	-0.046667	0.000813
TFCP2	-0.046668	0.000832		GLO1	-0.049999	0.000889
PSPC1	-0.049999	0.061279		RAB6A	-0.049999	0.000838
RPL23A	-0.05	0.000814		GTPBP10	-0.050001	0.000892
RTRAF	-0.05	0.000884		ATP6V1H	-0.050001	0.059696
VARS1	-0.05	0.000873		LAS1L	-0.053333	0.133604
RAC2	-0.050001	0.000839		MTHFD1	-0.053334	0.108301

CYP51A1	-0.053333	0.000932		NME2	-0.053334	0.000879
RRAS2	-0.053333	0.000901		PUS1	-0.053334	0.06921
EIF2B3	-0.053333	0.000949		SRP72	-0.053334	0.000976
ATP6V1H	-0.053334	0.068934		MDN1	-0.056666	0.001032
GPI	-0.053334	0.00092		PDCD6	-0.059999	0.001012
PLEC	-0.053334	0.052866		GTF3C5	-0.06	0.00101
NSUN2	-0.053335	0.08668		PFKM	-0.060001	0.001053
CYB5R3	-0.056666	0.108842		SNRPA1	-0.060001	0.001017
GNA13	-0.056666	0.00098		ARF4	-0.063334	0.001051
NOP56	-0.056666	0.000981		PSMB2	-0.063334	0.00111
SAR1A	-0.056666	0.000938		SLC25A5	-0.063334	0.173
EXOC4	-0.056667	0.001002		POLDIP2	-0.066666	0.001161
LYAR	-0.059999	0.001044		LYAR	-0.066666	0.00116
ELAVL1	-0.06	0.152601		NMT1	-0.066666	0.248553
NUBP2	-0.06	0.001084		PES1	-0.066666	0.001202
RBM25	-0.06	0.001046		CDK4	-0.066667	0.001141
NTPCR	-0.06	0.001025		PEBP1	-0.066667	0.001118
MTHFD1	-0.060001	0.147691		SLC27A4	-0.066667	0.001179
PDIA4	-0.063332	0.001087		NUP205	-0.069998	0.166234
COPG1	-0.063333	0.444734		ACTR3	-0.07	0.143581
IMMT	-0.063334	0.324941		PSMD1	-0.07	0.001244
SLC25A5	-0.063334	0.227436		RCL1	-0.07	0.001245
SMARCA5	-0.063334	0.131578		CALU	-0.07	0.001246
AP2B1	-0.066666	0.106819		THOC2	-0.070001	0.001233
RAB8A	-0.066666	0.001159		WDR1	-0.070001	0.001236
SMC4	-0.066666	0.376807		YWHAZ	-0.073333	0.232332
ABCB7	-0.066667	0.138443		PSMA5	-0.073334	0.001284
AP3B1	-0.066667	0.479624		UBA1	-0.073335	0.417763
NCKAP1	-0.066667	0.127005		QARS1	-0.076665	0.122489
RPA1	-0.066667	0.001133		ABCF3	-0.076667	0.001342
PSMD14	-0.066668	0.108045		KIF1A	-0.076667	0.001347
AHCY	-0.069999	0.32928		NARS1	-0.076667	0.001364
PPP2R5D	-0.069999	0.001255		ROCK1	-0.076667	0.001369
ARF6	-0.07	0.001228		TRIP6	-0.076667	0.001293
LBR	-0.07	0.910155		YWHAH	-0.076667	0.001353
LMAN1	-0.07	0.075321		RAB3GAP1	-0.076667	0.044118
ORC5	-0.07	0.001253		SRRT	-0.076667	0.001354

TCP1	-0.070001	0.514005		RPS27	-0.080001	0.34592
DRG1	-0.073333	0.219984		AGPS	-0.083333	0.001465
HACD3	-0.073333	0.499579		DNMT1	-0.083333	0.0015
POLDIP3	-0.073333	0.001308		VAPB	-0.083333	0.227773
MYO1C	-0.073334	0.00135		SLC25A4	-0.083335	0.001399
AASS	-0.076666	0.001358		BASP1	-0.086666	0.001507
CKB	-0.076667	0.001324		ATP13A1	-0.086667	0.001514
RPL23	-0.076667	0.136088		ERGIC1	-0.09	0.001564
TOMM40	-0.076667	0.483377		MAD2L1	-0.09	0.001517
YWHAB	-0.076667	0.182765		NIPBL	-0.09	0.00163
RAB1B	-0.076667	0.001318		ATP6V0D1	-0.09	0.001571
MSN	-0.076668	0.001337		LIMA1	-0.09	0.001541
TARS2	-0.076668	0.001338		NIPSNAP2	-0.09	0.001558
EEF2	-0.08	0.389792		DNAAF5	-0.093333	0.001649
LRRC40	-0.08	0.392864		PSMA1	-0.093333	0.00159
ARHGAP21	-0.080001	0.001431		GPR107	-0.093334	0.001714
HADHB	-0.080001	0.308419		SLC12A7	-0.096666	0.001786
SLC25A4	-0.080001	0.001343		KIFBP	-0.096666	0.001706
TRAF2	-0.083335	0.001431		KEAP1	-0.096667	0.001707
SARS1	-0.086666	0.878351		ALG6	-0.1	0.001748
FANCI	-0.086666	0.001566		IGF2BP3	-0.1	0.576528
PSMD2	-0.086666	0.240754		MGST3	-0.1	0.001669
GTPBP6	-0.086667	0.001614		HM13	-0.103333	0.001791
MYO6	-0.086667	0.37609		COQ5	-0.103333	0.001799
PSMB5	-0.086667	0.001497		RAB9A	-0.103333	0.001776
SLC25A1	-0.086667	0.559434		MSH2	-0.103334	0.483209
CCDC88A	-0.09	0.001621		ATP5PB	-0.106665	0.001799
TRMT5	-0.09	0.001571		HSPH1	-0.106667	0.001884
TUBB4A	-0.09	0.001592		TBC1D4	-0.106667	0.001864
IGF2BP2	-0.093332	0.300175		UGGT1	-0.106667	0.001869
PDHA1	-0.093332	0.001561		SSR3	-0.106667	0.001822
CDIPT	-0.093333	0.001658		0	-0.109999	0.001905
DHX57	-0.093333	0.001738		HLA-B	-0.109999	0.001896
LRCH2	-0.093333	0.001674		UBE2M	-0.109999	0.107145
PSMD4	-0.093333	0.001569		RBFOX2	-0.11	0.001933
SMC2	-0.093333	0.193322		TBCB	-0.113333	0.002005

HSD17B4	-0.093334	0.384051		CDC27	-0.116666	0.002072
SAFB2	-0.096666	0.001726		RPL36AL	-0.116666	0.00195
CALR	-0.096667	0.12694		SAFB2	-0.116666	0.002086
SNRNP200	-0.096667	0.478669		MIPEP	-0.116667	0.002119
EIF4A1	-0.099999	0.450757		IPO4	-0.123333	0.002124
G3BP1	-0.099999	0.00171		NCLN	-0.123333	0.002167
CNN3	-0.1	0.062658		CTBP2	-0.123334	0.002154
ROCK1	-0.1	0.001789		OPA1	-0.123334	0.002152
RPS18	-0.1	0.225649		HNRNPC	-0.126667	0.002136
EEF1A2	-0.103333	0.001829		MOB1B	-0.126667	0.002215
HSP90AB1	-0.103333	1.474701		EIF3D	-0.129999	0.386222
PNP	-0.103333	0.001814		DRG2	-0.129999	0.002296
UHRF1	-0.103333	0.001838		TTLL12	-0.129999	0.18672
PSMD11	-0.106667	0.001832		LMNB1	-0.13	0.002269
TMEM33	-0.106667	0.289946		SEPTIN9	-0.13	0.002254
RPL9	-0.106668	0.677837		CAP1	-0.13	0.002257
TBL2	-0.109999	0.001918		RPN1	-0.133333	1.51443
DHX30	-0.11	0.443874		SLC25A1	-0.133333	1.336644
DNAJB1	-0.11	0.001832		WDR26	-0.133334	0.002371
PEBP1	-0.110001	0.001849		XPO5	-0.133334	0.00241
PRPF8	-0.110001	0.291822		DLD	-0.136666	0.002375
MYH9	-0.110001	0.188447		TUBA1B	-0.136666	0.178446
RPL26L1	-0.113333	0.001869		FLOT2	-0.136667	0.11822
ESYT2	-0.113333	0.001976		NAA10	-0.136667	0.002314
MAP2K1	-0.113333	0.001918		PNPLA6	-0.136667	0.002403
DYNLL1	-0.113334	0.001978		PRMT1	-0.136667	0.002376
ATP6V0D1	-0.113335	0.00198		YARS1	-0.136667	0.002365
SF3B1	-0.116666	0.237135		ATP6V1A	-0.136668	1.109464
SEC61A1	-0.116666	0.757744		DHRS2	-0.139999	0.002441
AAAS	-0.116667	0.002013		PELO	-0.143332	0.002463
BASP1	-0.116667	0.002032		ACADVL	-0.143333	0.152851
NUP88	-0.116667	0.002023		SLFN11	-0.143333	0.002512
RPS23	-0.116667	0.244698		CLTA	-0.146666	0.002492
ARAF	-0.116667	0.002165		LIPA	-0.146666	0.002539
RPN2	-0.116667	1.923727		ARF5	-0.146667	0.002486
GSTP1	-0.12	0.883938		RTCB	-0.146668	0.153481

TUBG1	-0.12	0.276845		ATL2	-0.15	0.002533
RPL19	-0.123332	0.002037		SEC61A1	-0.153333	0.652022
ASNS	-0.123333	0.002126		EFTUD2	-0.153334	0.00268
CEP112	-0.123333	0.002093		SURF4	-0.153334	0.427246
ARF4	-0.123334	0.002051		HMGCS1	-0.153334	0.002651
RUFY1	-0.123334	0.002205		NFS1	-0.153334	0.002659
DIS3	-0.126666	0.002181		DCAKD	-0.156666	0.002833
PNPLA6	-0.126666	0.002226		PPA1	-0.156667	0.233571
SMARCC2	-0.126666	0.002273		PSMB5	-0.156667	0.002718
NAA10	-0.126667	0.002143		RPL9	-0.156667	0.757377
SERPINH1	-0.129999	0.860587		TUBB	-0.156667	0.281812
SMS	-0.129999	0.176666		ZC3H18	-0.156667	0.00279
ATP2A2	-0.13	1.208504		HNRNPH3	-0.159999	0.438677
MRPL10	-0.13	0.002336		UBLCP1	-0.159999	0.002725
PFKP	-0.13	0.555504		CMAS	-0.16	0.002815
PSMA1	-0.13	0.002218		RPS23	-0.16	0.320534
MCM4	-0.13	0.513491		UCHL1	-0.16	0.002685
MCM7	-0.13	1.494241		RAB1A	-0.160001	0.00274
ALDH9A1	-0.133333	0.002259		HSPE1	-0.163334	0.002887
SLC12A7	-0.133333	0.002469		RPL15	-0.163334	0.580171
MRPS17	-0.133333	0.002285		YARS2	-0.163334	0.248288
HNRNPK	-0.136667	0.851885		PIGT	-0.166666	0.665858
DSTN	-0.136667	0.14048		RAB2A	-0.166666	0.002916
GMPS	-0.136668	0.002346		ALG10	-0.166667	0.002864
ADAR	-0.139999	0.284441		RPS6	-0.166667	1.540387
CUL2	-0.139999	0.002475		LRRC40	-0.169999	0.561458
RPL34	-0.14	0.620432		PDLIM7	-0.169999	0.002993
MRPS2	-0.143333	0.002478		ARPC4	-0.17	0.002991
NIPBL	-0.143333	0.002605		DDX18	-0.17	0.002851
ILF2	-0.149999	0.724022		HDHD5	-0.17	0.210419
MYL12B	-0.149999	0.002578		MBOAT7	-0.176666	0.003102
SETSIP	-0.149999	0.002506		PSMC5	-0.176666	0.562192
DRG2	-0.15	0.002652		AFG3L2	-0.176667	0.282562
ECHS1	-0.15	0.002632		FLOT1	-0.176668	0.196975
TMTC3	-0.15	0.002641		ILVBL	-0.18	0.214891
ATP13A1	-0.15	0.002627		NUP85	-0.183333	0.247441

GNAS	-0.15	0.404385		PRRC2A	-0.183334	0.003079
MRPS5	-0.15	0.002571		TIMM50	-0.183334	0.593106
XPO5	-0.15	0.002714		CAND1	-0.186667	0.905983
TIMM50	-0.153332	0.67805		HAX1	-0.186667	0.003336
NACA	-0.153333	0.002661		CYP51A1	-0.19	0.003347
G6PD	-0.153334	0.317468		PPM1F	-0.19	0.003306
YTHDC1	-0.153334	0.002687		PRPF19	-0.19	0.003261
ANAPC7	-0.153334	0.002849		SMC1A	-0.19	1.972436
ARF3	-0.156666	0.002661		AIFM1	-0.190001	0.700718
PDS5B	-0.156666	0.52096		CSE1L	-0.190001	0.8971
RPS27	-0.156667	1.117784		PDE12	-0.190001	0.003487
SF3B3	-0.156667	0.002748		FARSB	-0.193334	0.75088
SUGP2	-0.156667	0.002696		FXR2	-0.193334	0.099796
SMC3	-0.159999	0.863762		TMEM33	-0.193334	0.505734
SLC25A11	-0.16	1.140137		BRIX1	-0.196667	0.003373
ZNF326	-0.16	0.317599		CAPN1	-0.199998	0.157845
IPO9	-0.160001	0.237569		GSTO1	-0.2	0.003361
PRKCSH	-0.160001	0.002806		MYL12B	-0.2	0.003447
MAGED1	-0.163333	0.002848		RCC2	-0.2	0.003512
SNTB2	-0.163333	0.002929		PDHX	-0.200001	0.003475
TBRG4	-0.163333	0.002822		SUPT16H	-0.200001	0.003332
EIF4A3	-0.163334	0.802912		TMTC3	-0.203334	0.003588
RFC2	-0.163334	0.002792		DHX9	-0.203335	2.596792
NELFB	-0.166665	0.002996		CLIC1	-0.206666	0.003544
TMEM97	-0.166666	0.002727		ILF3	-0.206666	0.003585
ARCN1	-0.166667	0.887682		EIF2AK2	-0.206667	0.600414
PPFIA1	-0.166667	0.003065		SLC25A11	-0.206667	1.976928
PDHX	-0.166667	0.002892		RPL18A	-0.209999	0.813756
STK4	-0.166667	0.002873		ADAR	-0.21	0.488912
YARS1	-0.166667	0.002889		PSMD4	-0.21	0.003553
CCT6A	-0.166668	1.642502		RPL19	-0.213333	0.003536
SRP68	-0.169999	0.002952		TECR	-0.213333	0.959132
ATAD3A	-0.17	0.473559		LMF2	-0.213333	0.003541
IGF2BP3	-0.17	0.932258		RBM25	-0.213333	0.003742
CCT3	-0.170001	1.696147		RTRAF	-0.213333	0.003798
FTL	-0.170001	0.002939		NFKB2	-0.213334	0.003761
PIGT	-0.173332	0.478279		PRMT3	-0.213334	0.003765

ALG6	-0.173333	0.003039		DIMT1	-0.213334	0.003723
CALCOCO1	-0.173334	0.003091		DLAT	-0.216665	0.902504
RPL35A	-0.173334	0.002833		MAP2K2	-0.216666	0.003692
RTCA	-0.173334	0.479035		DDX47	-0.216667	0.272655
HNRNPA0	-0.173334	1.173626		PNP	-0.216667	0.003828
LDHA	-0.173334	0.803627		RPS11	-0.219999	1.031356
ATP1A1	-0.176666	1.692225		ALDH9A1	-0.22	0.003746
AGPS	-0.176666	0.003117		MTREX	-0.22	0.003929
RAB18	-0.176666	0.003062		RAB35	-0.22	0.003867
SGPL1	-0.176666	0.003025		KANK1	-0.220001	0.003843
NIPSNAP2	-0.176668	0.003074		DDX19A	-0.223333	0.00389
TCOF1	-0.176668	0.003089		MSN	-0.223333	0.003916
TUBB	-0.176668	0.456232		MRPS17	-0.223334	0.003846
PPIB	-0.18	0.003106		RPL37A	-0.223334	0.003584
PSMD7	-0.18	0.003201		ETF1	-0.226666	1.41609
RAB2A	-0.18	0.003151		ANAPC7	-0.226667	0.00423
SFPQ	-0.18	0.736095		RAB5C	-0.226667	0.57166
WDR26	-0.18	0.00321		TUBG1	-0.226667	0.707507
PDIA3	-0.180001	0.523867		HSPA4	-0.226669	0.680472
PTPMT1	-0.180001	0.003138		SETSIP	-0.23	0.00386
PSMD3	-0.183332	1.087851		AGAP3	-0.233334	0.003999
CHD4	-0.183333	0.886934		CDK9	-0.233334	0.004003
HMGCS1	-0.183333	0.003175		RFC2	-0.233334	0.004005
FSCN1	-0.183334	0.817702		XPO7	-0.233334	0.004024
MRPL47	-0.183334	0.003358		MRPS2	-0.236666	0.004107
TRAP1	-0.183334	1.253783		SUCLG1	-0.24	0.249942
MARS1	-0.186666	0.790713		MSH3	-0.24	0.004345
RCL1	-0.186666	0.003336		NSUN2	-0.240001	0.800007
RARS2	-0.186667	0.003285		ELAC2	-0.243332	0.004175
TOMM70	-0.186667	0.003342		DHX40	-0.243333	0.004377
ATP2C1	-0.186667	0.003236		NACA	-0.243333	0.004245
LRP1	-0.186668	0.09018		ARF6	-0.243334	0.004313
TUBB4B	-0.189999	0.744409		LYN	-0.243334	0.004179
HNRNPH2	-0.19	0.291722		SDHA	-0.243334	0.283132
MMUT	-0.19	0.003553		SLC25A6	-0.243334	0.662307
TMPO	-0.19	0.003382		HSP90AB	-0.246665	2.081466

				1		
CCT4	-0.190001	1.103459		ECHS1	-0.246667	0.004353
NONO	-0.190001	0.822399		SLC25A3	-0.246667	1.425048
CUL4B	-0.193333	0.195269		PSMD11	-0.246669	0.004259
RHOT2	-0.193333	0.003419		RPL23A	-0.249999	0.004098
MBOAT7	-0.193333	0.003398		RCC1	-0.25	0.004528
TRIP12	-0.193333	0.003391		SRP68	-0.25	0.004355
PFKM	-0.193334	0.003412		PRKCSH	-0.250001	0.004407
XPO1	-0.193334	0.810618		ATP5PO	-0.253332	0.521161
GSTO1	-0.196666	0.003305		CDIPT	-0.253333	0.00453
AKAP13	-0.196667	0.003484		BCCIP	-0.253333	0.00446
CDK9	-0.196667	0.003369		TRMT10C	-0.253333	0.602248
HARS2	-0.196667	0.003481		COPG1	-0.256667	1.854973
KNTC1	-0.196667	0.003489		PCBP2	-0.256668	1.565382
RPL18A	-0.199999	1.113566		TCOF1	-0.256668	0.004501
CCT7	-0.2	0.857446		DNAJA3	-0.26	0.004716
ITGB1	-0.2	0.003585		ERLIN2	-0.26	1.378084
MAIP1	-0.2	0.00348		MAP2K1	-0.26	0.004424
ACAA2	-0.200001	0.003363		ME2	-0.260001	0.00454
RPS11	-0.203332	1.310949		ADRM1	-0.263332	0.004575
BUB3	-0.203332	0.003459		HACD3	-0.263332	1.478969
YWHAZ	-0.203333	0.846411		HSPB1	-0.263333	1.087708
EIF5B	-0.203334	0.003593		H1-2	-0.263334	0.004303
OGDH	-0.203334	0.003728		GTF2I	-0.263334	0.004647
SEC61B	-0.203334	0.00354		CCT2	-0.266666	1.532709
UBLCP1	-0.203334	0.003469		SLC25A24	-0.266666	0.004544
MDH1	-0.206666	0.00347		TEX10	-0.266666	1.43905
FLOT1	-0.206668	0.242925		ACTC1	-0.269999	0.004522
GTF2I	-0.206668	0.003635		SERPINH1	-0.27	1.34827
PEX11B	-0.206668	0.003635		CLPTM1L	-0.270001	0.00476
GOT2	-0.209999	0.00365		GNA13	-0.270001	0.004729
ABCF3	-0.21	0.003696		LDHA	-0.270001	0.81853
HNRNPA1	-0.21	1.445805		ABCB7	-0.273333	0.411993
HSPA5	-0.21	1.374373		MPRIP	-0.273333	0.004664
CDK1	-0.21	0.486939		APMAP	-0.276666	0.004682
PDLIM7	-0.21	0.003706		CEP112	-0.276666	0.004737

RBBP4	-0.210001	0.00369		EIF5A	-0.276667	0.873333
DEK	-0.213333	0.003672		BZW1	-0.279999	1.536343
KEAP1	-0.213333	0.003792		DRG1	-0.279999	1.395306
MSH3	-0.213334	0.003857		GNB1	-0.28	2.071188
RPSA	-0.213334	0.82509		RAB32	-0.28	0.441112
STAT3	-0.213334	0.003747		APRT	-0.283333	0.00483
CAT	-0.213334	0.003616		EEF2	-0.283333	2.256713
ALDH2	-0.216666	0.110338		NXF1	-0.283333	0.004918
DDX19A	-0.216666	0.003772		DDX42	-0.283334	0.004981
PPP2R2D	-0.216666	0.003697		HNRNPA 2B1	-0.283334	1.523298
HNRNPF	-0.216667	2.661235		TRMT5	-0.283334	0.005
RPL10	-0.216667	0.936166		KHDRBS1	-0.286666	0.630071
CSK	-0.219999	0.003868		PPP2R2D	-0.286666	0.004911
PC	-0.219999	0.914322		U2SURP	-0.286667	0.00525
RPL21	-0.219999	1.120715		ERLIN1	-0.286668	0.391018
TM9SF3	-0.219999	0.00375		IGF2BP2	-0.289999	0.854218
MCM6	-0.22	1.177079		MIF	-0.289999	1.947461
RAB1A	-0.22	0.003777		TUBB4B	-0.289999	0.855457
RPL32	-0.22	0.003605		C1QBP	-0.29	0.00494
TBCB	-0.220001	0.003909		ERAP1	-0.290001	0.005126
GLRX3	-0.223333	0.25345		RPL3	-0.293333	1.036147
NUP85	-0.223333	0.230046		AKR7A2	-0.293334	0.005365
DDOST	-0.223333	0.901927		DNAJB1	-0.293334	0.004936
GTPBP1	-0.226666	0.004009		SUCLA2	-0.293334	0.772286
KIF1A	-0.226666	0.004008		TCP1	-0.293334	2.124908
PCNT	-0.226666	0.004045		TMEM97	-0.293334	0.004821
TUFM	-0.226666	0.277386		YTHDC1	-0.293334	0.005182
MOB1B	-0.226667	0.003987		AKAP13	-0.296667	0.005287
SSX2IP	-0.226667	0.004118		H1-10	-0.296667	0.005314
SRSF4	-0.226667	0.003889		SMARCA 5	-0.296667	0.844334
AASDHP PT	-0.23	0.003971		ZNF326	-0.296667	0.622838
DHRS7B	-0.23	0.686707		MRPL16	-0.296667	0.00503
MAPK1	-0.230001	0.003963		PSMD13	-0.296667	0.005162
RBM14	-0.230001	0.746654		CBR1	-0.3	0.005279
VPS4B	-0.230001	0.65536		DHRS7B	-0.3	0.79921
CDC27	-0.233333	0.004173		PKP2	-0.300001	0.343672

HNRNPA3	-0.233333	0.003975		DDX54	-0.303333	0.005443
MYH14	-0.233333	0.004151		PDHA1	-0.303333	0.005112
AIFM1	-0.233334	0.790013		CAT	-0.306667	0.005226
APMAP	-0.233334	0.003939		PHB2	-0.306667	1.415536
H1-2	-0.233334	0.003806		STRAP	-0.306667	0.005433
MRPS22	-0.233334	0.004118		PRKAR2A	-0.306667	0.005393
DDX18	-0.236666	0.003979		SUGP2	-0.310001	0.005366
ATP5PB	-0.236666	0.00402		PRPS1	-0.313332	0.005341
PRDX6	-0.236666	1.847622		GFM1	-0.313334	0.723119
RPL8	-0.236666	1.344343		FMR1	-0.316666	0.387663
RPN1	-0.236667	1.731406		CLPB	-0.316667	0.005574
VWA8	-0.239999	0.004324		EIF2S1	-0.316667	0.005319
ACTR3	-0.24	0.660016		MT-CO2	-0.316667	1.851512
MYL6	-0.24	0.794463		XPO1	-0.316668	1.574493
SKIV2L	-0.24	0.004272		USP7	-0.319998	1.430911
GTPBP10	-0.24	0.004317		ALDH1B1	-0.32	0.005722
ATP5F1B	-0.240001	1.181386		RAB5B	-0.32	0.005436
SMC1A	-0.240001	1.728863		RPL35A	-0.32	0.005258
SSR3	-0.240001	0.004121		ZC3HAV1	-0.32	0.666266
MT-CO2	-0.243333	1.005616		DIS3	-0.323333	0.005609
PHB2	-0.243334	1.470735		FANCI	-0.323333	0.005927
RPL3	-0.246667	0.715051		RPL34	-0.323333	0.979994
ARL8A	-0.246667	0.004423		ACAA2	-0.326666	0.005518
GANAB	-0.246667	0.902608		RIF1	-0.326667	0.005878
PCCA	-0.246667	2.129177		TRAP1	-0.326667	1.632673
OAT	-0.246668	0.66701		FBXO22	-0.330001	0.005702
RPL4	-0.249999	1.536372		GSTP1	-0.330001	1.793028
RPS15A	-0.249999	2.042027		RBBP4	-0.330001	0.005825
XPOT	-0.249999	0.206254		FARSA	-0.333333	0.005581
AP2A2	-0.25	0.004402		PPIB	-0.333333	0.005786
CDK2	-0.250001	0.004228		NOP56	-0.333334	0.005835
PSMA7	-0.253332	0.76446		PMPCB	-0.333334	0.740429
AGAP3	-0.253333	0.004347		DDX17	-0.336666	1.021104
DHRS2	-0.253333	0.004437		TOP2A	-0.336666	0.005821
GPR89A	-0.253333	0.004656		MAGT1	-0.336667	0.005565
HNRNPM	-0.253333	1.735078		RPL21	-0.34	1.2082
LIMA1	-0.253333	0.004379		RPS15A	-0.34	1.99057

RPS2	-0.253333	1.204061		SLC25A10	-0.34	0.726623
UQCRC2	-0.253333	1.28268		DPM1	-0.340001	1.443226
CEP170	-0.253334	0.004413		GSPT1	-0.343333	0.00606
EEF1A1	-0.256668	1.096626		SGPL1	-0.343333	0.005916
ATP5MG	-0.259999	0.004423		UHRF1	-0.343333	0.006166
BRIX1	-0.26	0.004471		YTHDF2	-0.343334	0.005981
CDK5RAP1	-0.26	0.004708		MPDU1	-0.346667	0.006123
MPDU1	-0.26	0.004576		USP14	-0.346668	0.747187
EIF2S1	-0.263333	0.004414		CSK	-0.349999	0.006185
IDH2	-0.263333	0.676276		ILF2	-0.349999	1.525433
MDN1	-0.263333	0.004856		SF3B1	-0.353333	1.365416
LMNB1	-0.263334	0.00462		RPL13	-0.356666	0.557953
NKRF	-0.263334	0.004673		EIF2S3	-0.356667	2.36486
RPL27	-0.263334	1.062041		HNRNPF	-0.356667	3.013191
RPS24	-0.263334	1.066956		NELFB	-0.359999	0.006522
RAB35	-0.266666	0.004695		ACADSB	-0.36	1.31936
LYN	-0.266666	0.004586		HNRNPH1	-0.360001	2.398699
DDX42	-0.266667	0.004684		PDCD4	-0.363333	0.363724
MCM3	-0.266667	0.975395		POLA1	-0.363333	0.964168
TPR	-0.266668	0.240109		RAB10	-0.363333	0.006198
AARS2	-0.269999	0.00464		SLC25A12	-0.363333	0.00656
PAFAH1B3	-0.269999	1.411951		ZADH2	-0.363333	0.006448
DNAJA3	-0.27	0.0049		FSCN1	-0.366667	1.819949
NDUFA10	-0.27	0.788288		RPS24	-0.366667	1.999757
POGZ	-0.27	0.004782		NDUFS1	-0.369999	0.006541
POLDIP2	-0.27	0.004738		LONP1	-0.37	0.731223
PRKACA	-0.27	1.177523		MCM6	-0.37	1.577
RPS9	-0.27	1.707056		RPS26	-0.37	2.04036
SLC25A3	-0.27	1.655719		DEK	-0.37	0.006426
AP3D1	-0.270001	0.00474		SMAD5	-0.37	0.006569
DIMT1	-0.270001	0.004722		YWHAG	-0.37	0.006316
EIF4A2	-0.273333	0.004654		EIF4A1	-0.373333	1.27207
RPS26	-0.273333	1.801443		IDH2	-0.373333	1.245359
TRMT10C	-0.273333	0.883881		NONO	-0.376665	1.39262
RAN	-0.276665	1.940202		RPL26L1	-0.376666	0.006273

ATP5F1C	-0.276666	1.087304		HSD17B12	-0.38	1.017609
MLEC	-0.276666	0.004764		MCM7	-0.38	2.470555
CRNKL1	-0.276667	0.004942		MRPS22	-0.38	0.006745
RPL26	-0.276668	2.127057		RAB8A	-0.38	0.006688
DARS2	-0.279999	0.649699		PRDX3	-0.383333	0.575856
ACAT1	-0.28	1.420324		IDH3B	-0.383333	0.586717
ENO1	-0.28	0.950908		POLDIP3	-0.383333	0.006923
GCC2	-0.28	0.005338		PRPF8	-0.383335	1.340954
ANXA5	-0.280001	0.543087		IDH3A	-0.386666	0.893846
MGST3	-0.280001	0.004704		PGM3	-0.393333	0.007076
ACADVL	-0.283332	0.238205		TIGAR	-0.393333	1.142309
COQ5	-0.283332	0.004966		POLD1	-0.393334	0.549153
RPL28	-0.283332	1.098399		TIMM44	-0.396666	1.147124
ACTN1	-0.283333	0.005073		AP2A2	-0.396666	0.007045
ACSF3	-0.283334	0.004925		SMARCA1	-0.396666	0.006854
HMOX2	-0.283334	0.004802		PRPSAP2	-0.396667	0.006855
PAPOLA	-0.283334	0.005023		TM9SF3	-0.399999	0.006864
VDAC1	-0.283334	0.675213		MLEC	-0.4	0.00692
FBL	-0.286666	1.084439		RPL28	-0.403333	2.109473
HSDL2	-0.286667	1.402311		HNRNPA3	-0.403334	0.006916
LDHB	-0.286667	1.365857		HSP90AA1	-0.406666	3.301791
OPA1	-0.286667	0.005048		RPA2	-0.406666	0.006783
PMPCB	-0.286667	0.659867		SLC16A1	-0.406666	1.017061
SBDS	-0.286667	0.004982		RPL17	-0.406667	2.752296
SULT1A1	-0.286668	0.004853		CALCOCO2	-0.41	0.007041
LRPPRC	-0.293332	1.098053		MIA3	-0.41	0.007224
PRPS1	-0.293332	0.004996		POLR2A	-0.41	0.007305
PCCB	-0.293334	1.634229		ATP5F1C	-0.413333	1.271532
PSMD12	-0.293334	0.005072		MMTAG2	-0.413334	1.31472
HNRNPU	-0.296667	1.637423		VDAC1	-0.413334	1.093645
RPA2	-0.296667	0.004919		PHB	-0.416666	1.933127
KHDRBS1	-0.299998	1.11688		CHD4	-0.416667	1.343929
EIF3F	-0.299999	0.827567		EEF1B2	-0.416667	0.007065
WDR18	-0.299999	1.82797		PSMD12	-0.416668	0.007238
HSPA9	-0.3	1.080949		MCM2	-0.42	1.367145

RPS6	-0.3	2.106797		PSMA4	-0.42	1.187286
TARDBP	-0.3	1.546713		BUB3	-0.426667	0.007321
ACACB	-0.300001	1.256641		GARS1	-0.426667	1.375277
CKMT1A	-0.300001	1.100787		RPL38	-0.426667	2.103988
PRKAR2A	-0.300001	0.005274		SARS1	-0.426667	3.3708
PTBP1	-0.300002	0.945045		WDR3	-0.43	1.267568
BZW1	-0.303333	1.61622		GLUD1	-0.433332	0.860236
HDAC1	-0.303333	2.19685		ETFA	-0.433334	1.709464
HNRNPC	-0.303335	0.00515		RPS18	-0.433334	1.403997
MCCC2	-0.306666	1.48484		EEF1A2	-0.436667	0.007883
SLC1A5	-0.306666	0.51447		PCNT	-0.436667	0.007889
RPL17	-0.306667	2.556734		PYGB	-0.436667	1.485517
RPS3	-0.306667	2.779954		TRIP12	-0.436667	0.007767
DHX40	-0.31	0.005591		FAM98A	-0.436668	0.007499
NAMPT	-0.31	0.948956		MTPAP	-0.439999	2.302588
PCID2	-0.31	0.005755		HSPA9	-0.44	1.966053
SFXN1	-0.31	0.999465		STAG2	-0.440001	0.007903
TRMT2B	-0.31	0.005742		EEF1A1	-0.440001	1.660971
RPL14	-0.310001	1.452036		TRIM28	-0.443332	1.718875
ATIC	-0.313332	0.632049		RPS3	-0.443333	3.288662
SDHA	-0.313334	0.382086		ATP5MG	-0.446665	0.007652
EIF2AK2	-0.313334	1.465336		EXD2	-0.446667	0.007815
YARS2	-0.313335	0.824308		PDS5B	-0.446667	1.289864
DDX46	-0.316666	0.84955		ARHGDIA	-0.453332	0.00788
H3C15	-0.316666	0.00502		RPS2	-0.453333	2.582238
SUCLA2	-0.316666	1.041707		ACO2	-0.456666	0.007898
PRRC2A	-0.316667	0.005358		EIF4A2	-0.456666	0.007829
QARS1	-0.319998	0.926807		CCT3	-0.459999	3.858365
PHB	-0.32	1.66797		CCT5	-0.459999	2.192951
PYCR1	-0.32	0.005541		PSMD7	-0.46	0.008272
PRIM1	-0.32	0.005604		ACOT9	-0.460001	1.934925
HARS1	-0.320001	0.005514		GANAB	-0.460001	1.718799
GARS1	-0.323333	1.476245		DHX15	-0.463333	1.48343
RPL7A	-0.323333	1.404409		GOT2	-0.463333	0.008133
SHMT2	-0.323334	0.941327		RPS8	-0.463333	1.715185
SLC25A10	-0.323334	0.922325		AHSA1	-0.463334	0.007825
RPL38	-0.323335	2.239108		ERAP2	-0.463334	1.106417

DNAAF5	-0.326666	0.005826		RPL4	-0.463334	2.185503
PMPCA	-0.326666	0.295984		SSRP1	-0.463334	0.008031
RAB10	-0.326666	0.005564		NAMPT	-0.466667	1.952596
EIF3A	-0.326667	0.333193		CCT6A	-0.466669	3.263239
RAB11A	-0.326667	1.650472		ASS1	-0.469999	2.498381
RPL13A	-0.326668	1.589992		RO60	-0.469999	3.867993
RPL7	-0.329999	1.588659		NDRG1	-0.47	2.195814
NUP62	-0.330001	0.005788		SFXN1	-0.47	1.253705
PRDX4	-0.330001	0.850973		H2BC12	-0.470003	2.245652
PIK3R4	-0.333333	0.006026		DECR1	-0.473333	0.008428
NDUFA13	-0.333333	0.005858		RPL6	-0.473333	1.976098
OXCT1	-0.333333	1.266733		RPS3A	-0.473333	1.96849
RPS4X	-0.333333	2.185635		TARDBP	-0.473333	2.180547
CLTA	-0.336666	0.005782		CDK16	-0.476667	0.008364
NUP205	-0.336666	1.337968		HSPA5	-0.476667	2.79836
TSFM	-0.336666	0.491295		MATR3	-0.476667	1.864826
CLPTM1L	-0.336667	0.00595		BCKDK	-0.483332	0.008416
CYB5R1	-0.34	0.005741		PDK3	-0.483334	1.953732
RPL37	-0.34	2.231251		SULT1A1	-0.49	0.008358
TECR	-0.34	1.760165		HNRNPU	-0.490001	2.403315
CCT5	-0.343334	1.445163		HSDL2	-0.493333	1.759972
DSP	-0.343334	0.416744		ARF3	-0.493333	0.008488
SLC25A12	-0.343334	0.006191		UQCRC2	-0.493333	1.929784
CORO7	-0.343335	0.323313		RPL13A	-0.496667	1.979704
SLC25A6	-0.343336	1.333589		RPRD1B	-0.496667	0.008765
RPS8	-0.346665	1.751012		ACAT1	-0.499999	1.860824
ACOT9	-0.346666	1.589195		PRKACA	-0.5	1.620496
RAB5B	-0.346666	0.005895		NTPCR	-0.500001	0.008687
IKBKG	-0.346667	0.006117		SLC1A5	-0.500001	0.729669
ACACA	-0.349999	1.955366		RFC5	-0.503332	2.077557
RPL13	-0.35	0.820153		AK2	-0.503333	0.008738
ATP2B4	-0.35	0.006194		PDHB	-0.503333	0.008577
HNRNPUL1	-0.35	0.006129		PSMA6	-0.503333	2.645819
XRCC5	-0.35	1.743093		GTF3C4	-0.503334	1.134219
LMF2	-0.353333	0.005909		HNRNPA0	-0.503334	2.075201
MRPL16	-0.353334	0.00601		PSMA7	-0.506666	1.574372

RPLP0	-0.353334	1.275714		RPS9	-0.506666	2.769361
RPS3A	-0.356667	2.064491		ACTR1A	-0.506667	0.008818
MYO1B	-0.359999	1.515176		SYNE2	-0.506667	0.362193
ATP5F1A	-0.36	1.450668		LRPPRC	-0.506667	1.573333
HADHA	-0.36	0.686956		STT3A	-0.506667	1.412295
RAB21	-0.36	0.987328		RPL24	-0.509999	2.334537
PDE12	-0.360001	0.006676		RPL7A	-0.513333	2.411824
PSMA6	-0.360001	2.208575		IDH3G	-0.513334	0.498464
RACK1	-0.363332	2.380243		RPL32	-0.513334	0.008501
ERAP2	-0.363333	0.864937		SSB	-0.513334	0.008938
KHSRP	-0.366669	1.05663		LDHB	-0.513334	2.240234
DLAT	-0.369999	1.586873		NDUFA4	-0.513334	0.008636
ASS1	-0.37	1.674208		PRDX6	-0.513334	3.344715
PYGL	-0.37	0.979817		HNRNPAB	-0.516667	1.528472
IGF2BP1	-0.370001	2.243868		MDH1	-0.516667	0.008775
ACTC1	-0.373332	0.006276		CCT4	-0.52	2.878682
SLC25A24	-0.373334	0.006387		SF1	-0.52	0.009364
IPO8	-0.373334	0.006574		TOP1	-0.523333	0.009132
PARP1	-0.38	1.658889		HNRNPK	-0.523335	2.142821
POLRMT	-0.38	0.007006		NDUFA13	-0.526666	0.009359
SLC2A3	-0.383333	1.113446		PRPF31	-0.526667	0.009293
MCCC1	-0.383334	2.472681		MCM4	-0.526667	1.494296
TEX10	-0.383334	1.709553		PDIA6	-0.529999	2.478783
ALDH7A1	-0.386667	0.666904		PPME1	-0.529999	1.175577
HSPE1	-0.386667	0.006925		P4HB	-0.530001	3.106798
CHCHD3	-0.389999	1.885545		DARS2	-0.536665	1.167858
EFTUD2	-0.389999	0.00688		HADHA	-0.536666	1.525329
ACADSB	-0.390001	1.605395		RPL22	-0.536666	2.128342
NDUFS1	-0.390001	0.006902		TPP2	-0.54	0.009448
ALG5	-0.393333	0.804744		GPI	-0.54	0.009491
PDIA6	-0.393333	1.755513		IGF2BP1	-0.54	2.430807
CTPS1	-0.393333	0.488612		NDUFA10	-0.543333	1.786117
DECR1	-0.396666	0.007042		SF3B3	-0.543333	0.009676
SSB	-0.396666	0.006861		FDXR	-0.543334	1.190295
NUDT19	-0.4	0.007213		RPS5	-0.543334	1.946597
SUCLG1	-0.4	0.703878		MYH10	-0.543335	0.925334
C1QBP	-0.400001	0.006843		EEF1G	-0.546667	2.394151

TRIM28	-0.403332	1.516125		RECQL	-0.550001	1.814647
PSMA4	-0.403334	1.409259		RPS12	-0.550001	2.42176
GLUD1	-0.406666	1.08273		ACSF2	-0.553333	0.010159
UGP2	-0.406666	0.00722		KHSRP	-0.553335	1.5393
MMTAG2	-0.406667	1.598242		CFL1	-0.556666	3.203115
PYCR2	-0.406668	0.634697		SMARCA4	-0.556666	0.973509
RPL6	-0.406668	1.727038		RPL14	-0.556667	2.665108
GTF3C4	-0.410001	0.603863		DDOST	-0.556667	2.189324
HSPD1	-0.410001	2.121898		FTL	-0.556667	0.009841
ETFA	-0.410001	1.987172		CPOX	-0.56	0.009997
RPS27A	-0.410001	0.541497		GTPBP1	-0.56	0.010035
DDX39B	-0.413333	2.556855		PYGL	-0.56	1.766298
ERLIN2	-0.413333	2.029025		RPL10	-0.560001	2.567397
FEN1	-0.413333	0.763069		RPL8	-0.560001	3.38688
PRIM2	-0.413333	0.007378		ATP5F1A	-0.563333	2.483968
RPL31	-0.413333	1.71943		DDX6	-0.563334	3.83708
YWHAG	-0.413333	0.007067		RPSA	-0.563334	2.288657
MSH6	-0.416667	1.543276		HARS1	-0.570001	0.009917
RPL24	-0.416667	1.977025		HSP90B1	-0.573334	3.097479
ANKFY1	-0.42	0.007203		PSMD3	-0.576666	2.873996
CPS1	-0.42	0.007652		HNRNPA1	-0.576667	2.330591
P4HB	-0.42	3.040396		INPPL1	-0.579999	0.010192
CFL1	-0.42	2.601113		PSMD6	-0.579999	1.759005
SAFB	-0.42	0.007342		ANXA5	-0.58	1.725243
ERLIN1	-0.420001	0.709517		RPL11	-0.58	1.90051
STT3A	-0.423334	1.288899		CCT7	-0.580001	1.87043
RPL11	-0.426668	1.822722		JUP	-0.583333	1.045667
RO60	-0.433332	3.57569		ARCN1	-0.586667	2.694931
RPL22	-0.433334	1.198559		ANKFY1	-0.589999	0.010185
NCAPG	-0.436666	0.826012		PAPOLA	-0.59	0.010649
XRCC6	-0.436666	1.551293		PRPF40A	-0.59	0.011005
RPS7	-0.436667	2.7509		AASDHPPT	-0.593334	0.010388
RPS20	-0.439999	2.151267		CYB5R1	-0.596666	0.010173
IARS2	-0.440001	0.531378		SNRNP200	-0.596667	2.057996
NPM1	-0.443333	2.2202		HNRNPUL1	-0.6	0.010608

PPIA	-0.446668	0.986275		HSD17B4	-0.6	3.041036
SNRPD3	-0.45	0.00792		RPA1	-0.6	0.010408
TOP2A	-0.45	0.007813		RPLP0	-0.6	2.624511
EIF5A	-0.450001	1.079206		OAT	-0.603333	2.105528
FH	-0.453334	0.007666		CDK1	-0.603334	1.140337
HSP90B1	-0.453334	2.494049		RAN	-0.606665	3.098468
TOP1	-0.456666	0.007948		GMPS	-0.606667	0.010604
LONP1	-0.456668	1.251446		HDAC1	-0.606667	3.69456
USP7	-0.459999	1.948732		UQCRC1	-0.606667	1.69817
ATL2	-0.46	0.007904		ARGLU1	-0.606667	0.783109
COQ8A	-0.463333	0.561004		HSPD1	-0.606668	3.477691
GBF1	-0.463333	0.483349		CENPV	-0.61	1.403602
H4C1	-0.463334	0.007688		LGALS3BP	-0.613333	1.826037
NNT	-0.463334	2.308269		SAFB	-0.613333	0.010842
MIA3	-0.463334	0.008189		MCCC2	-0.616667	2.710284
RFC5	-0.466667	1.70972		G3BP2	-0.616667	0.011263
HNRNPAB	-0.469999	1.178539		PRPF4	-0.620001	0.010988
FAU	-0.47	2.662634		RPS7	-0.623333	2.774105
MCM5	-0.470001	2.869257		EIF4A3	-0.623334	2.850523
RPS13	-0.470001	1.937168		RPN2	-0.626666	4.141463
PDHB	-0.473333	0.008057		RPS16	-0.626666	3.029728
MDH2	-0.473334	0.008064		CHD1L	-0.63	0.011201
DDB1	-0.476667	0.514609		RACK1	-0.633333	3.395109
SNX2	-0.476667	2.731299		ALDH7A1	-0.633333	1.525463
SMAD5	-0.476667	0.008516		HNRNPM	-0.636666	3.277953
ACTR1A	-0.48	0.008345		ACTR2	-0.636667	0.78467
RBM39	-0.483332	1.203743		SFPQ	-0.636667	2.032718
RPS12	-0.483333	1.556309		SHMT2	-0.64	1.912568
PKP2	-0.483334	0.918451		RPL26	-0.643335	2.893942
CPOX	-0.486666	0.008663		MCU	-0.646666	0.011237
AP2M1	-0.489999	0.008297		ARHGAP21	-0.646666	0.011961
GTF3C5	-0.49	0.008452		PDIA3	-0.646667	2.590372
RPL18	-0.49	1.630219		ATP5F1B	-0.646668	3.386991
OGA	-0.493333	0.008669		TKT	-0.649999	1.308817
CHD1L	-0.493334	0.008725		PPIA	-0.67	1.123639
UQCRC1	-0.496667	1.791095		PRIM1	-0.673334	0.011956

VAPB	-0.496667	1.239242		SLC25A13	-0.673334	1.40697
POLR2A	-0.499999	0.00894		CS	-0.673334	2.012213
DDX54	-0.5	0.009076		EIF3F	-0.676666	1.795899
RPS16	-0.503333	2.058954		RPS14	-0.676667	3.755572
TBC1D4	-0.503333	0.009001		RPL31	-0.683332	2.524393
HSD17B12	-0.503333	1.203696		CDK2	-0.69	0.011864
PRPF31	-0.506667	0.008933		RBM14	-0.690001	1.857722
ILVBL	-0.506667	1.054054		MSH6	-0.696667	2.6941
ADO	-0.51	0.008479		RPS20	-0.699999	3.561893
PCNA	-0.520001	1.541471		MCM5	-0.7	4.173925
MACROD1	-0.523333	0.00964		DDB1	-0.7	0.939497
SAE1	-0.523333	1.830342		NNT	-0.7	3.668662
MYO1D	-0.523334	2.092011		RPL27	-0.7	2.780318
ATP5PO	-0.526666	1.060041		RPS4X	-0.700001	4.16813
MTPAP	-0.526666	3.037201		RPL27A	-0.703332	2.58786
UBA2	-0.526666	3.356728		ENO1	-0.706667	1.892225
ETFB	-0.526667	1.834624		NUP62	-0.706668	0.012578
NUDT21	-0.529999	0.751299		PARP1	-0.71	1.998689
CS	-0.53	1.527181		PSPC1	-0.71	1.41121
RPS14	-0.533334	2.66767		FN1	-0.71	0.012517
EARS2	-0.536666	0.009683		CUL4B	-0.713334	0.73218
LYPLAL1	-0.536666	0.009992		MDH2	-0.72	0.01238
WDR3	-0.536666	2.108541		MRPS34	-0.720001	2.301582
HNRNPD	-0.54	1.954216		PICALM	-0.723333	0.012746
PRPF40A	-0.54	0.010052		AP2A1	-0.723334	0.012643
SMARCA1	-0.543333	0.009467		RPL7	-0.729999	2.745076
RPRD1B	-0.546666	0.009665		PTBP1	-0.730001	2.015676
PDK3	-0.546668	2.303235		RPL36A	-0.733333	2.805457
RPL27A	-0.549999	1.902798		ARL2	-0.733334	1.651038
RPL5	-0.553333	1.86913		STAT3	-0.736668	0.013206
RPL12	-0.553335	2.085069		MCCC1	-0.736668	4.138466
LGALS3BP	-0.556667	1.412181		NPM1	-0.74	2.988528
KRT5	-0.563334	0.009623		AP2M1	-0.743333	0.012707
RAB5C	-0.566666	1.228101		NHLRC2	-0.743333	0.013014
RBM15	-0.57	0.573645		PC	-0.743333	2.67523

RIF1	-0.57	0.010357		PSMD14	-0.743335	2.087619
ACSF2	-0.570001	0.010475		RPL5	-0.749999	2.792203
LUC7L2	-0.570002	1.445949		H2AC11	-0.75	0.01271
STOML2	-0.576668	1.005366		PCCB	-0.75	2.95027
UBR4	-0.580001	0.875846		RTCA	-0.753333	1.524157
SLC25A13	-0.59	1.330626		RPL37	-0.756667	2.851069
MRPS34	-0.590001	1.605077		PCCA	-0.756667	3.913299
ATP6V1C1	-0.593333	0.010283		OXCT1	-0.756668	3.181907
FMR1	-0.596666	1.172232		XRCC5	-0.76	3.291471
OSBPL3	-0.596666	0.010706		PAFAH1B3	-0.776667	3.037514
RCN1	-0.603333	0.01061		FH	-0.776667	0.013293
HSPB1	-0.603334	2.450433		RCN1	-0.776667	0.013749
EEF1B2	-0.610001	0.010418		RPS25	-0.779999	0.013233
DHFR	-0.616667	2.682162		H4C1	-0.78	0.013091
TFRC	-0.62	1.31102		RPL30	-0.78	2.045249
MMS19	-0.623333	1.161867		XRCC6	-0.78	2.587905
RPL30	-0.623333	1.493357		HNRNPD	-0.786668	2.081693
SRM	-0.623333	0.982054		NDUFA9	-0.789998	1.352444
ZC3HAV1	-0.623333	1.024541		PMPCA	-0.803333	1.234253
ARHGDIA	-0.626665	0.01097		LUC7L	-0.806667	0.014988
ELAC2	-0.629999	0.010969		SNRPD3	-0.806667	0.014395
NDRG1	-0.633333	2.813597		XRN2	-0.810001	0.786112
MIPEP	-0.643333	0.012062		DDX39B	-0.813333	3.387314
HDHD5	-0.646666	1.428253		RPS27A	-0.823334	1.173688
PRPF4	-0.646667	0.011473		GNL3	-0.826667	2.0959
RPL36A	-0.646668	2.5114		ATIC	-0.829999	1.708829
NOC2L	-0.673334	1.001756		RPL18	-0.83	2.532805
BLVRA	-0.676667	1.002613		SBDS	-0.83	0.01473
PDCD4	-0.686667	0.756987		ACAD9	-0.833333	2.265919
CALD1	-0.69	0.943407		CRNKL1	-0.833333	0.015219
EXD2	-0.693333	0.012302		RHOC	-0.836666	0.015305
ARL2	-0.696667	1.651693		WDR18	-0.836667	3.193585
ARGLU1	-0.696667	1.436661		MCM3	-0.839999	3.068436
USP14	-0.703335	0.965697		RPL12	-0.846667	2.565964
MRPS27	-0.706667	1.919918		PRIM2	-0.856667	0.015562
PTPN11	-0.706668	0.012266		MRPS27	-0.86	2.48081

RAB32	-0.71	0.769555		RPS13	-0.873333	2.326159
UGDH	-0.720001	1.418272		ACACA	-0.876666	3.462302
CALCOCO2	-0.723333	0.012642		UBA2	-0.876666	3.481399
MAT2A	-0.726666	0.0128		PIK3C2A	-0.876668	0.551638
PGK1	-0.726666	1.397411		HNRNPH2	-0.88	1.291923
RPL29	-0.730001	3.102587		SAE1	-0.886667	2.37704
WASHC5	-0.746666	0.013216		WASHC5	-0.886667	0.01578
PA2G4	-0.750001	1.59834		ATP6V1C1	-0.896666	0.015721
CCPG1	-0.750001	0.0136		USP54	-0.896666	0.015686
KIFBP	-0.753333	0.013647		FAU	-0.896667	3.919518
PIK3C2A	-0.753334	0.49288		TSFM	-0.900001	1.342605
XRN2	-0.766667	0.627433		CCPG1	-0.903334	0.016528
H2AC11	-0.770001	0.013059		DHFR	-0.916666	3.491911
TALDO1	-0.790001	0.013394		FADS1	-0.916667	0.016214
SLC16A1	-0.793334	1.678084		XPOT	-0.916667	0.947333
ACOT7	-0.796666	0.99664		STOML2	-0.936667	1.669585
BCKDK	-0.799999	0.014183		FEN1	-0.95	1.210581
AK1	-0.8	0.014127		ACACB	-0.976667	3.547344
MYH10	-0.803335	1.727104		RBM39	-0.983332	1.816201
U2AF2	-0.806668	1.589473		LUC7L2	-0.986668	2.185114
CPSF6	-0.81	1.862851		UGDH	-0.99	2.177083
TPP2	-0.816666	0.01444		CALR	-0.996666	1.618288
CENPV	-0.82	1.441786		SLC2A3	-1.016665	2.805216
GNL3	-0.820001	2.36323		SNX2	-1.03	4.496209
RPS25	-0.823333	0.014002		BLVRA	-1.030001	1.247789
AP2A1	-0.823334	0.014446		NOC2L	-1.04	1.387756
MYBBP1A	-0.829999	0.597599		TMED10	-1.049999	2.238043
PPP1R12A	-0.830001	0.890532		TUBA1C	-1.09	0.979585
PICALM	-0.876666	0.015539		MYBBP1A	-1.1	0.910977
PGAM1	-0.876668	0.780159		PA2G4	-1.11	2.023311
RAB3GAP1	-0.88	0.680697		DDX46	-1.113333	3.262828
CDK16	-0.883333	0.015866		SPECC1L	-1.113333	0.019918
ACAD9	-0.883333	1.658825		ACAD11	-1.136667	2.757031
FADS2	-0.883334	2.066565		PCNA	-1.153333	2.54153
AK2	-0.903334	0.015924		GOLGA5	-1.163333	0.020411

YTHDF2	-0.916667	0.016501		RPS17	-1.176667	0.862191
MCU	-0.923333	0.016211		LRP1	-1.206668	0.582383
JUP	-0.926666	1.464184		ERC1	-1.216666	0.02071
NHLRC2	-0.936668	0.016517		CPSF6	-1.22	2.153762
TPI1	-0.943334	0.85997		TALDO1	-1.236668	0.021318
ATP5MF	-0.95	0.016341		RBM15	-1.25	1.056606
RPS17	-0.986666	0.896916		SRM	-1.250001	1.725968
DDX47	-0.99	0.963162		SARM1	-1.273333	0.022178
EIF3M	-0.99	0.779425		ATP5MF	-1.293333	0.022534
ACAD11	-1.02	2.213115		RPL29	-1.293333	4.079355
KCTD12	-1.043333	1.213834		PGK1	-1.296667	2.16638
H2BC12	-1.056669	4.416801		PGAM1	-1.313334	0.945806
FADS1	-1.113334	0.019841		U2AF2	-1.320002	2.124352
ERC1	-1.123334	0.019025		EIF3M	-1.380001	1.319414
NCL	-1.163332	1.23839		NUDT21	-1.396666	1.676938
SPECC1L	-1.223333	0.022023		AK1	-1.436667	0.025996
USP54	-1.25	0.022305		NCL	-1.459999	1.453977
TMED10	-1.329999	2.326378		ACOT7	-1.51	2.515266
PYGM	-1.33	0.022817		KRT5	-1.54	0.027779
TUBA1C	-1.360001	1.266917		PKM	-1.543333	2.987304
PKM	-1.376666	2.657025		TPI1	-1.793334	1.298996
SARM1	-1.393333	0.024429		FADS2	-1.870001	2.567313
RAP2C	-1.66	0.03036		PYGM	-2.093334	0.037428
				KRT82	-2.423333	0.042617
				ALB	-2.726666	1.155161
				KRT10	-3.58	1.221948
				KRT9	-3.683333	2.04221

Table S7. Key Resource Table

RESOURCE TYPE	RESOURCE NAME	SOURCE	IDENTIFIER	NEW/REUSE
Antibody	ATG2A	Cell Signaling Technologies	AB_2732797	REUSE
Antibody	P62	BD BioSciences	AB_398151	REUSE
Antibody	GAPDH	Abcam	AB_307274	REUSE
Antibody	LC3B	Cell Signaling Technologies	AB_2137707	REUSE
Antibody	RB1CC1/ FIP200	Thermo Fisher Scientific	AB_10666428	REUSE
Antibody	Rab1a	Cell Signaling Technologies	AB_2665537	REUSE
Antibody	Rab1b	Proteintech	AB_2237881	REUSE
Antibody	ARFGAP1	Proteintech	AB_2058621	REUSE
Antibody	FLAG	Sigma-Aldrich	AB_262044	REUSE
Antibody	GFP	Cell Signaling Technologies	AB_1196615	REUSE
Antibody	mCherry	Invitrogen	AB_2552323	REUSE
Antibody	ECL anti-rabbit IgG horseradish peroxidase-linked	Cytiva	AB_2722659	REUSE
Antibody	ECL anti-mouse	Cytiva	AB_772210	REUSE

	IgG horseradish peroxidase-linked			
Antibody	Biotin	Rockland	AB_2611059	REUSE
Antibody	GFP	Massive Photonics	AB_2744600	REUSE
Antibody	Sec31A	BD BioSciences	AB_399717	REUSE
Antibody	Sec24C	Cell Signaling Technologies	AB_2798565	REUSE
Antibody	MIA3/Tango1	Sigma-Aldrich	AB_2682971	REUSE
Antibody	TFG	Abcam	AB_3677764	REUSE
Antibody	COPI/CMIA10	Rothman Lab	AB_3678745	REUSE
Antibody	LC3B	MBL	AB_2274121	REUSE
Antibody	Sec16A	Abcam	AB_1270588	REUSE
Antibody	Sec24D	Cell Signaling Technologies	AB_2798574	REUSE
Antibody	GM130	BD BioSciences	AB_398142	REUSE
Antibody	LMAN1/ERGIC53	Abcam	AB_10973984	REUSE
Antibody	Alexa Fluor 405 goat anti-mouse IgG	Invitrogen	AB_3251389	REUSE
Antibody	Alexa Fluor 594 goat anti-rabbit IgG	Invitrogen	AB_3251387	REUSE

Antibody	Alexa Fluor 647 goat anti-rabbit IgG	Invitrogen	AB_3251388	REUSE
Antibody	Alexa Fluor 647 goat anti-mouse IgG	Invitrogen	AB_3668624	REUSE
Recombinant DNA	pLVX Puro GFP-ATG2A	Valverde and Yu et al, 2019	Addgene_250863	REUSE
Recombinant DNA	pLVX Puro APEX2-GFP-ATG2A	This paper	Addgene_250864	NEW
Recombinant DNA	pcDNA3 APEX2-NES	Addgene	Addgene_49386	REUSE
Recombinant DNA	pCMV 3xFLAG-ATG2A	Valverde and Yu et al, 2019	Addgene_250865	REUSE
Recombinant DNA	pLVX Neo TagBFP-LC3B	This paper	Addgene_250866	NEW
Recombinant DNA	pLVX-EGFP-IRES-Neo	Addgene	Addgene_128660	REUSE
Recombinant DNA	pDESt47 Sar1-GFP	Addgene	Addgene_67409	REUSE
Recombinant DNA	Sar1b-mOrange2	Addgene	Addgene_166899	REUSE
Recombinant DNA	Sar1bH79G2-mOrange2	Addgene	Addgene_166900	REUSE
Recombinant DNA	Sar1bH79G-3xFLAG	This paper	Addgene_250867	NEW
Recombin	Sar1bH79	This	Addgene	NEW

ant DNA	G2-BFP	paper	_250873	
Recombinant DNA	Sar1b-BFP	This paper	Addgene _250872	NEW
Recombinant DNA	mRuby-Sec23A	Addgene	Addgene _36158	REUSE
Recombinant DNA	EGFP-Sec23A	Addgene	Addgene _66609	REUSE
Recombinant DNA	pEGFP-Sec24A	This paper	Addgene _250868	NEW
Recombinant DNA	pEGFP-Sec24B	This paper	Addgene _250869	NEW
Recombinant DNA	EGFP-Sec24C	This paper	Addgene _250870	NEW
Recombinant DNA	pEYFP-Sec24C	Addgene	Addgene _66608	REUSE
Recombinant DNA	pEGFP-Sec24D	Addgene	Addgene _32678	REUSE
Recombinant DNA	GFP-Sec31A	Addgene	Addgene _42124	REUSE
Recombinant DNA	GFP-Sec16A	Addgene	Addgene _36155	REUSE
Recombinant DNA	ARFGAP1-TagRFP	Gift from the Rothman lab	N/A	NEW
Recombinant DNA	ARFGAP1-GFP	Gift from the Antonny Lab	N/A	REUSE
Recombinant DNA	pMRX IB HaloTag7-mGFP	Mizushima Lab	Addgene _184903	REUSE
Recombinant DNA	pMRX No HaloTag7-mGFP-LC3B	Mizushima Lab	Addgene _184901	REUSE
Recombinant DNA	pLVX puro GFP	This paper	Addgene _250871	NEW
Recombinant DNA	GFP-Rab1a	Gift from the Rothman lab	N/A	REUSE
Recombinant DNA	SNAP-Rab1a	Gift from the	N/A	REUSE

		Rothman lab		
Recombinant DNA	pGEX2T GST-GFP-RAB1A	This paper	Addgene_250877	NEW
Recombinant DNA	pGEX2T GST-GFP-GABARAPL1	This paper	Addgene_250874	NEW
Recombinant DNA	psPAX2	Addgene	Addgene_12260	REUSE
Recombinant DNA	pCMV-VSV-G	Addgene	Addgene_8454	REUSE
Oligonucleotide	APEX2_f	Keck Oligonucleotide Synthesis	N/A	GTATGAATTCATGggaaagtcttacccaactgtg
Oligonucleotide	APEX2_r	Keck Oligonucleotide Synthesis	N/A	GGAAGTGAATTCggcatcagcaaacccaag
Oligonucleotide	BamFLAGNotf	Keck Oligonucleotide Synthesis	N/A	CATGAGGATCCAGACTACAAAGACCATGACGGTGATTATAAAGATCATGACATCGATTACAAGGATGACGATGACAAGTAGGCGGCCGCACTAG
Oligonucleotide	BamFLAGNotr	Keck Oligonucleotide Synthesis	N/A	CTAGTGCGGCCGCCTACTTGTCAT

				CGTCATCCTTGTAATCGATGTCATGATCTTTATAATCACCGTCATGGTCTTTGTAGTCTGGATCCTCATG
Oligonucleotide	24A_f	Keck Oligonucleotide Synthesis	N/A	GATCACTCGAGGTAGTGGAAGTGGAAGTATGTCCCAGCCGGGAATACC
Oligonucleotide	24A_r	Keck Oligonucleotide Synthesis	N/A	GATCATTAATTAATCATTTATTCACTTGTTGCTGTATATGCAACAGGAATTCATAATATG
Oligonucleotide	24B_f	Keck Oligonucleotide Synthesis	N/A	GATCACTCGAGGTAGTGGAAGTGGAAGTATGTCGGCCCCCGCCGGGTCCTCTCAC
Oligonucleotide	24B_r	Keck Oligonucleotide Synthesis	N/A	GATCATTAATTAATCACTTACAAAT

				CTGCTG CTGAAC ATGAAG CAAAAA TTCATA GTAAG
Oligonucleotide	pLVX-GFP_f	Keck Oligonucleotide Synthesis	N/A	gatctcgag ctcaagcttc gaattcAT GGTGAG CAAGGG CGAG
Oligonucleotide	pLVX-GFP_r	Keck Oligonucleotide Synthesis	N/A	agaattatct agagtcgc gggatccT TACTTG TACAGC TCGTCC ATG
Oligonucleotide	Negative Control siRNA	Horizon Biosciences	D-001810-10-05	REUSE
Oligonucleotide	siFIP200	Horizon Biosciences	L-021117-00-0005	REUSE
Oligonucleotide	siRab1a	Horizon Biosciences	L-0082383-00-0005	REUSE
Oligonucleotide	siRab1b	Horizon Biosciences	L-008958-01-0005	REUSE
Oligonucleotide	siARFGAP1	Horizon Biosciences	L-013321-02-005	REUSE
Oligonucleotide	Anti-GFP label	Integrated DNA Technologies	N/A	TCTTCA TTAGCG
Oligonucleotide	Anti-TFG label	Integrated DNA Technologies	N/A	ATAGTG ATTGGA
Oligonucleotide	Anti-Tango1 label	Integrated DNA Technolo	N/A	TTATGTT CTGCT

		gies		
Oligonucleotide	Anti-Sec24C label	Integrated DNA Technologies	N/A	ATGTTA ATGGGT
Oligonucleotide	Anti-Sec16A label	Integrated DNA Technologies	N/A	ATTTAG TGTAGC
Oligonucleotide	Anti-LC3B label	Integrated DNA Technologies	N/A	ATATGA TCTCCG
Oligonucleotide	Anti-Sec31A label	Integrated DNA Technologies	N/A	AAAAAG TTCGAG
Oligonucleotide	Anti-ARFGAP1 label	Integrated DNA Technologies	N/A	ATAATG GATGGG
Oligonucleotide	Anti-COPI/CMIA10 label	Integrated DNA Technologies	N/A	ATAATC ATGCTC
Oligonucleotide	Anti-P62 label	Integrated DNA Technologies	N/A	ATAACA GAATCG
Oligonucleotide	Imager	Integrated DNA Technologies	N/A	TGGTGG
Oligonucleotide	A3-5xR2	Integrated DNA Technologies	N/A	ACCACC ACCACC ACCACC A AA CGCTAA TGAA
Oligonucleotide	A15-5xR2	Integrated DNA Technologies	N/A	ACCACC ACCACC ACCACC A AA TCCAAT

				CACT
Oligonucleotide	A39-5xR2	Integrated DNA Technologies	N/A	ACCACCACCACCACCACCA AAAGCAGAACAT
Oligonucleotide	A8-5xR2	Integrated DNA Technologies	N/A	ACCACCACCACCACCACCA AAACCCATTAAC
Oligonucleotide	A38-5xR2	Integrated DNA Technologies	N/A	ACCACCACCACCACCACCA AAGCTACACTAA
Oligonucleotide	A20-5xR2	Integrated DNA Technologies	N/A	ACCACCACCACCACCACCA AACGGAGATCAT
Oligonucleotide	A27-5xR2	Integrated DNA Technologies	N/A	ACCACCACCACCACCACCA AACTCGAACTTT
Oligonucleotide	A10-5xR2	Integrated DNA Technologies	N/A	ACCACCACCACCACCACCA AACCCATCCATT
Oligonucleotide	A25-5xR2	Integrated DNA Technologies	N/A	ACCACCACCACCACCACCA AAGAGCATGATT
Oligonucleotide	A36-5xR2	Integrated DNA	N/A	ACCACCACCACC

		Technologies		ACCACCA AA CGATTCTGTT
Oligonucleotide	E3-5xR2	Integrated DNA Technologies	N/A	TTCATTAGCG TT TGG
Oligonucleotide	E15-5xR2	Integrated DNA Technologies	N/A	AGTGATTGGA TT TGG
Oligonucleotide	E39-5xR2	Integrated DNA Technologies	N/A	ATGTTCTGCT TT TGG
Oligonucleotide	E8-5xR2	Integrated DNA Technologies	N/A	GTTAATGGGT TT TGG
Oligonucleotide	E38-5xR2	Integrated DNA Technologies	N/A	TTAGTGTAGC TT TGG
Oligonucleotide	E20-5xR2	Integrated DNA Technologies	N/A	ATGATCTCCG TT TGG
Oligonucleotide	E27-5xR2	Integrated DNA Technologies	N/A	AAAGTTCGAG TT TGG
Oligonucleotide	E10-5xR2	Integrated DNA Technologies	N/A	AATGGATGGG TT TGG
Oligonucleotide	E25-5xR2	Integrated DNA Technologies	N/A	AATCATGCTC TT TGG
Oligonucleotide	E36-5xR2	Integrated DNA Technologies	N/A	AACAGAATCG TT TGG

Experimental model: Cell line	HEK293	WT Parental	ATCC CRL-1573	CVCL_0045
Experimental model: Cell line	HEK293	ATG2 DKO	Valverde and Yu et al	CVCL_E8CG
Experimental model: Cell line	HEK293	ATG2 DKO + APEX2-EGFP-ATG2A	This study	CVCL_E8GU
Experimental model: Cell line	HEK293	ATG2 DKO + GFP-ATG2A	Valverde and Yu et al	CVCL_E8CH
Experimental model: Cell line	HEK293	ATG2 DKO + GFP-ATG2A + TagBFP-LC3B	This study	CVCL_E8GV
Experimental model: Cell line	HEK293	WT + HaloTag7-mGFP	This study	CVCL_E8GW
Experimental model: Cell line	HEK293	WT + HaloTag7-mGFP-LC3B	This study	CVCL_E8GX
Protocol	Immunoprecipitation with GFP-Trap Beads	protocols.io	dx.doi.org/10.17504/protocols.io.kqdg3k6b7v25/v1	NEW
Protocol	HaloTag autophagy flux assay	protocols.io	dx.doi.org/10.17504/protocols.io.36wgq65xxlk5/v1	NEW
Protocol	APEX2-based	protocols.io	dx.doi.org/10.17504	NEW

	proximity biotinylation of ATG2A		/protocols.io.4r3l2686qv1y/v1	
Protocol	Immunoblotting	protocols.io	dx.doi.org/10.17504/protocols.io.yxmvmyxyov3p/v1	NEW
Protocol	Immunofluorescence staining	protocols.io	dx.doi.org/10.17504/protocols.io.5jyl8e5p8l2w/v1	NEW
Protocol	Sample Preparation for FLASH-PAINT	protocols.io	dx.doi.org/10.17504/protocols.io.ewov11ry7vr2/v1	NEW
Protocol	GST tagged recombinant protein expression and purification with thrombin cleavage	protocols.io	dx.doi.org/10.17504/protocols.io.4r3l21d53g1y/v1	NEW
Protocol	3D FIBSEM CLEM	protocols.io	dx.doi.org/10.17504/protocols.io.6qpvr63rzvmk/v1	REUSE
Dataset	Figures 1 and S1	Zenodo	https://zenodo.org/records/17817401	NEW
Dataset	Figures 2 and S2	Zenodo	10.5281/zenodo.17820324	NEW

Dataset	Figures 3 and S3	Zenodo	10.5281/zenodo.17822357	NEW
Dataset	Figures 4 and S4	Zenodo	10.5281/zenodo.17831992	NEW
Dataset	Figures 5 and S5	Zenodo	10.5281/zenodo.17856725	NEW
Dataset	Figures 6 and S6	Zenodo	10.5281/zenodo.17871794	NEW
Chemical, peptide, or recombinant protein	DMEM	Thermo Fisher Scientific	11965-092	REUSE
Chemical, peptide, or recombinant protein	Earle's Balanced Salt Solution (EBSS)	Thermo Fisher Scientific	24010043	REUSE
Chemical, peptide, or recombinant protein	Hank's Balanced Salt Solution (HBSS)	Thermo Fisher Scientific	14025092	REUSE
Chemical, peptide, or recombinant protein	FBS	Thermo Fisher Scientific	16140-071	REUSE
Chemical, peptide, or recombinant protein	PBS	Thermo Fisher Scientific	10010023	REUSE
Chemical, peptide, or	Penicillin/ Streptomicin	Thermo Fisher Scientific	15140122	REUSE

recombinant protein	(10,000 U/mL)			
Chemical, peptide, or recombinant protein	Blasticidin	Gibco	A11139-03	REUSE
Chemical, peptide, or recombinant protein	Puromycin	Clontech	631306	REUSE
Chemical, peptide, or recombinant protein	Geneticin	Thermo Fisher Scientific	10131035	REUSE
Chemical, peptide, or recombinant protein	Opti-Mem	Thermo Fisher Scientific	31985062	REUSE
Chemical, peptide, or recombinant protein	Lipofectamine 3000	Thermo Fisher Scientific	L3000008	REUSE
Chemical, peptide, or recombinant protein	Dharmafect	Horizon Discovery	T-2001-01	REUSE
Chemical, peptide, or recombinant protein	TMR-conjugated HaloTag ligand	Promega	G8251	REUSE

Chemical, peptide, or recombinant protein	Tris	American Bio	AB02000-05000	REUSE
Chemical, peptide, or recombinant protein	NaCl	Ambion	AM9759	REUSE
Chemical, peptide, or recombinant protein	Ultrapure water	Invitrogen	10977-015	REUSE
Chemical, peptide, or recombinant protein	NaCl	Sigma-Aldrich	S9888-25G	REUSE
Chemical, peptide, or recombinant protein	Potassium chloride	Sigma-Aldrich	P3911-25G	REUSE
Chemical, peptide, or recombinant protein	Urea	Sigma-Aldrich	U5128-5G	REUSE
Chemical, peptide, or recombinant protein	Hydrochloric Acid	J.T. Baker	9535	REUSE
Chemical, peptide, or	Tris	Sigma-Aldrich	648310-500GM-M	REUSE

recombinant protein				
Chemical, peptide, or recombinant protein	Sodium deoxycholate	Sigma-Aldrich	D6750-10G	REUSE
Chemical, peptide, or recombinant protein	SDS	American Bio	AB01920-00500	REUSE
Chemical, peptide, or recombinant protein	EDTA	Sigma-Aldrich	3690	REUSE
Chemical, peptide, or recombinant protein	Triton X-100	Sigma-Aldrich	X100	REUSE
Chemical, peptide, or recombinant protein	Saponin	Sigma-Aldrich	47036-50G	REUSE
Chemical, peptide, or recombinant protein	Tween-20	Thermo Fisher Scientific	CAS 9005-64-5	REUSE
Chemical, peptide, or recombinant protein	Nonidet P40 Substitute	Roche	1.1755E+10	REUSE

Chemical, peptide, or recombinant protein	NuPAGE ™ LDS Sample Buffer (4X)	Thermo Fisher Scientific	NP0007	REUSE
Chemical, peptide, or recombinant protein	Glycerol	Sigma-Aldrich	G5516-500ml	REUSE
Chemical, peptide, or recombinant protein	(+_)-6-hydroxy-2,5,7,8-tetra-methylchromane-2-carboxylic acid (Trolox)	Sigma-Aldrich	238813-5G	REUSE
Chemical, peptide, or recombinant protein	3,4-dihydroxybenzoic acid (PCA)	Sigma-Aldrich	37580-25G-F	REUSE
Chemical, peptide, or recombinant protein	protocatechuate 3,4-dioxygenase pseudomonas (PCD)	Sigma-Aldrich	P8279	REUSE
Chemical, peptide, or recombinant protein	16% Paraformaldehyde	Electron Microscopy Sciences	15710	REUSE
Chemical, peptide, or recombin	Triton X-100	Sigma-Aldrich	T8787-50ML	REUSE

ant protein				
Chemical, peptide, or recombinant protein	1_ Phosphate Buffered Saline (PBS) pH 7.2	Gibco	10010-023	REUSE
Chemical, peptide, or recombinant protein	bafilomycin A1	Enzo	BML-CM110-0100	REUSE
Chemical, peptide, or recombinant protein	L-Arginine-13C6,15N4 hydrochloride	Sigma-Aldrich	608033	REUSE
Chemical, peptide, or recombinant protein	L-Lysine·2HCl (__C_, 99%; __N_, 99%)	Cambridge Isotope Laboratories, Inc.	CNLM-291-H-PK	REUSE
Chemical, peptide, or recombinant protein	L-Lysine·2HCl (4,4,5,5-D_, 96-98%)	Cambridge Isotope Laboratories, Inc.	DLM-2640-PK	REUSE
Chemical, peptide, or recombinant protein	L-Arginine·HCl (__C_, 99%)	Cambridge Isotope Laboratories, Inc.	CLM-2265-H-PK	REUSE
Chemical, peptide, or recombinant protein	Biotinyl Tyramide	Sigma-Aldrich	SML2135	REUSE

Chemical, peptide, or recombinant protein	Hydrogen Peroxide (H2O2)	Sigma-Aldrich	H1009-100ML	REUSE
Chemical, peptide, or recombinant protein	Sodium Ascorbate	Sigma-Aldrich	A4034-100G	REUSE
Chemical, peptide, or recombinant protein	GFP-Trap beads	Proteintech	gtma-20	REUSE
Chemical, peptide, or recombinant protein	Streptavidin Magnetic Beads	Pierce	88817	REUSE
Chemical, peptide, or recombinant protein	ampicillin	Sigma-Aldrich	S2002-100G	REUSE
Chemical, peptide, or recombinant protein	Sodium hydroxide	Sigma-Aldrich	221465-500G	REUSE
Chemical, peptide, or recombinant protein	Glutaraldehyde solution	Sigma-Aldrich	G5882-10X1ML	REUSE
Chemical, peptide, or	Sodium cacodylate	Sigma-Aldrich	C0250-10G	REUSE

recombinant protein	trihydrate			
Chemical, peptide, or recombinant protein	Osmium tetroxide	Sigma-Aldrich	419494-250MG	REUSE
Chemical, peptide, or recombinant protein	Potassium hexacyanoferrate(II) trihydrate (K4Fe(CN)6)	Sigma-Aldrich	P3289-5G	REUSE
Chemical, peptide, or recombinant protein	1% Uranyl Acetate Solution	Electron Microscopy Sciences	22400-1	REUSE
Chemical, peptide, or recombinant protein	B-mercaptoethanol	Sigma-Aldrich	M3148	REUSE
Chemical, peptide, or recombinant protein	HEPES (pH 7.4)	Thermo Fisher Scientific	15630-080	REUSE
Chemical, peptide, or recombinant protein	Glutathione agarose	Sigma-Aldrich	G4510	REUSE
Chemical, peptide, or recombin	Thrombin	Sigma-Aldrich	T6884	REUSE

ant protein				
Chemical, peptide, or recombinant protein	DMSO	Sigma-Aldrich	D2650	REUSE
Chemical, peptide, or recombinant protein	COmplete mini EDTA Free	Roche	1.1836E+10	REUSE
Chemical, peptide, or recombinant protein	Bovine serum albumin (BSA)	Jackson ImmunoResearch	001-000-162	REUSE
Chemical, peptide, or recombinant protein	Bovine serum albumin (BSA)	Sigma-Aldrich	A9647	REUSE
Chemical, peptide, or recombinant protein	Non-Fat Dry Milk Omniblock	American Bio	AB10109-01000	REUSE
Chemical, peptide, or recombinant protein	0.45 um Nitrocellulose Membrane	Thermo Fisher Scientific	1620115	REUSE
Chemical, peptide, or recombinant protein	SuperSignal West Pico PLUS Chemiluminescence Substrate	Thermo Fisher Scientific	34580	REUSE

Chemical, peptide, or recombinant protein	SuperSignal West Femto Maximum Sensitivity Substrate	Thermo Fisher Scientific	34095	REUSE
Chemical, peptide, or recombinant protein	Methanol	J.T. Baker	9070-05	REUSE
Chemical, peptide, or recombinant protein	Ethanol	Decon Laboratories	2716	REUSE
Chemical, peptide, or recombinant protein	Ampicillin	Sigma-Aldrich	A0166	REUSE
Chemical, peptide, or recombinant protein	Paraformaldehyde	Electron Microscopy Sciences	19202	REUSE
Chemical, peptide, or recombinant protein	Fisherbrandô Superfrostô Disposable Microscope Slides	Thermo Fisher Scientific	12-550-143	REUSE
Chemical, peptide, or recombinant protein	Microscope Cover Slips (12 mm)	Carolina Biological Supply	633029	REUSE
Chemical,	Q5 High-	NEB	M0492S	REUSE

peptide, or recombinant protein	Fidelity 2X Master Mix			
Chemical, peptide, or recombinant protein	HIFI DNA Assembly Master Mix	NEB	E2621L	REUSE
Chemical, peptide, or recombinant protein	One-Shot STABL3	Invitrogen	C7373-03	REUSE
Chemical, peptide, or recombinant protein	Fluoromount-G	Southern Biotech	0100-01	REUSE
Software/ Code	Prism 10	Graphpad	SCR_002798	REUSE
Software/ Code	2.14.0/1.54f	FIJI	SCR_002285	REUSE
Software/ Code	FlowJo	BD Life Sciences	SCR_008520	REUSE
Software/ Code	Zen	ZEISS ZEN Microscopy Software	SCR_013672	REUSE
Software/ Code	Nikon Elements	NIS-Elements	SCR_014329	REUSE